**ANKARA YILDIRIM BEYAZIT UNIVERSITY**

**GRADUATE SCHOOL OF NATURAL AND APPLIED SCIENCES**




# PLASMONIC $TiO_2$ COMPOSITES FOR DYE-SENSITIZED SOLAR CELLS APPLICATIONS

**M.Sc. Thesis by**

**Hilal YILDIRIM**

**Department of Material Engineering**

**June, 2019**

**ANKARA**

# PLASMONIC $TiO_2$ COMPOSITES FOR DYE-SENSITIZED SOLAR CELLS APPLICATIONS

**A Thesis Submitted to**

**The Graduate School of Natural and Applied Sciences of**

**Ankara Yıldırım Beyazıt University**

**In Partial Fulfillment of the Requirements for the Degree of Master of Science in Material Engineering, Department of Material Engineering**

**by**

**Hilal YILDIRIM**

**June, 2019**

**ANKARA**

## M.Sc. THESIS EXAMINATION RESULT FORM

We have read the thesis entitled **"PLASMONIC $TiO_2$ COMPOSITES FOR DYE-SENSITIZED SOLAR CELLS APPLICATIONS"** completed by **HİLAL YILDIRIM** under the supervision of **ASSIST. PROF. DR. KOUROUSH SALİMİ** and we certify that in our opinion it is fully adequate, in scope and in quality, as a thesis for the degree of Master of Science.

Assist. Prof. Dr. Kouroush SALİMİ

Supervisor

Assist. Prof. Dr. Begüm ÜNVEROĞLU

Jury Member

Assist. Prof. Dr. Mehmet Fatih ÖKTEM

Jury Member

Assoc. Prof. Dr. Yusuf ERDOĞDU

Jury Member

Prof. Dr. Sefer Bora LİŞESİVDİN

Jury Member

Prof. Dr. Ergün ERASLAN

Director

Graduate School of Natural and Applied Sciences

# ETHICAL DECLARATION

I hereby declare that, in this thesis which has been prepared in accordance with the Thesis Writing Manual of Graduate School of Natural and Applied Sciences,

- All data, information and documents are obtained in the framework of academic and ethical rules,
- All information, documents and assessments are presented in accordance with scientific ethics and morals,
- All the materials that have been utilized are fully cited and referenced,
- No change has been made on the utilized materials,
- All the works presented are original,

and in any contrary case of above statements, I accept to renounce all my legal rights.

**Date:** **Signature:……..**

**Name & Surname:…….**

# ACKNOWLEDGMENTS

I owe my deepest gratitude to my supervisor Asst. Prof. Kouroush SALİMİ for his keen interest from the beginning of the work and his support during thesis period. His encouragement making this project successful with his valuable guidance, support and advice. I am thankful for his constructive criticism and kind help. And also, I would like to thank to Assoc. Prof. Dr. Nuray ÇELEBİ for her support to complete my characterization measurements on the Central Laboratory of Middle East Technical University.

This thesis would not have been possible unless working at the Yıldız Research Group. I had a chance to practice laboratory work about the production of solar cells. I would like to extend my thanks to those who offered support: my co-supervisor Prof. Dr. Abdullah YILDIZ and his laboratory team. I am very grateful for having many helpful people around; here I would like to thank the ones, by contributing in direct or indirect ways: Assist. Prof. Dr. Furkan SOYSAL, PhD student Abdullah ATILGAN and PhD student Mustafa Yasir AYDIN.

Additionally, I would like to thank my mother and father who have educated me with love for all my life, my brother Furkan who has always been with me with respect. My family have never denied me an opportunity to further my education. And I have warmest thanks to my fiancé Metin, he has been a great moral support of any time I give up.

Finally, my dear Mirabelle, she always gives me strength and hope for the future. I am truly thankful for her presences in my life.

**2019, 27 June** **Hilal YILDIRIM**

# PLASMONIC $TiO_2$ COMPOSITES FOR DYE-SENSITIZED SOLAR CELLS APPLICATIONS


## ABSTRACT

Dye-sensitized solar cells (DSSCs) have attracted considerable attention of scientists because of their low cost, flexible design, ease of fabrication and low toxicity, since first reported by Grätzel in 1991. In order to prevent the charge recombination at the $TiO_2$/dye/electrolyte interface, engineering of an alternative functional photoanodes still to be challenged. Recently, cooperation between surface plasmon resonance and photosensitizer electrodes led to achieve different properties of dye sensitized solar cells (DSSC). Particularly, plasmonic nanoclusters have ability to concentrate the incident light in their optical field as well as enhancement the efficiency of photovoltaic devices based on strong light scattering and local field improvements. For example, noble metal nano-particles (*i.e.,* Au and Ag) have been utilized for surface modification of $TiO_2$ to improve the power conversion efficiency (PCE) of a DSSC.

In this study, plasmonic $TiO_2$ photoanodes were synthesized by multi-stage methods using solvothermal and silanization procedures, respectively. The physical and chemical properties of the plasmonic photoanodes were characterized using SEM, XRD, XPS, BET, UV-vis, and EIS as well. Based on the specific surface area, pore size distribution, and enhanced localized surface plasmon resonance properties of the synthesized photoanodes, the designed DSSCs showed remarkable power conversion efficiency (*i.e.,* 7.62%) compare to the control groups (*i.e.,* bare $TiO_2$ and P25 paste).



**Keywords:** Dye sensitized solar cells, light harvesting, surface plasmon, photoanodes

# PLAZMONİK $TiO_2$ KOMPOZİT MALZEMELER VE BOYA DUYARLI GÜNEŞ PİLLERİNDE KULLANIMI

## ÖZ

Boyaya duyarlı güneş pilleri (DSSC'ler), 1991'de Grätzel tarafından ilk rapor edildiğinden beri düşük maliyetli, esnek tasarımları, üretim kolaylıkları ve düşük toksisiteleri nedeniyle bilim adamlarının dikkatini çekmiştir. $TiO_2$/boya/elektrolit arayüzünde yük rekombinasyonunu önlemek için, alternatif bir fonksiyonel fotoanodun geliştirilmesi için çalışmalar hala devam etmektedir. Son zamanlarda, yüzey plazmon rezonansı ve foto-hassaslaştırıcı elektrotları arasındaki işbirliği, boyaya duyarlı güneş pillerinin farklı özelliklerinin elde edilmesini sağlamıştır. Özellikle, plazmonik nanoparçacıklar, gelen ışığı optik alanlarına yoğunlaştırma yeteneğinin yanı sıra, güçlü ışık saçılımı ve yerel alan iyileştirmelerine dayanan fotovoltaik cihazların verimliliğini arttırma kabiliyetine sahiptir. Örneğin, bir boya duyarlı güneş pilinin güç dönüşüm verimliliğini (PCE) geliştirmek için $TiO_2$'nin yüzey modifikasyonuyla asil metal nanoparçacıklar (yani Altın ve Gümüş) kullanılmıştır.

Bu tez çalışmasında, plazmonik $TiO_2$ fotoanotları, sırasıyla solvotermal ve silanizasyon prosedürleri kullanılarak çok aşamalı metotlarla sentezlenmiştir. Plazmonik fotoanotların fiziksel ve kimyasal özellikleri, SEM, XRD, XPS, BET, UV-vis ve EIS kullanılarak karakterize edilmiştir. Özel yüzey alanı, gözenek ebadı dağılımı ve geliştirilmiş lokalize yüzey plazmon rezonans özelliklerine dayanarak, sentezlenen fotoanotların tasarlanan boya duyarlı güneş pillerinin kontrol gruplarına kıyasla (yani, katkısız $TiO_2$ ve P25 macunu) karşılaştırıldığında dikkate değer bir güç dönüşüm (%7,62) verimliliği gösterdiği not edilmiştir.

**Anahtar Kelimeler:** Boya duyarlı güneş pilleri, ışık verimliliği, yüzey plazmonu, fotoanotlar

# CONTENTS

M.Sc. THESIS EXAMINATION RESULT FORM ..... ii
ETHICAL DECLARATION ..... iii
ACKNOWLEDGMENTS ..... iv
ABSTRACT ..... v
ÖZ ..... vi
NOMENCLATURE ..... ix
LIST OF TABLES ..... xii
LIST OF FIGURES ..... xiii

**CHAPTER 1 - INTRODUCTION ..... 1**
1.1 Energy Demand and Energy Consumption ..... 1
1.1.1 Environmentally Energy Sources ..... 2
1.1.2 Solar Spectrum and Solar Irradiation ..... 3
1.1.3 Solar Energy Conversion ..... 5
1.2 Solar Cells ..... 5
1.2.1 History of Solar Cells ..... 5
1.2.2. Types of Solar Cells ..... 6
1.2.2.1 Wafer Based Solar Cells ..... 6
1.2.2.2 Thin Film Solar Cells ..... 7
1.2.2.3 Emerging Solar Cells ..... 8
1.3 Dye Sensitized Solar Cells ..... 9
1.3.1 Introduction: DSSC ..... 9
1.3.2 Components of DSSC ..... 10
1.3.3 Working Principle of DSSC ..... 13
1.3.4 Parameters of DSSC ..... 15
**CHAPTER 2 - PLASMONIC $TiO_2$ COMPOSITE FOR ENHANCING LIGHT ABSORBTION IN DSSC ..... 17**
2.1 General Principles of Semiconductor Materials ..... 17
2.2 Mesoporous $TiO_2$ Nano-particles ..... 19
2.2.1 Crystal Structure of $TiO_2$ ..... 19
2.2.2 Photocatalytic Properties of $TiO_2$ ..... 20
2.2.2 Synthetic Methods for $TiO_2$ ..... 23
2.3 Plasmon Enhanced Nano-particles ..... 25
2.3.1 LSPR & Sensing Principle with Nano-particle Plasmon ..... 25

2.3.2 Plasmonic Response of Metal Nano-particles ..... 26
**CHAPTER 3 - EXPERIMENTAL ..... 29**
3.1 Nano-particle Synthesis ..... 29
3.1.1 Synthesis of Mesoporous $TiO_2$ Particles ..... 29
3.1.1 Incorporating Plasmonic Nano-particles into Mesoporous $TiO_2$ Particles ..... 30
3.1.1.1 Synthesis of Au@$TiO_2$ Particles ..... 30
3.1.1.2 Synthesis of Ag@Au@$TiO_2$ Particles ..... 30
3.2 DSSC Fabrication ..... 31
3.2.1 Deposition Process ..... 31
3.2.1.1 FTO Coated Glass Cleaning ..... 31
3.2.1.2 Preparation of Photoanode Pastes ..... 32
3.2.1.3 Anchoring of Dye Sensitizer to Oxide Surface ..... 34
3.2.1.4 Preparation of Electrolyte ..... 35
3.2.1.5 Preparation of Counter Electrode ..... 35
3.2.2 Assembly of DSSC ..... 35
3.3 Characterization Methods Devices ..... 36
3.3.1 Characterization Methods Devices of $TiO_2$ ..... 36
3.3.2 Characterization Methods Devices of DSSC ..... 36
**CHAPTER 4 – RESULTS AND DISCUSSION ..... 38**
4.1 Scanning Electron Microscope Results ..... 38
4.2 X-Ray Diffraction Results ..... 39
4.3 X-Ray Photoelectron Spectroscopy Results ..... 40
4.4 Surface Area Measurement (BET) Results ..... 41
4.5 Device Characterization Results ..... 43
4.6 Current-Voltage Measurements Results ..... 46
4.7 Electrochemical Impedance Spectroscopy Results ..... 49
**CHAPTER 5 - CONCLUSION ..... 53**
**REFERENCES ..... 55**
**CURRICULUM VITAE ..... 75**

# NOMENCLATURE

## Symbols

| | |
|---|---|
| Ef | Fermi energy |
| hϑ | Light quantum |
| Imp | Current at the maximum power point |
| Isc | Short-circuit current |
| Vmp | Voltage at the maximum power point |
| Pin | Power of the incident light |
| Pmp | Power at the maximum power point |
| S | Sensitizer |
| S* | Excited energy state of the sensitizer |
| S+ | Oxidized state of the sensitizer |
| λ | X-ray wavelength |
| I | Current |
| J | Current density |
| Jsc | Short circuit current density |
| Voc | Open circuit voltage |
| FF | Fill factor |
| η | Efficiency |
| V | Potential |

## Acronyms

| | |
|---|---|
| $AgNO_3$ | Silver nitrate |
| AM | Incident air mass |
| a-Si | Amorphous silicon |
| APTES | (3-Aminopropyl) triethoxysilane |
| BET | Brunauer, Emmet, Teller |
| CB | Conduction band |
| DSSC | Dye-sensitized solar cell |
| EC | Ethyl cellulose |
| EIS | Electronic Impedance Spectroscopy |
| FTO | Fluorine-doped tin oxide |
| HAc | Acetic acid |

| | |
|---|---|
| $HAuCl_4$ | Gold(III) chloride hydrate |
| HCHO | Formaldehyde |
| HOMO | Highest occupied molecular orbital |
| IPA | Isopropanol |
| ITO | Indium-tin oxide |
| LUMO | Lowest unoccupied molecular orbital |
| LSPR | Localized surface plasmon resonance |
| Mtoe | Million tonnes of oil equivalent |
| $NH_3$ | Ammonia |
| NIR | Near-infrared |
| NREL | National Renewable Energy Laboratory |
| PV | Photovoltaic |
| Red/Ox | Reduction /Oxidation |
| rpm | Revolution per minute |
| SEM | Scanning Electron Microscopy |
| SPR | Surface plasmon resonance |
| TCO | Transparent conductive oxide |
| TEA | Triethylamine |
| $TiO_2$ | Titanium dioxide |
| $TiCl_4$ | Titanium(IV) Chloride |
| TSC | Trisodium citrate dihydrate |
| TTIP | Titanium(IV) isopropoxide |
| UV-Vis | Ultraviolet-visible |
| VB | Valence band |
| QD | Quantum Dot |
| XPS | X-ray Photoelectron Spectroscopy |
| XRD | X-ray Diffraction |

# LIST OF TABLES

**Table 2.1** LSPR Frequencies of Various Metals ……..….. 27
**Table 3.1** The Mixing Percent of Paste and Bare & Plasmon…….…..... 34
**Table 4.1** Area-Volume-Pore Size Summary of Synthesized Materials ……..….. 41
**Table 4.2** JV Characteristics for Different Sample Ratios……...….. 46
**Table 4.3** EIS Characteristics for Different Sample Ratios ……...…… 51

# LIST OF FIGURES

**Figure 1.1** Primary Energy Demand……..... 2
**Figure 1.2** Consumption According to Types of Energy……...…….….. 2
**Figure 1.3** Solar Radiation Spectrum ……..…….... 4
**Figure 1.4** Best Research Cell Efficiencies…….……..... 6
**Figure 1.5** Band Gap and Lattice Constant for Various III–V and
Group-IV Material Alloys ……..…….…...….. 7
**Figure 1.6** Sandwich Structure of Dye Sensitized Solar Cell ……..…....10
**Figure 1.7** Some Ruthenium Based Dyes ……...…….. 12
**Figure 1.8** Energy Levels in DSSCs ……..……..…….... 13
**Figure 1.9** Working Mechanism of DSSCc…….…….... 14
**Figure 2.1** Energy Bands and Fermi Levels Of Semiconductors……..... 18
**Figure 2.2** The Band Positions of Some Semiconductors ……..... 18
**Figure 2.3** Crystal Structures of $TiO_2$ ……...…….... 20
**Figure 2.4** Photocatalytic Properties of $TiO_2$ ……..……..….... 21
**Figure 2.5** Comparison of Recombination Processes Within Anatase and Rutile Phases..22
**Figure 2.6** Schematic Drawing of Surface Plasmons ……..…….…….... 26
**Figure 3.1** Representation of The Experimental Procedure ……..……..... 29
**Figure 3.2** Au Attachment Procedure of $TiO_2$ Nano-particles ……..…….... 30
**Figure 3.3** Schematic Drawing of the Planned DSSC Structure ……...……..... 31
**Figure 3.4 a)** FTO Cutting and **b)** Cleaning Processes ….…….... 32
**Figure 3.5** Spin Coating Process ……...…….... 33
**Figure 3.6** Samples after Dye Loading …….…….….. 34
**Figure 3.7** a) Electrolyte Solution Applying b) DSSC Assembling ……..…..... 35
**Figure 3.8** Working Mechanism of Produced DSSC ……..…….…..……..... 37
**Figure 3.9** Current- Voltage Measurement Process ……..……..... 38
**Figure 4.1**. SEM Images of A-B) $TiO_2$ nano-particles, C) Au@$TiO_2$ nano-particles, D)
Ag@Au@$TiO_2$ nano-particles ……..……..... 38
**Figure 4.2** SEM Images of Au@$TiO_2$ and Ag@Au@$TiO_2$ nano-particles ……...…..... 39
**Figure 4.3** XRD Result of Bare $TiO_2$ , Au@$TiO_2$ and Ag@Au@$TiO_2$ nano-particles …..39
**Figure 4.4** XPS Images of Bare $TiO_2$, Au@$TiO_2$ and Ag@Au@$TiO_2$ nano-particles ..... 40
**Figure 4.5** BET Pore Volume Results …….……..…….... 42

**Figure 4.6** A)$N_2$ Adsorption/ Desorption Isotherm of Synthesized Materials, B)BET Plot of Synthesized Materials……..……..... 43
**Figure 4.7** Absorption Spectra of All Samples …...……..……..... 44
**Figure 4.8** Absorption Spectra of Before and After Dye Loading of Bare $TiO_2$……..... 44
**Figure 4.9** Absorption Spectra of Before and After Dye Loading of Au@$TiO_2$ nano-particles……..……. 45
**Figure 4.10** Absorption Spectra of Before and After Dye Loading of Ag@Au@$TiO_2$ nano-particles ..……..……..... 45
**Figure 4.11** JV Characteristics of All Synthesized Nano-particles ……...……..... 47
**Figure 4.12** JV Characteristics of A) Au@$TiO_2$ and B) Ag@Au@$TiO_2$ nano-particles ... 47
**Figure 4.13** Efficiency Graph of Bare $TiO_2$, Au@$TiO_2$ and Ag@Au@$TiO_2$ Nano-particles……48
**Figure 4.14** $\tau_e$ Coefficient Comparison of All Synthesized Nano-particles……..51
**Figure 4.15** Impedance Graph of All Synthesized Nano-particles ……... 52
**Figure 4.16** Impedance graph of A) Au@$TiO_2$ and B) Ag@Au@$TiO_2$ Nano-particles .. 52

# CHAPTER 1

## INTRODUCTION

At present, through looking for after a superior life and better advancements, the quality of human life relies upon a prepared and reliable supply of energy [1]. In modern society, humans consume energy for many different purposes in fact. Together with the growing world population, the expansion in global output and prosperity is also coming with a huge energy need. As the world economy grows rapidly and industrialization of developing countries continues, energy consumption in the world is increasing very rapidly [2]. This demand in energy has economic impact, as well. So that the economic growth is directly related with the usable energy sources.

### 1.1 Energy Demand and Energy Consumption

The progress in living standards by the changing economic status all over the world causes energy demand to increase by around a third over driven especially by India, China and Asia. It is easy to understand the various viewpoints of energy progress with the help of the BP: Energy Outlook. The Figure 1.1 considers the diff erent parts of the change: the sectors wherein energy is utilized; the regions wherein it is devoured and created; and the consumption and generation of diff erent fuels [3].

Figure 1.1. shows a scenario that; in spite of significant development in prosperity and consumption throughout the following 20 years, a significant extent of the total still consumes moderately low levels of energy. [3].

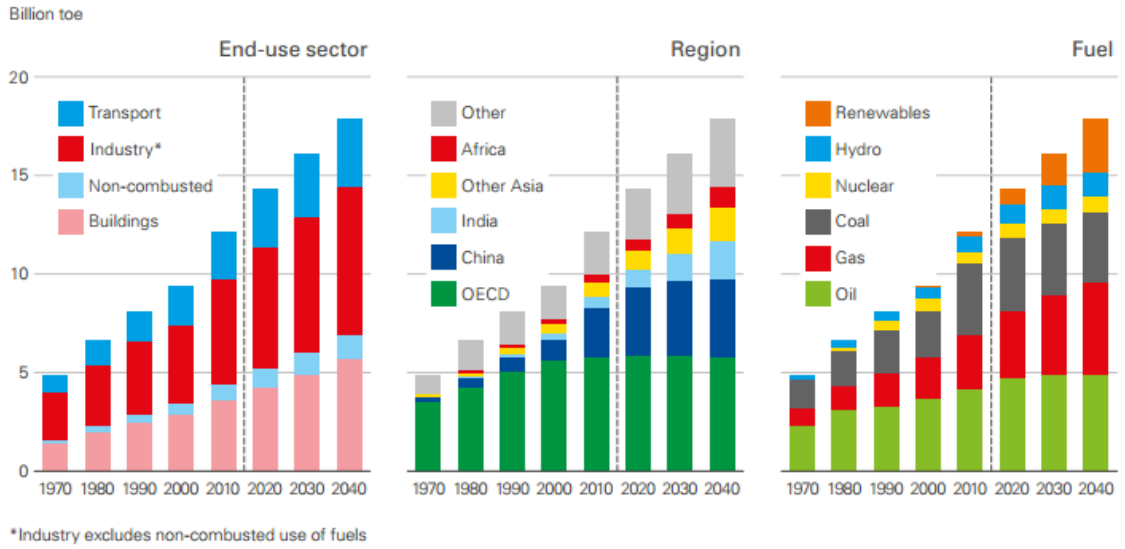


**Figure 1.1** Primary Energy Demand [3]

The priorities in energy policy in Turkey is determined according to the share of Turkey's main energy policy in general will be on oil and gas. As it can be seen in the Figure 1.2, are the largest energy items at the final consumption of petroleum products in Turkey. It followed by natural gas and other fuels, respectively. In brief, with the help of the report of Institute for Energy Markets and Policy- EPPEN we can argue what really drives Turkey's energy demand [4,5].

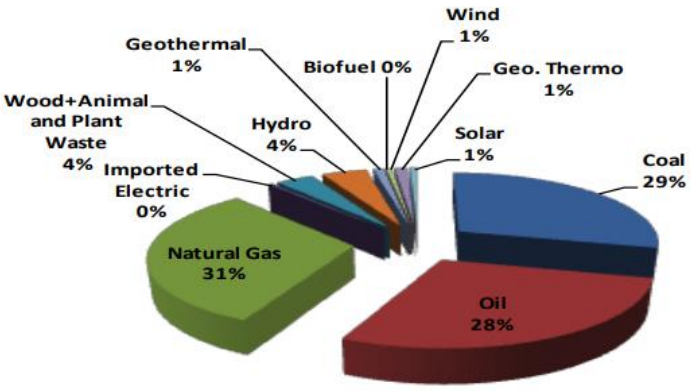


**Figure 1.2** Consumption According to Types of Energy [4]

### 1.1.1 Environmentally Energy Sources

Various types of energy are used in our life including nonrenewable and renewable sources. The modern life of human, critical energy supply primarily relies upon in the form of fossil fuels (coal, oil and natural gas), hydroelectric and nuclear energy, and biomass. Fossil fuels

are thoroughly overwhelming, contributing around 80 % of the world's expanding energy need [3,6].

Humans began to turn towards utilization of fossil fuels, for example, renewable forms of ancient biomass because its storage and transportation being easily and having higher energy density than elective sources [7]. This sort of fuel was formed by the decomposition of living organisms covered in the ground millions of years ago. But as it can be clearly seen with the unbalanced changing of the climate, the life quality of future generations decreases because of various issues arise from fossil-powered energy conversion. [8-11]

Therefore, the people canalize toward sustainable energy and find new energy sources to meet their growing needs. The generation, investment and use of renewable energy source is growing all around the world [12]. From the ancient ages, humanity carried out various renewable energy forms from sunlight, wind, rain, tides, and geothermal heat. It was the main need for the habitat of planet due to it is most plentiful or inexhaustible sustainable power source. Solar energy is a foundation of life because not only humans, the plants and animals also primarily need it to grow and increase the popularity [7,13].

In this regard, in addition to being a renewable energy source, solar energy has been considered to be the most promising and long-lasting source due to its superiority such as the absence of environmental pollution, its local application and lack of complex technology, which is an important problem for the living and living creatures on the world. [14]. The technical capability of solar energy conversion is huge and ready-to-use. And clean source of energy is a powerful candidate for the energy problem that we are trying to solve.

The transformation of solar energy directly into electrical energy is the most appropriate way to the energy cycle of nature. With this regard, energy storage systems such as photovoltaics are essential and useful for storing the energy produced from renewable power sources [15] [12]. With solar cells, electrical energy can be produced near end users, which eliminates transport losses and costs and minimal environmental pollution [16,17].

### 1.1.2 Solar Spectrum and Solar Irradiation

As the largest energy source, the sun sends about $3.9 \times 10^{24}$ J of energy to the earth's surface every year [18-20]. This amount can also be called solar constant and is equal to $1.08 \times 10^{18}$ kW/hour. This amount of energy is about 10000 times the energy that the world needs as the

primary [21]. The atmosphere reduces the incoming radiation by about 20% by reflection and by about 16% by damping. and thus, the highest solar energy achievable at sea level is reduced to around 1000 W/m$^2$ [22,23]. This energy is a small part of the world, even more than the current human energy consumption.

The solar energy is homogeneous on the outside of the sun. While passing through the atmosphere, the solar radiation is constricted by scattering from the light absorption of the air molecules due to the kilometers among sun and the earth. So that this results the solar radiation spectrum on the earth's surface. The effect of atmosphere on solar radiation spectrum relation can be given by followed equation:

$$\text{Airmass} = 1/\cos\theta$$

where θ is the angle between vertical direction and incident radiation [24, 25].

The energy of the sun is determined according to the hours of sunshine, daylight of the sun, the time of day, season, weather conditions and latitude. For example, between 20° and 30° latitude, there is a total yearly solar irradiation on horizontal surface distribution called solar belt, which starts at approximately 700 kWh/m$^2$ from the north of Europe to the equator and continues up to 2500 kWh/m$^2$ [26].

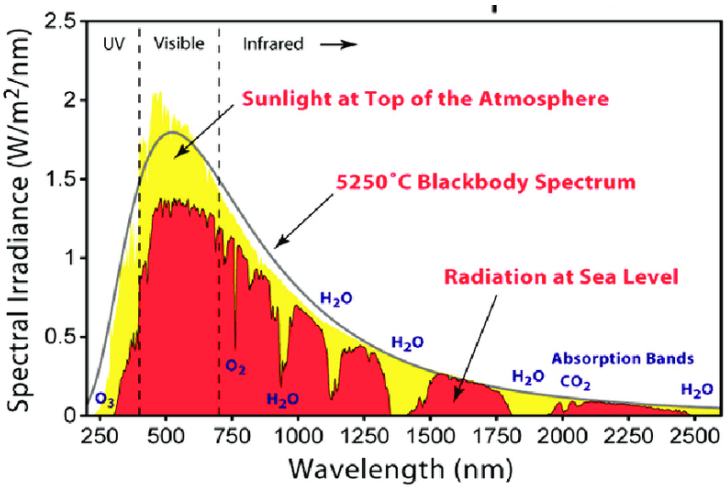


**Figure 1.3** Solar Radiation Spectrum [27,28]

Figure 1.3 shows that even the solar spectrum has very broad range from 100nm to 1mm, the highest intensity of the incoming radiation is in the visible wavelengths (400-700nm) for air mass (AM) 0. The wavelength is from blue to red light, which corresponds to 47% of the total solar radiation received [27,28].

### 1.1.3 Solar Energy Conversion

Solar energy can be used for heating, use or electricity generation. With using solar energy, we take less fuel (coal, oil, natural gas) together. Less fuel consumption, cleaner and healthier environmental management [13,29]. Solar energy must be captured, transformed and stored in a practical way in order to provide a truly common primary energy source [30,31].

Solar energy is transformed into another type of energy with a suitable technology according to the area to be used. The energy types we need most today are heat and electric energy. Therefore, the majority of the work done today is aimed at obtaining heat and electric energy from solar energy. The photovoltaic system is only one of them, but it is separated from the others due to its structure and its function [32]. The energy of solar photons can be converted directly into electrical energy by means of photovoltaic solar cells, this is the key step for capture this energy.

## 1.2 Solar Cells

### 1.2.1 History of Solar Cells

Electrical energy from solar energy is possible with photovoltaic systems [11,12]. The photovoltaic effect was first discovered by French physicist Alexandre Edmond Becquerél in 1839. Becquerél observed and reported the formation of current with light drop on silver bars immersed in electrolyte solution [33]. In the past, photovoltaic batteries consisted of metal / semiconductor interfaces. Their yields were very low. This was due to the relatively large dark current that reduced the photovoltaic effect. Later, semiconductor / semiconductor interfaces were found to yield better yields. [33-37]. In the 1960-1970 years, the aviation industry has been a pioneer in the development of photovoltaic cells [38]. Efforts have been accelerated to be more economical with the energy crisis and environmental awareness that emerged in the 1970s [40]. In the Figure 1.4 The chart of best research-cell efficiencies by National Renewable Energy Laboratory (NREL) can be found [39].

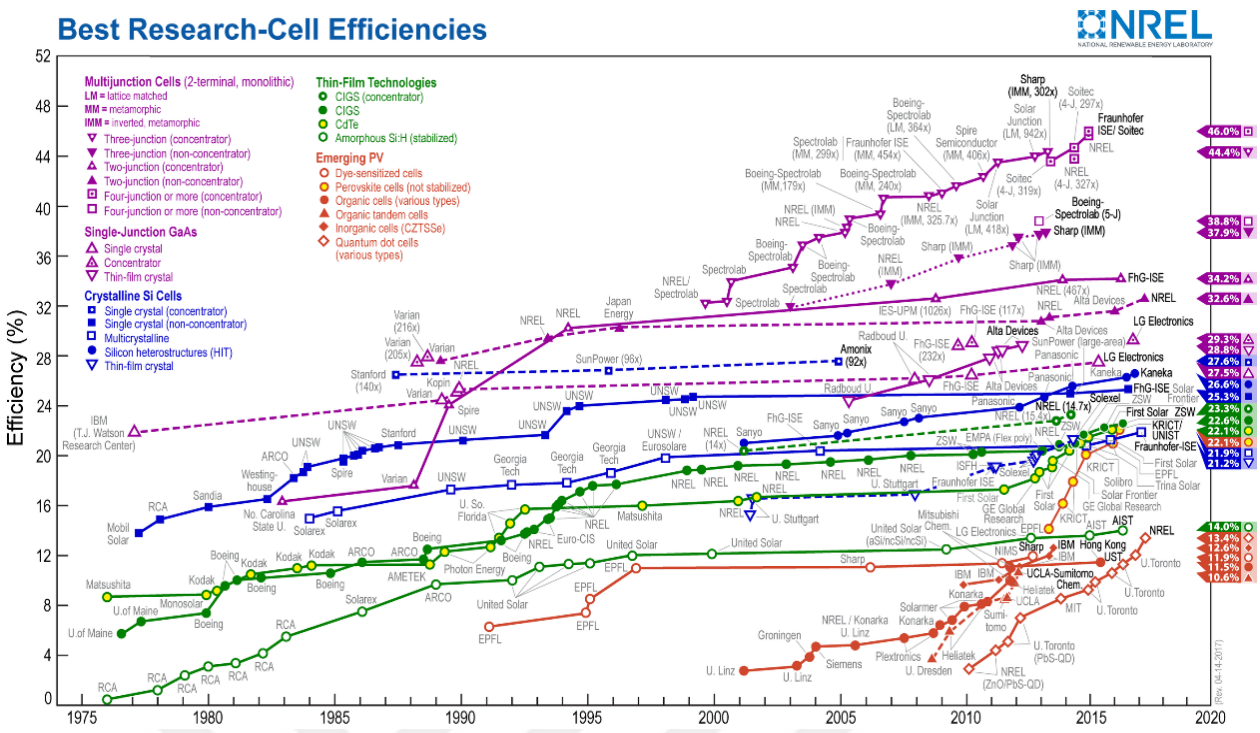


**Figure 1.4** Best Research Cell Efficiencies [39]

### 1.2.2 Types of Solar Cells

Thanks to the growing knowledge and developing technology, more efficient and cheaper solar systems can be made. It is possible to divide solar cells into 3 basic groups [24].

- Wafer-based Solar Cells:
- Thin film Solar Cells:
- Emerging Solar Cell Technologies:

#### *1.2.2.1 Wafer Based Solar Cells*

Wafer-based Solar Cells are silicon-based single and multiple crystal structures that have been used for many years. The distinguishing properties of these cells are about their crystal structures. Single order and regular placement of the atoms in the structure of silicon increases the yield values. During production, a multi-crystalline structure can be obtained depending on the cooling and slicing parameters. The cost of these batteries is low, but their efficiency is lower [41] Based on the data of the NREL, in these solar cells, 24% efficiency is obtained in laboratory conditions and 15% in commercial modules [39].

Another gathering of crystalline solar cells are the III-V group semiconductor materials based on the elements with three valence electrons like aluminum (Al), gallium (Ga) or indium (In) and elements with five valence electrons like phosphorus (P), arsenic (As) and antimony (Sb) [24]. The alloys of these elements such as GaAs, InP, InAs, InSb have much higher absorption coefficients than Si because of they are direct bandgap semiconductors. Figure 1.5 shows the available band gap and lattice constant for the III–V elements such as N, P, As, and Sb alloys [42].

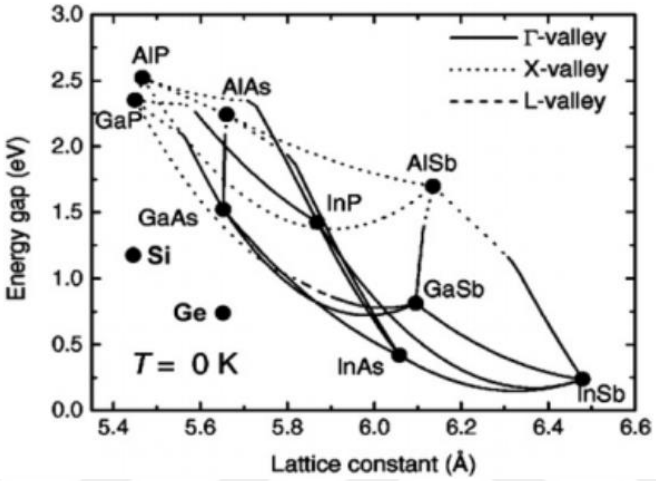


**Figure 1.5** Band gap and lattice constant for various III–V and group alloys [42]

The III-V PV technology is expensive and is used for very specific purposes such as space work and optical systems where performance is more important than cost [38]. The solar concentrator systems can be preferred to reduce the cost. With this system, the irradiance of a large area is concentrated onto the small wafer. GaInP, GaInAs, Ge, GaAlAs, GaInAsP are most known concentrator systems.

### *1.2.2.2 Thin Film Solar Cells*

The most important reason for starting the production of thin film solar cells is that they are more advantageous in terms of cost. Amorphous silicon can absorb light more than crystal silicon. They can therefore be produced in thinner layers. These thin layers can be sliced and used in the cells inside the panels [43]. As of 2014, the efficiency of thin-film solar cells reached 23.3% [39] Thin film solar cells can be divided into two main categories as thin film Si alloys and chalcogenide solar cells.

Thin Film Si Alloys are generally known as microcrystalline silicon, hydrogenated amorphous silicon (a-Si: H) and hydrogenated nanocrystalline silicon (nc-Si: H) structures,

has some of the valance electrons in the silicon lattice that are passivated by hydrogen. Similarly, hydrogenated amorphous germanium (a-Ge: H) and hydrogenated nanocrystalline germanium (nc-Ge: H) also a challenge to make alloys like Si.

Chalcogenide Solar Cells, the term chalcogenides refer to the chemical compounds consisting of chalcogen anion from the group VI (oxygen (O), sulphur (S), selenium (Se), tellurium (Te), and the radioactive polonium (Po)) with electropositive elements. CdTe, a highly crystalline material, is the most well-known example of this group and yields 16% in laboratory type small cells and 7% in commercial type modules [38] Chalcogenides have a sub-class of a tetragonal systems as chalcopyrites that mostly consist of copper iron disulfide, ($CuFeS_2$). The most common chalcopyrite used for solar cells are copper indium diselenide ($CuInSe_2$, CIS), copper gallium diselenide ($CuGaSe_2$, CGS), copper indium gallium arsenide (CuInGaAs (CIGS)) [27,44]

And also some of laboratories are producing new types of solar cells which can be named as kesterites for example: copper zinc tin sulfide ($Cu_2ZnSn(S,Se)_4$ (CZTS)), copper zinc tin selenide ($Cu_2ZnSnSe_4$ (CZTSe)) or ones using a mixture of sulphur and selenium like $Cu_2ZnSn(SSe)_4$ (CZTSS) or $Cu(InGa)(Se,S)_2$ (CIGSS) [24].

#### *1.2.2.3 Emerging Solar Cell Technologies*

Organic solar cells are produced by the development of low-cost, conductive, organic and polymer photovoltaic materials that can be easily produced and processed in large areas. Organic materials used in solar cells contain conductive polymers, dyes, pigments and liquid crystals [11,15,32,45-51].

Hybrid Organic- Inorganic Solar Cells, junction is formed from both organic and inorganic materials.

Perovskite Solar Cells: Perovskite is a crystal structure described with a chemical formula $ABX_3$, where “A” and “B” are two different cations with varied sizes and “X” is an anion which halogen or oxygen atom [52-56]. Perovskite films are suitable for thin, semi-transparent, light and flexible devices due to their adjustable bandgaps, high absorption coefficients, long charge carrier diffusion lengths. Naturally, electronic designers and researchers agree that these features will open up more space for solar cells. It has still challenges with efficiencies increasing to 22% [57].

Dye Sensitized Solar Cells: In the simplest sense, dye-sensitive solar cells are third-generation photovoltaic batteries that convert light into electrical energy with organic dye molecules. The photo-active dye of DSSC can produce electricity once it becomes light sensitive [58]. This dye captures photons from natural or artificial light, making the electrons stimulated by the energy coming from here. Then the electrons which stimulated by dye are sent to semiconductor Titanium Dioxide ($TiO_2$) film, which is a white synthetic pigment and applied to the cell [59] .DSSCs have achieved efficiencies of up to 12.3% and may benefit of Ability to operate in low radiation conditions, High temperature operation, High efficiency with low energy requirements, Environmentally friendly structure, Adaptability to continuous / on-site production conditions and They are structurally strong and lighter [60]. Chemists who synthesize advanced dye through organic synthesis studies, continue to increase the efficiency of solar cells every day.

Quantum Dot Solar Cells: Quantum dot solar cells, have basically the same structure as DSSCs, but with dye molecules replaced by use semiconducting inorganic nanocrystals, also known as quantum dots (QDs), to absorb light. Quantum dots, which are semiconductor metal compounds, can be obtained from the II-VI, III-V group. Due to their quantum confinement effects, they have a higher bandgap. In contrast to bulk materials, their bandgap can be tuned by just controlling the size of the crystal [61,62].That is make it possible to change the color of the glow, which is a unique feature for its use in engineering applications. They also produce lower production costs per watt because their production is cheaper than conventional materials [63]. Highest achieved efficiency is 5.4% with the Cd based quantum dot sensitized solar cells [44].

## 1.3 Dye Sensitized Solar Cells

### 1.3.1 Introduction: Dye Sensitized Solar Cells

When we look at the solar cell industry, we unfortunately see that silicon solar cells need to be produced from very pure material to prevent regeneration problem. Because of that issue, the costs are quite high and this type of solar cells can not find a wide range of applications. Therefore, there is an urgent need for cheaper materials and easy-to-produce photovoltaic systems and materials. One of the strongest candidates for such solar cells is the photo-electrochemical solar cells. [33, 53]

In 1991, Prof.Dr. Michael Grätzel and Brian O'Regan produced a photoelectrochemical battery system by sensitizing the nano-crystalline $TiO_2$ film with Ruthenium bipyridyl complex dyes and it achieved 7% efficiency [40] .Nowadays, this efficiency up until % 11 [64-66].

After the publication of Grätzel [67], such cells began to be called cheap solar cells. The most important parameters that make the system cheaper are that the materials used do not require much purity so that the cost of clean room technology used in the production of silicon based solar cells is eliminated [68,69].Additionally, with the use of natural dye extracts, devices provide natural, non-toxic developments with high absorbance level of UV, visible and NIR.

### 1.3.2 Components of Dye Sensitized Solar Cells

As the sandwich structure can be seen in the Figure 1.6, the DSSC device consists of [64] conductive glass sheet: transparent conducting (ITO or FTO), semiconducting electrode (anode): n-type $TiO_2$ and p-type NiO, dye-sensitizer: light harvesting and electronic transition, redox electrolyte solution: $I^-$ / $I_3^-$ or Co-II / Co-III complexes, counter electrode (cathode): carbon or Pt coated catalyst.

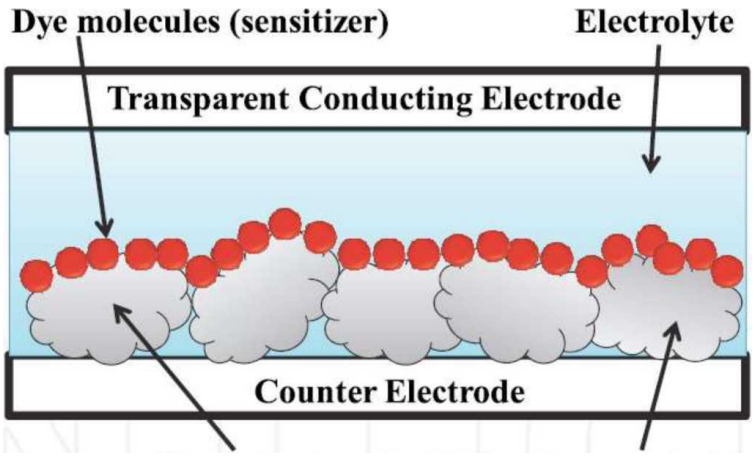


**Figure 1.6** Sandwich Structure of Dye Sensitized Solar Cell [64]

Transparent Substrate for Both the Conducting Electrode and Counter Electrode: The working electrode forms the negative end of the dye sensitized solar cells. This section contains the transparent conductive oxide thin film coated conductive glass (TCO) and semiconductor layer ($TiO_2$) coated with the of PVD (physical vapor deposition) technique. Indium doped tin oxide (ITO) or fluorine doped tin oxide (FTO) is used as TCO glass [70].

The main task of the conductive glass in the solar cell is to provide electrical conductivity and optical transparency. Optically, its transparent and low resistance for visible and near infrared lights enables TCO glass to be used in many opto-electronic applications. They are also resistant to high temperatures. $TiO_2$ is generally used as a semiconductor layer in dye sensitized solar cells. Although it is possible to use materials such as ZnO, $SnO_2$ and $Nb_2O_5$ as a semiconductor layer [71,72], $TiO_2$ is abundant in the market, relatively cheap, non-toxic, chemically and mechanically stable that makes preferable it [73]. $TiO_2$ has three basic functions in dye sensitive solar cells. First, to create a surface area for adsorption (holding) of the dye; the second is to accept the electron from the dye, and thirdly to transmit the incoming electron to the conductive glass surface.

Nanostructured Semiconducting Photoelectrode (Anode): As well known that, in the classical types of solar cells bulky semiconductor materials for example, Si, GaAs or CdS was preferred. In any case, when presented to light they have photocorrosion issue with poor stability problem. However, for DSSCs, because of their photocorrosion resistance, using of sensitized wide bandgap semiconductors, for example, $TiO_2$, or ZnO brought better stability of the device [50]. The material commonly used as a semiconductor matrix is titanium dioxide. The most important reason for this is that $TiO_2$ is a semiconductor which has a wide bandgap, cheap, comfortable and has no health hazards [74]. The main task of $TiO_2$ in the cell is to move the electron from the dye material to the conductive glass. The broadband range prevents the stimulation of $TiO_2$ and electron delivery under the visible light spectrum in which the dyes is active. On the basis of the binding of dyes molecules to the $TiO_2$ surface, $TiO_2$ is required to have a large surface area and to bind more dye. The $TiO_2$ anode is the heart of the solar cell with dye and it is the main study of this thesis. $TiO_2$ nanocomposite information will be given in Chapter 2 in detail.

Photosensitizer: Dye is an organic semiconductor component that is the electron source of the battery. When the wavelength of light reachs on the band gap, it passes to the electron conduction band in the valence band of the dye and leaves the dye to reach the $TiO_2$ surface. The stimulated dye is reduced again by redox reactions in the electrolyte and thus continues its operation. Among the first sensitizers, the polypeptide compounds of Ru (II) were used extensively. E.g. $Ru(dcb)(bpy)_2$, $Ru(dcbH_2)(bpy)_2(PF_6)_2$, $Os(dcbH_2)(bpy)_2$-$(PF_6)_2$. In recent years, natural dyes derived from plants such as Natural dye- shiso leaf pigments, black rice, rosella, natural anthocyanins, henna etc. used as an alternative to ruthenium complexes have been tested in solar cells [75]. Approximately 45% of the light reaching the earth from the

sun is visible (VIS), 47% is composed of infrared (IR) and 8% is composed of ultraviolet (UV) light spectrum [76]. Ruthenium-based dye is often preferred because it is well-stimulated by visible and especially near-infrared (NIR) spectra of sunlight [77].

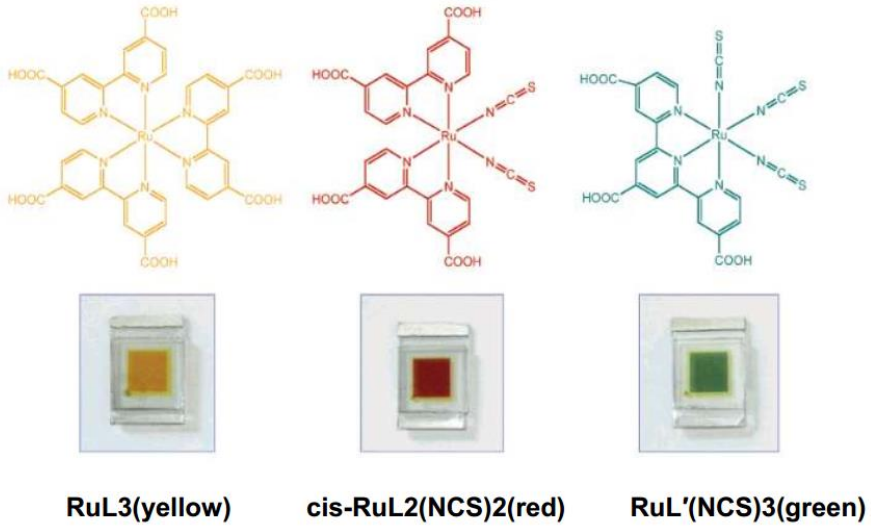


**Figure 1.7** Some Ruthenium Based Dyes [78]

As shown in the Figure 1.7 [78], generally, the structure of Ruthenium complexes are $ML_2(X)_2$. The N3 dye molecule consists of 2 bipridyl and 2 carboxylic acids and 2 isothiocyanides, the ruthenium metal in the center [74]. An ideal dye molecule must be stable enough to withstand approximately 20 years (under the sun).

Redox electrolyte: The electrolytes are prepared by dissolving $I_2$ in acetonitrile and KI, NaI, $R_4NI$ or LiI. The electrolyte is a conductive liquid containing different ions in which oxidation and reduction occurs [79]. The electrolyte, usually composed of acetonitrile solutions containing the tri-iodide / iodide redox pair, allows the dye to re-gain the lost electron and complete the electrical circuit [80]. Redox pairs are quickly reduced and oxidized for efficient and rapid transfer of electrons [81].

The reactions in the electrolyte are shown in the equations *(1.1)* and *(1.2)* [82].

$$I_3^- + 2e^- \rightarrow 3I^- \qquad (1.1)$$

$$3I^- \rightarrow I_3 + 2e^- \qquad (1.2)$$

Platin Coated Electrode (Cathode): In DSSCs, the counter electrode forms the positive end of the electrical circuit. In this part of the DSSC, there is a layer of platinum (Pt), graphite

or polymers that act as catalysts on the conductive glass [83,84]. The task of platinum is to catalyze the reaction on the electrode. Reduction of tri-iodide takes place in this part. The platinum reduces the excess voltage required for triiodide reduction, allowing the reaction to occur very quickly [85]. In addition, platinum has a high level of reflectivity. Because of these properties, platinum is frequently preferred in DSSCs [86].

### 1.3.3 Working Principle of Dye Sensitized Solar Cells

The most generic solar cell needs the absorbing dye (to create an electron-hole pair), an electron donor (to fill the hole absence in the HOMO (highest occupied molecular orbital)), and an electron acceptor (to take the extra electron from the LUMO (lowest unoccupied molecular orbital)). These main energy levels of the components that make up the dye sensitized solar cell can be seen in Figure 1.8, and are selected to be suitable for the desired direction of electron transfer and it is a key to the performance of a device [87,88].

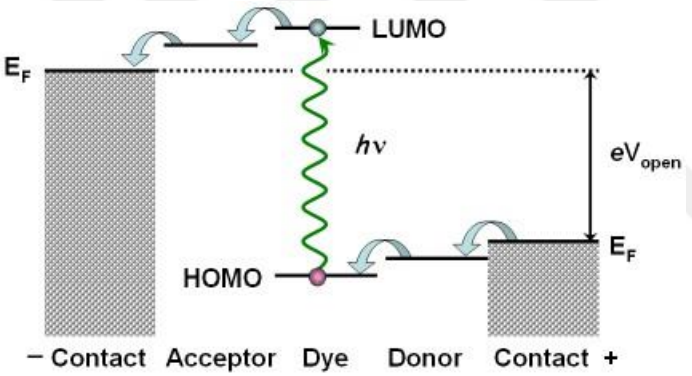


**Figure 1.8** Energy Levels in DSSCs [87]

The working mechanism starts by the absorbing light by dye molecules impregnated onto nanocrystalline $TiO_2$. Because the bandgap energy of the semiconductors used in solar cells (3.2 eV for $TiO_2$) is very high and covers the ultraviolet zone ($\lambda = 390$nm) of the light spectra, the visible light cannot be absorbed by the semiconductor. Therefore, the absorption of visible light occurs in dye molecules [89]. Ruthenium-based metal-organic dyes are generally stimulated by light with a near-infrared wavelength ($\lambda = 720$ nm, 1.72 eV) [90,91]. The working principle of dye sensitized solar cells is represented by equations and shown in the Figure 1.9 below [60,72,69,92].

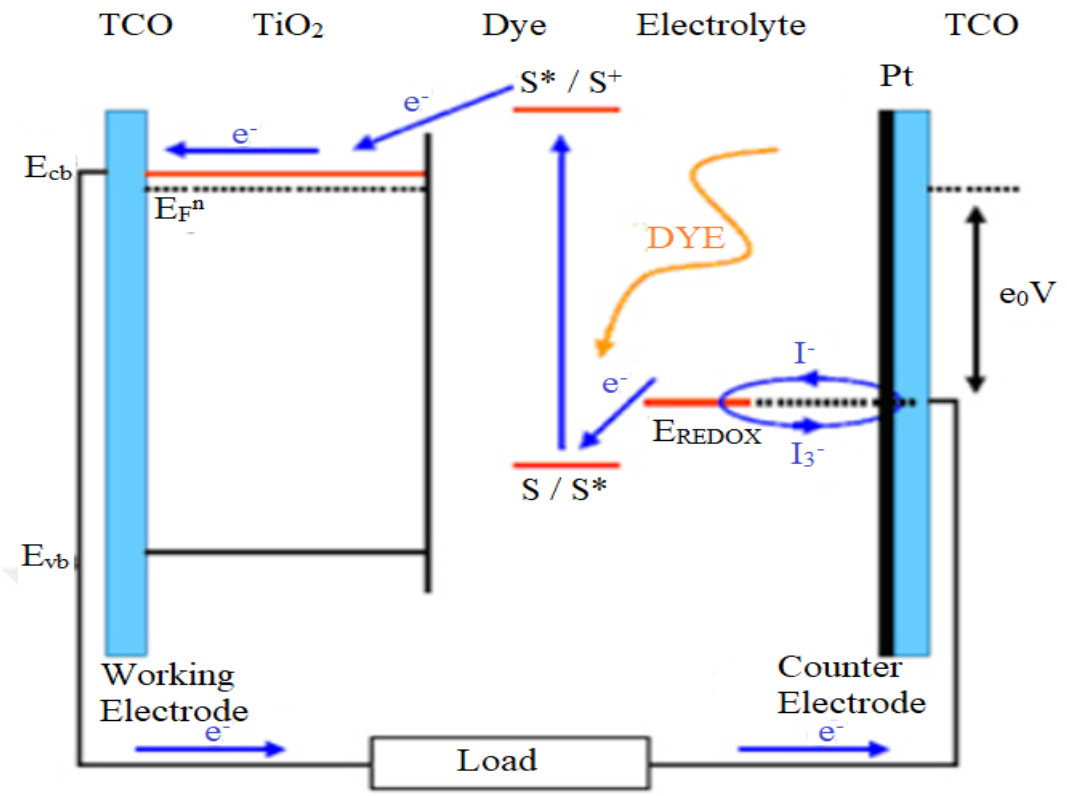


**Figure 1.9** Working Mechanism of DSSC [74]

The dye absorbs light and becomes excited.

$$S_{(ground)} + hv \rightarrow S^*_{(excited)} \text{ (excitation process)} \quad (1.3)$$

The excited dye molecule injects an electron into the conductivity band (CB) of the $TiO_2$. The injected electrons move through the nanocrystalline network in the $TiO_2$ film to reach the transparent electrode and from there to the external circuit.

$$S^*_{(excited)} \rightarrow S^+ + e^-_{(TiO2)} \text{ (injection process)} \quad (1.4)$$

And energy is generated;

$$S^+ + e^-_{(TiO2)} \rightarrow S_{(ground)} \text{ (energy generation)} \quad (1.5)$$

The electrons separated from the dye reach the counter electrode and complete the circuit by reducing the tri-iodide ($I_3^-$) ions in the solution with the help of the catalyst coating.

$$I_3^- + 2e^-_{(Pt)} \rightarrow 3I^- \text{ (recapture reaction)} \quad (1.6)$$

The dye molecules which are excited with a pozitive (+) charge are reduced to neutral state by the iodide ($I^-$) ions in the electrolyte.

$$S^+ + 3/2\ I^- \rightarrow S_{(ground)} + 1/2 I_3^-$$ (regeneration of dye) (1.7)

In electrolyte, ion transfers are carried out by diffusion of ions depending on the concentration gradient. When an electron is removed from the dye molecule and recovered at the counter electrode, the net charge is always zero and does not change chemically. (from semiconductor-electrolyte interface to counter electrode and from counter electrode-electrolyte interface to semiconductor). When an electron is removed from the dye molecule and recovered at the counter electrode, the net charge is always zero and there is no chemical change.

At the end of these electron transfer processes photo-current occurs. These redox reactions need to be repeated to obtain continuous flow in the dye sensitized solar cell [93,94].

### 1.3.4 Parameters of DSSC

The efficiency of the solar cell is determined by the voltage (V) current (I) curve. This graph shows the characteristics of the cell and the cell parameters that determine the efficiency in solar cells. These important electrical parameters are I-V curve, η, Voc, Isc, FF and IPCE [69].The current-voltage characteristic of the solar cell can be defined according to the Schottky equation [101].

First of all, fill factor (FF) is an important parameter affecting efficiency. As explained in Equation 1.8 and 1.9, Fill Factor is equal to the maximum power received (theoretically) to the maximum power [24].

$$\mathbf{FF} = {}^{\mathbf{Vmp}.\mathbf{Imp}}/_{\mathbf{Voc}.\mathbf{Isc}} \quad (1.8)$$

$$\mathbf{Pmp} = \mathbf{Vmp}.\mathbf{Imp} \quad (1.9)$$

The fill factor indicates the internal resistance of the cell. For dye sensitized solar cells, it is desired to have a fill factor of 0.60-0.70. The power of the solar cell is directly related to the power of the incoming light [69]. The standard case corresponds to AM 1.5, 1000 W/$m^2$ and is considered the standard of measurement. The ratio of the output power obtained from the circuit to the light intensity on the cell gives the efficiency. In order to be able to calculate

the efficiency, it is necessary to know the open circuit voltage, the short circuit current, the filling factor and the light intensity per $cm^2$ of the cell (Equation 1.10) [102-104].

$$\eta = {Voc. Isc. FF}/{Pin} \quad (1.10)$$

Short circuit current Isc is the maximum value that current can take when zero voltage passes through the circuit. The short-circuit current depends on the optical properties of the cell, the photon capture capability and the spectrum of the incident light. The open circuit voltage Voc is the voltage at which the net current on the circuit is zero. The most important factor affecting the open circuit voltage is the reduction and oxidation reactions [105].

IPCE measurements are another important parameter in determining cell performance. The main purpose of this measurement is to determine which wavelength of light falling on the cell becomes more efficient. IPCE is calculated in Equation 1.11 as follows [106].

$$IPCE\ (\lambda) = {Isc}/{\lambda Pin} \quad (1.11)$$

# CHAPTER 2

## PLASMONIC $TiO_2$ COMPOSITE FOR ENHANCING LIGHT ABSORBTION IN DSSC

In dye sensitized solar cells, an alternative functional photoanode material needs to be developed to prevent charge recombination at the $TiO_2$ / dye / electrolyte interface. As described in the Nanostructured Semiconducting Photoelectrode part in Chapter 1, semiconductor materials are generally preferred and works are underway to improve them. This section focus on $TiO_2$, which is one of the materials used as photoanodes, and give information about plasmonic nanocomposites with their use of DSSCs.

### 2.1 General Principles of Semiconductor Materials

The number of electrons contributing to electrical conductivity in a material depends on the electron states, or corresponding energy values, as well as the behavior of electrons[107] [108]. The electrons in an atom have an isolated electron array and specific energy levels independently of each other and tend to fill the lowest energy state [24,109]. The electrical properties of the materials basically depend on these electronic band structures. There are four different band structures in 0 K [24]. The top energy level, which is filled with electrons at 0 K, is called the Fermi energy level [110].

Such semiconductors are called n-type semiconductors and their fermi level is near the edge of the conductivity band. Differently, if the Fermi level is close to the valence band they called p-type semiconductors are. The majority of these two types of semiconductors are different from their charge carriers. In the n-type semiconductor, the majority charge carriers are electrons while the p-type spaces are holes as seen in Figure 2.1 [108, 113].

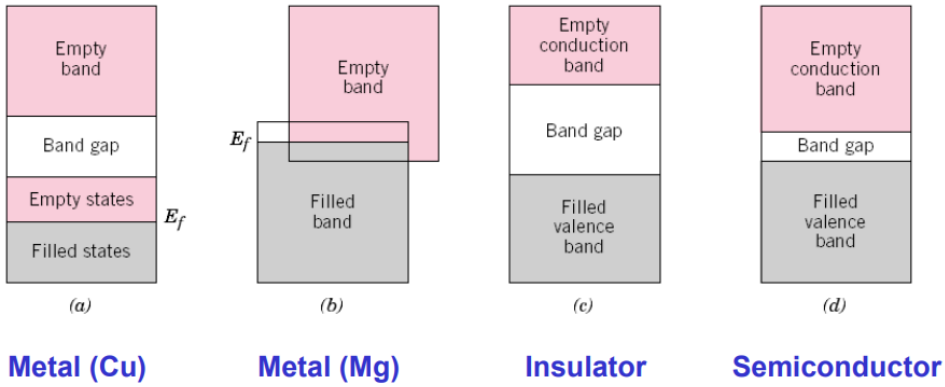


**Figure 2.1** Classification of Solids According to Their Electronic Structure [112]

When we look at the mechanism of n-type semiconductor, it is seen that the number of valence electrons of additive atom is more than the number of electrons added. In this case, the additive atom is released from the bonding of an electron and forms an additional level just below the conductivity band. When the band structure of $TiO_2$ is examined, it is seen that $TiO_2$ is also a semiconductor with n- type [112,114].

The semiconductors were used as working electrodes in many different areas, especially in the DSSC application, in early studies of them. Figure 2.2 shows the band positions of different semiconductors [115].

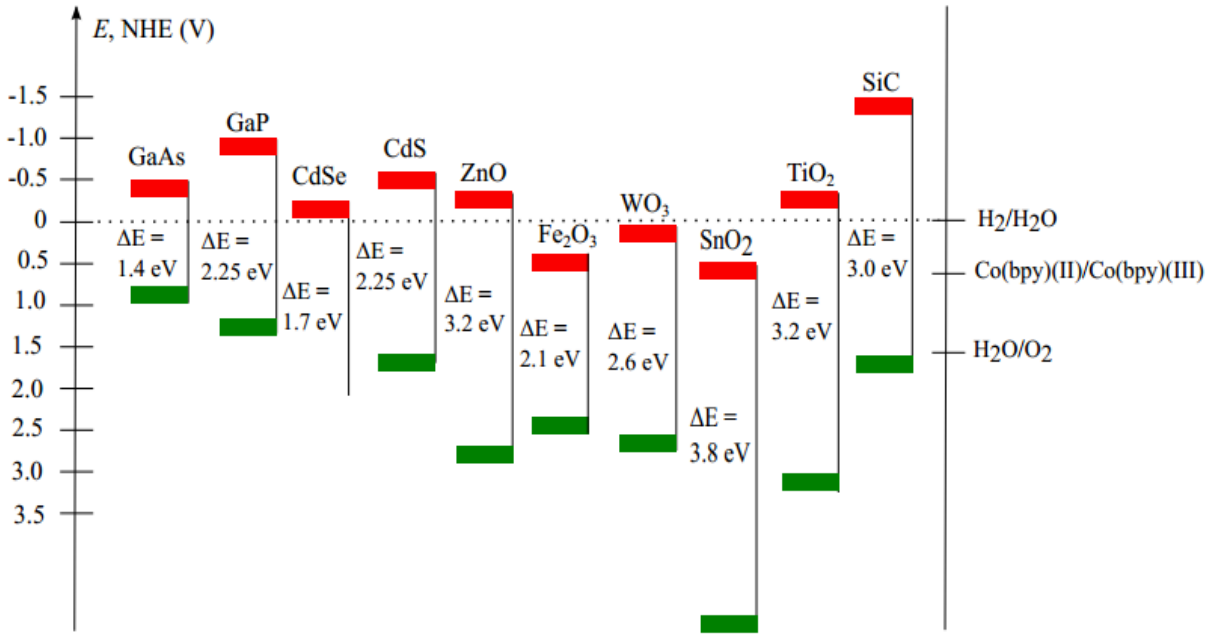


**Figure 2.2** The band positions of some semiconductors. CB: red color, VB: green color [115].

Oxide semiconductors, as a subtitle of semiconductors, exhibit considerable resistance to photocorrosion in the case of band gap stimulation and are therefore widely preferred in photoelectrochemical systems [116]. In dye sensitized solar cells, it is necessary to use a wide-band (Eg> 3) oxide semiconductors to provide transparency in the visible region. Although some semiconductors used in organic dye based nanocrystalline solar cells such as ZnO, $SnO_2$, CdS, CdSe, $WO_3$, $Fe_2O_3$, $Nb_2O_5$, $Ta_2O_5$ [106,117,118], $TiO_2$ remains the most popular semiconductor that used in this field.

## 2.2 Mesoporous $TiO_2$ Nano-particles

Titanium dioxide ($TiO_2$) is formed by the reaction of the Oxygen atom in the column VI with a titanium atom, which is a transition metal and contained in the IV-B group in the periodic table [119]. Another name of $TiO_2$ in the literature is Titania. The basic bond strength is covalent bond. Although it is known as a rare element, it is one of the most common elements in earth. This prevalence is one of the most important factor when broad production areas are considered.

$TiO_2$ is highly preferred as a colorant because of its high refractive index. Thanks to its physical and chemical properties, titanium dioxide is used in many industrial applications and scientific research such as dye, plastic, paper, ink, rubber, synthetic fibers, food, electronics, pharmaceuticals and cosmetics, and is one of the most important advanced technology ceramic materials [120,121] The use of titanium dioxide is highly resistant to chemicals, it has no toxic properties, its cost is low; so that with this features its usage are is increasing.

Additionally, $TiO_2$ is used as heterogeneous catalyst, hydrogen and electric energy producing solar cells, photocatalysis, gas sensor, corrosion protection coatings, optical coatings of ceramics and electrical devices. At the same time, it plays an important role in biological bone transplantation because of its biological compatibility [122]. $TiO_2$ is also used in water separation, anti-bacterial coatings and self-cleaning surfaces because of its photocatalytic properties when exposed to UV light [123].

### 2.2.1 Crystal Structure of $TiO_2$

The most used scientific and technological aspects of $TiO_2$; has mainly three different crystal structures named anatase, rutile and brookite [124]. In these three types of structures, one titanium is made up of two oxygen elements, but only the crystal structures are different

[93,125].While the rutile and anatase phases are tetragonal, the brookite is orthorhombic [126,127]. The anatase and rutile structure contain 12 and 6 atoms per unit cell, respectively. The distances between the two structures are different between neighboring atoms. While the distance between Ti-Ti is shorter than the rutile structure in the anatase structure, the distance between Ti-O is longer than the rutile structure [128].

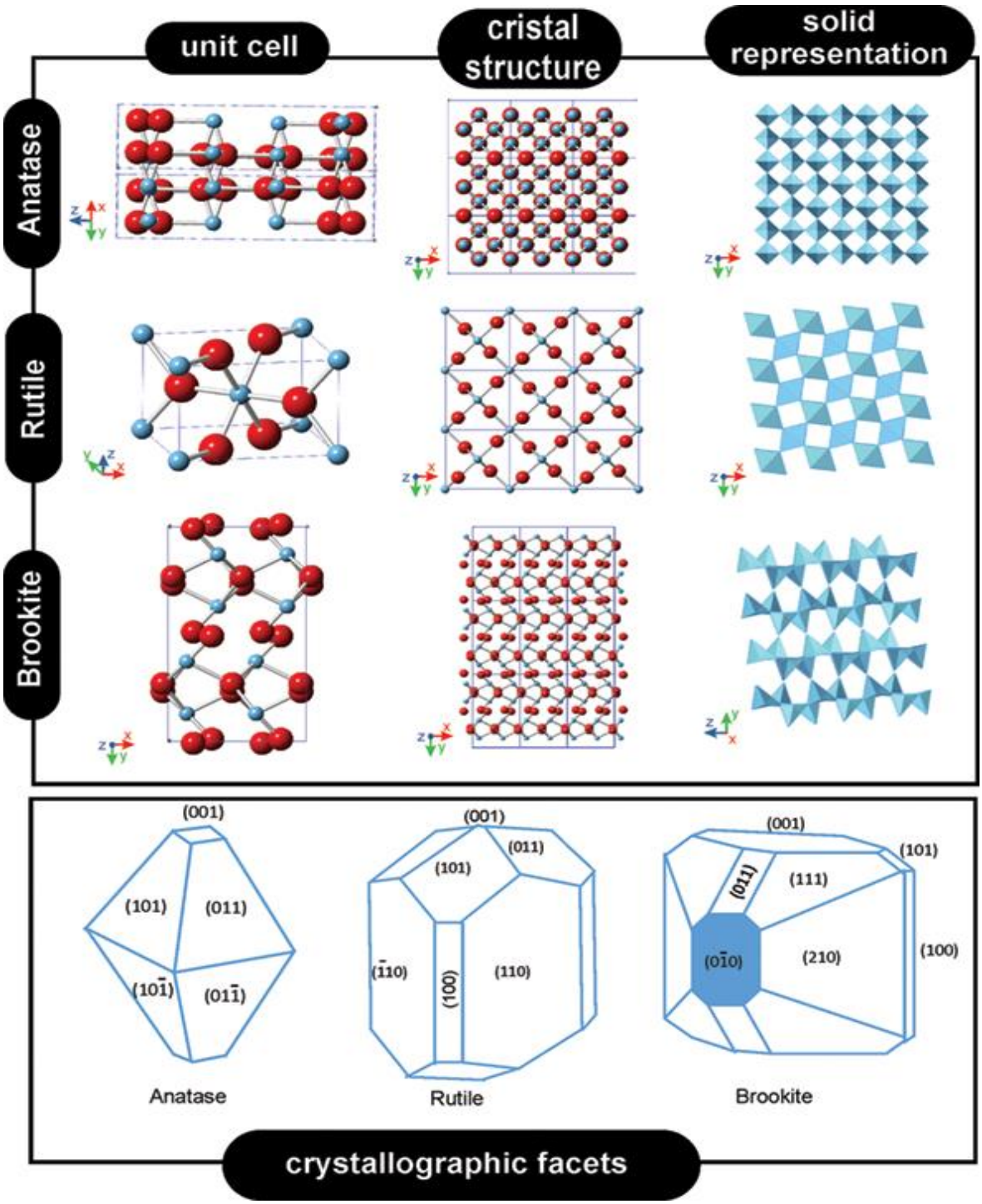


**Figure 2.3** Crystal Sturctures of $TiO_2$ [129].

As seen in both anatase and rutile crystal form, the basic building block $TiO_6$ contains a central $Ti_4^+$ ion surrounded by 6 $O_2$ atoms in slightly bent octahedral chains (Figure 2.3) [127]. In the anatase structure, octahedrons have been significantly distorted compared to those in the rutile structure [126]. And these differences cause different densities between anatase and brookite and change the electronic band structures [130].

### 2.2.2 Photocatalytic Properties of $TiO_2$

Photocatalysis can be defined as the acceleration of photoreaction in the presence of a catalyst. Photocatalytic reactions are carried out by absorbing the energy of photons from a light source. Titanium dioxide, which is widely used in many applications due to its electrical and optical properties, is a preffered material with photocatalytic properties [131]. When the particles of titanium dioxide interact with the UV and absorb a photon, they are oxidized from the valence band to an electron conduction band and thus create a gap in the valence band [132]. The excited semiconductors are unstable, but $TiO_2$ remains stable even in the excited state [133]. This is one of the reasons that makes $TiO_2$ a perfect photocatalyst [134]. In photocatalytic reactions, the bandgap energy determines the wavelength of light which is effective for stimulating the material, while the maximum point of the valence band determines the oxidation power of the photocatalyst [135].Figure 2.4, gives information about the photocatalytic applications of $TiO_2$ [134].

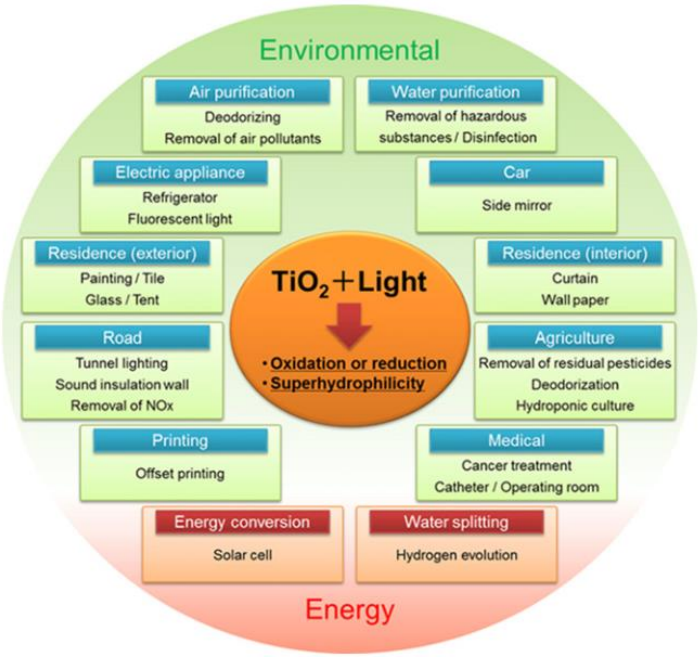


**Figure 2.4** Properties of $TiO_2$ [134]

Band gap energies of rutile, anatase and brookite crystal forms using UV-Vis spectrometer were determined as 3.02, 3.20 and 3.11 eV, respectively [116,125]. For anatase and rutile, these values correspond to the wavelength of 388 nm and 413 nm, respectively, for the ultraviolet light used [136]. This difference is thought to be a negative shift in the anatase structure of the transmission band [125].

The crystal structure of titanium dioxide nano-particles is mainly depending on the method of preparation. Anatase form is pyramidal and stable at low temperatures. The crystals of the rutile form are needle-shaped and occur at temperatures higher than 973 K [137,138].

While the density of the compound in the anatase structure is 3.89 g/cm$^3$, the density of the rutile compound is 4.26 g/cm$^3$. Because of the distance between the titanium ions in rutile structure is more than the distance between the titanium ions in the anatase structure, the rutile structure has a thermodynamically more stable structure than the anatase [93,139].

Rutile and anatase phases are generally used as photocatalyst. However, $TiO_2$ in the anatase phase showed a superior photocatalytic effect [140]. Due to the degradations in the crystal structure, the conductivity band electrons in the rutile $TiO_2$ have less reduction power than the anatase $TiO_2$ and therefore the amount of rutile phase adsorbed on the surface is also low [141,142]. "The activity of the rutile phase is therefore low since photocatalytic activity is directly related to crystalline regularity. In addition, the $TiO_2$ Rutile structure surface area is 25% less than the Anatase structure surface area. And Rutile absorbs less than 35% less dye. So that even if the open circuit potentials in rutile form are similar, circuit currents are reduced by 30% compared to anatase form [143-145]". As a result, this is one of the factors that make the photocatalytic activity of the anatase phase higher than the rutile phase [139].

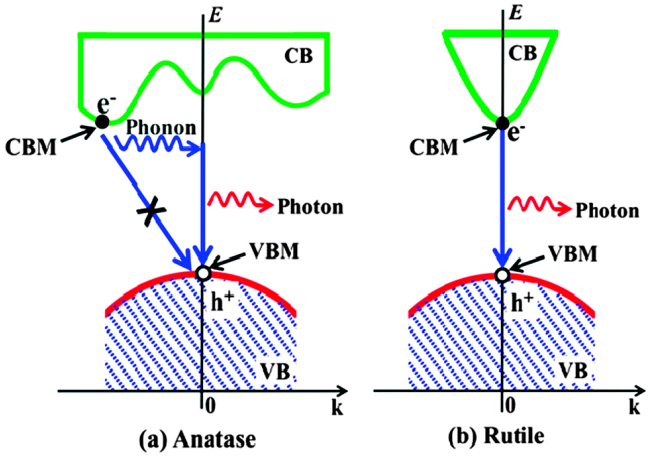


**Figure 2.5** Comparison of Recombination Processes within Anatase and Rutile Phases [146].

The recombination times of electron-hole pairs which have a significant effect on photocatalytic reactions are very short as shown in Figure 2.5. However, this period is longer in $TiO_2$ photocatalyst [121,147,148] However, in the rutile phase, the short recombination time for electrons and cavities affects the photocatalytic activity negatively. This phenomenon is due to the fact that the rutile phase has a direct bandgap and the anatase phase has an indirect bandgap [146,149].

The studies carried out in recent years reveal that photon-sensitive dye molecules with increasing surface area are better adsorbed and high efficiency is obtained, especially with the use of nano-sized titanium dioxide particles [150-153].

### 2.2.3 Synthetic Methods for $TiO_2$

Many different methods are used for the synthesis of $TiO_2$. These methods can be listed as follows[137,154-156]: sol-gel methods, micelle and ınverse micelle methods, sol method, hydrothermal method, solvothermal method, direct oxidation methods, chemical vapor deposition method, physical vapor deposition method, electrodeposition, sonochemical method, microwave assisted method, anodization, spray pyrolysis,templating.

Sol-Gel Method: In a typical sol-gel technique, the colloidal suspension or sol is obtained from the hydrolysis or polymerization reaction of the starting material. These starting materials are generally inorganic metal salts or organic metal compounds [157].

The $TiO_2$ nanomaterials can be obtained by the sol-gel technique by hydrolysis of a Titanium as a precursor. This process proceeds in the form of the acid-catalyzed Titanium(IV) alkoxide followed by the hydrolysis steps followed by the condensation reaction. The metal alkoxide is then subjected to hydrolysis to form the colloidal sol, then subjected to condensation reaction to form the gel.

Basically, the sol-gel technique consists of hydrolysis and polycondensation reactions to form metal oxide gel, as indicated below. M; Si, Ti, Zr, Al, R, are alkyl groups.

The relative speed of hydrolysis and condensation reacts to the structure and properties of metal oxide. Factors affecting the sol-gel process are based on the reactivity of the metal alkoxide, the pH of the reaction medium, the water / alkoxide ratio and the reaction temperature [158]. There are various case study about $TiO_2$ synthesis by solgel method. For example, Al doped $TiO_2$ with $TiCl_4$ precursor [159], Cr doped $TiO_2$ with Ti -isopropoxide

precursor [160], metal doped $TiO_2$ [161], and $TiO_2$ nano-particle synthesis[162,163]. Additionally, 14 nm of $TiO_2$ nano-particles were prepared using a sol-gel process of isopropoxide [164]. In the review of Lai *et al* 2018, they mostly focused on Sol- Gel method and found Anathase (50 nm), Rutile (20 nm) $TiO_2$ nano-particles. Oghaz et al performed a study by the Sol- Gel method (La-Nb codoped $TiO_2$ Pechini method) and found undoped $TiO_2$ (30- 40 nm) and Doped $TiO_2$ (20 nm). It is possible to find other works in the literature [154,157,165,166], due to the this production method is mostly preffered.

Sol Method: The sol method is a kind of nonhydrolytic sol-gel process which generally involves the reaction of the titanium halide with a variety of different oxygen donor molecules. As an example, Chang et al prepared Zr-doped anatase $TiO_2$ nanorods in anhydrous TOPO under dry inert gas protection, with the reactions being completed within 5 minutes [167]. There are many works done with nonhydrolic solution-based preparations of $TiO_2$ was also prepared [168-172].

Hydrothermal Method: In the hydrothermal method, the reaction is carried out in an aqueous solution in controlled temperature or pressure in a Teflon coated stainless steel autoclave [157,173]. Hydrothermal method has been widely used to prepare $TiO_2$ nanotube. Kasuga et al. in 1998 talked about this method and many examples can be given [174,175]. For example, Wang et al. prepared Fe(III)-doped $TiO_2$ nano-particles with a hydrothermal method and found that anatase, brookite, and a trace of hematite coexisted [154, 156,166,176]. Similarly, Xie et al used One step hydrothermal method, ($SnO_2$/$TiO_2$ composite) with Titanium tertrabutoxide precursor and obtained 5nm of particles [177]. One year before, self-assembly of cellulose nanocrystal (CNC) to prepare anatase $TiO_2$ nanocatalyst by controlling the hydrolysis of the sol-gel precursor and the followed hydrothermal treatment [178].

Solvothermal Method: Solvothermal method is very similar to the hydrothermal method, but the reaction is not carried out in aqueous media, organic solvents are used. However, the reaction is carried out at higher temperatures than the hydrothermal method. The size and shape distribution of the $TiO_2$ nano-particles in the solvothermal method can be better controlled [157]. Ramaknishnan et al modified solvothermal method with TTIP and Ethanol, and they obtained the average particle size of $TiO_2$ as 5 nm [179]. Many Works also done and still challenged about solvothermal synthesis [180,181].

Additionally there are many other methods such as Spray Pyrolysis [184], Anodization [155], Direct oxidation [185], Chemical Vapor Deposition (CVD) [186-188], Micelle & Reverse Micelle Method [60,116,182,183] and Templating [155,189] are widely used to produce Titania with nano structure.

## 2.3 Plasmon Enhanced Nano-particles

The surface plasmons are collective oscillations of conductive electrons in the noble metal film or nano-particle surfaces that are induced by light or electron at the interface of two different media with dielectric constants (i.e., metal and dielectric) [190-194]. Surface plasmons act as a particle and have the ability to control and change the direction of visible light in nanometer range [195,196]. The interface properties, the angle of incidence and the wavelength of the light are very important for the stimulation of plasmons [197-199].

When plasmonic nanostructures interact with light, they have the ability of absorbing (and thus also plasmon formation) as well as scattering light. The light-scattering characteristic of the nano-particle depends on the shape, size and the structure of the nano-particle. Plasmonic nano-particles are used in solar cells due to their high intensity of light, absorption capability in wide spectrum [200], adjustable color and intensity of scattering, and lack of photo cleavage [201] when exposed to high energy rays [202].

### 2.3.1 LSPR & Sensing Principle with Nano-particle Plasmon

Surface Plasmons can be classified under basic titles as surface plasmon polaritons and localized surface plasmon [203]. Localized surface plasmons are electrically oscillating electrons in nano-sized metallic structures on a focused dielectric material (such as nano-particles, gaps) [204]. Light in nano-sized metallic structures on a dielectric surface causes polarization on the surface and when they are stimulated, and they form plasmas localized on metal structures. One of the most important features of these structures is that they exhibit more intense resonance behavior due to the more localized electric field [205].

The electromagnetic wave with load density reaches its maximum value at the interface. And as it moves away from the interface, it is exponentially absorbed into the environments [206]. As shown in the Figure 2.6, the light from the surface causes an oscillation of electrons [207]. This leads to the formation of positive and negative regions on the surface and the formation of a zone in which the electric field changes periodically. The orange arrows indicate the

change in the electric field intensity relative to the distance. Plasmons cause the electric field to be strengthened on the surface[208,209].

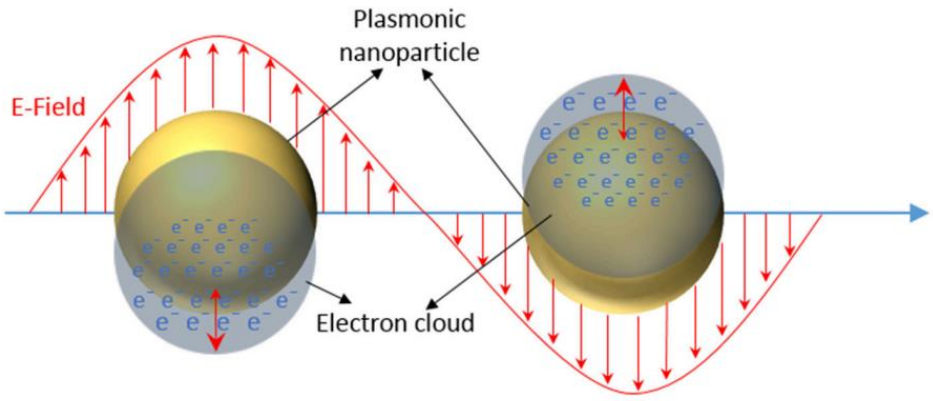


**Figure 2.6** Schematic Drawing of Surface Plasmons [207]

The resonance angle depends on the changes in the refractive index of the dielectric medium to be attached to the metal surface and the dielectric permeability of the media. Changes in the surface can be determined by the shifts in the resonance angle [210]. For the observation of the plasmon resonance, a prism is placed on the surface and the reflected power is measured against the angle of incidence of light. At a certain angle for a given wavelength, the plasmon is stimulated and the plasmons spread across the surface to reduce the intensity of the reflected light. When the wavelength of the incoming light matches the natural vibration frequency of the electrons, the intensity of the reflected light decreases. In order for plasmonic resonance to occur, the wave vector component which parallel to the dielectric surface of the incoming light must be equal to the plasmon wave vector component [211].

### 2.3.2 Plasmonic Response of Metal Nano-particles

The LSPR wavelength of an excited plasma is influenced by the nano-particle size and shape which allows the combined scattering and absorbance properties of the nano-particle to be adapted to the desired wavelengths [212,213]. Plasmonic effects can occur in many different materials with sufficient charge carrier density. In noble metals, plasmonic effects are very clear due to the high conductive band electron density in the material. The more electrons or charge carriers in the oscillation, the greater the electrostatic restoration force and therefore teh high resonance frequency.

For different metals, the wavelength of the resonating photons is different. In other words, ultraviolet (UV) and visible region (VIS) photons exhibit resonance behavior when they

interact with metal nanostructures. Such noble metals are of great interest since most of the sunlight are composed of UV-vis photons and have free conduction electrons. In the Table 2.1, it can be seen various metals and the frequency range. For the solar energy applicaitons, optical frequencies (400-700 nm) are mostly preffered [210].

**Table 2.1** LSPR Frequencies of various metals [210]

| **Various Metals with free electrons** | **LSPR frequencies** |
|---|---|
| Pb, In, Hg, Sn, Cd | UV |
| Cu, Ag, Au | VIS |

Silver and gold have been used extensively on plasmonic effects due to their high-quality plasmonic resonance. The superior optical properties of silver, for example, the greater dependence of the dielectric function on energy means less absorption losses [214]. As another metal, gold is more chemically and physically stable and resistant to oxidation, so it is often used [215]. Other materials may also exhibit plasmonic resonances such as aluminum and high doped semiconductors, metal oxides [216], but noble metals are commonly used for visible and NIR resonances.86 However, LSPR wavelength depend on the size, shape and crystal structure of the nanocrystalline and the surrounding environment [207,217,218].

Plasmonic nanostructures with unique properties such as strengthening the electromagnetic field, scattering the electromagnetic radiation or converting photon energy to heat have preffered in many applications. These applications for plasmonic metals; Surface Enhanced Raman Spectroscopy (SERS) [219], molecular detection in biological systems [220], single molecule spectroscopy [221-224] and solar cells[225,226].

In many applicaitons, plasmonic nano-particles are used to increase light absorption in PV devices [210] organic solar cells [227], perovskite solar cells [228-230] and DSSCs [231] have been shown to improve the performance of gold or silver nano-particles added to the electrode. Especially in DSSCs, these metal plasmons are used to improve the light absorption of the dye molecules and are integrated into the photoanode to increase the optical absorption or charge transfer of the sensitizer [232-235].This integrated system acts as an antenna for sunlight catching in the DSSC due to the strong local area development of metal nano-particles. The electromagnetic field on the metal surface can propagate 10-100 μm depending on the type of metal, film thickness and surface roughness, and forms an

electromagnetic field in the 200-300 nm range [236-238]. The Non-propagating surface plasmons are formed around an Au nano-particles and Ag nano-particles in an electromagnetic field of the several nm, unlike the thin film [237,239]. In this way, dense electric fields are formed which are localized on the surface of the plasmonic metal particle. When noble metal nano-particles are incorporated into a semiconductor material such as $TiO_2$ [240-242], The semiconductor band gap energy and the light illumination source overlap the wavelengths of the surface plasmon resonance; and thus it is possible to use the visible light spectrum of solar radiation [243]. Photons that are not initially absorbed by the dye may be dispersed by metal nano-particles during irradiation. Thus, the photons can pass through the photoactive layer and be absorbed by the dye. As the most important advantage of the system is to increase the efficiency of a cell by increasing the photon absorption. As aimed in this thesis, it is preferable to integrate metallic nanostructures into the cell layer and utilize their resonance with incoming light to increase light absorption in DSSCs [244].

# CHAPTER 3

## EXPERIMENTAL

### 3.1 Nano-particle Synthesis

Plasmonic $TiO_2$ photoanodes were synthesized by multi-stage methods using solvothermal and silanization procedures, respectively. Figure 3.1 represents the schematic pathway for the synthesis of plasmonic $TiO_2$ photoanodes.

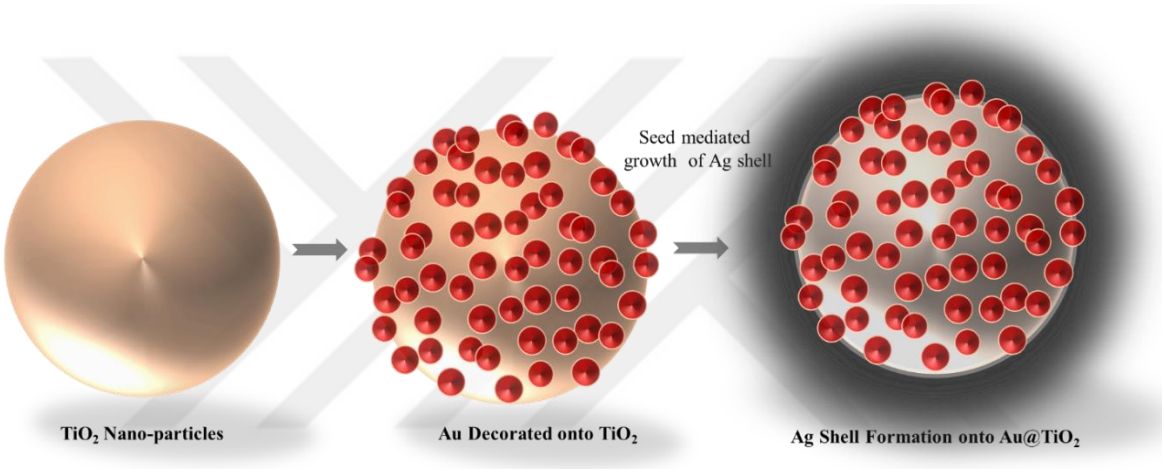


**Figure 3.1** Representation of the experimental procedure

#### 3.1.1 Synthesis of Mesoporous $TiO_2$ Nano-particles

The synthesis of bare $TiO_2$ nano-particles was carried out according to the previous reported procedure by Ahmed et al [245]. Typically, 330 µl of TTIP (Titanium(IV) isopropoxide, $Ti[OCH(CH_3)_2]$, Sigma Aldrich) was mixed with 10 mL of anhydrous Acetone (Sigma Aldrich). The as-prepared solution was stirred at room temperature for 10 min and then transferred into a Teflon-lined stainless-steel reactor under heating at 180°C for 12 hr. Then, the reaction medium was cooled to ambient temperature and $TiO_2$ nanoparticles precipitated by centrifugation and washed with acetone (2 times) and deionized water, respectively.

### 3.1.2 APTES attchment onto $TiO_2$ nanoparticles

For the silanization and attachment of the primary amine groups (-$NH_2$) onto bare $TiO_2$ nanoparticles, isopropanol (15 mL), APTES (2 mL), and TEA (0.3 mL) were added onto the particles and sonicated at room temperature for 10 min. The mixture was transferred into a T-shape glass reactor and heated in a water-bath at 80°C for 24 hr. The primary amine attached $TiO_2$ nanoparticles (-$NH_2$-$TiO_2$, APTES-$TiO_2$) were washed with isopropanol and ethanol and dispersed in water for further usage [246].

#### *3.1.2.1 Synthesis of Au@$TiO_2$ Particles*

The presence of primary amine groups (-$NH_2$-$TiO_2$) enables $TiO_2$ to adsorb Au nanoparticles on its surface (Figure 3.2).

Au nanoparticles were prepared by Turkevich method using sodium citrate reduction of the chloroauric acid solution. Typically, 123 mg of TSC (Trisodium citrate dihydrate, $HOC(COONa)(CH_2COONa)_2 \cdot 2H_2O$) was prepared in 8 mL of deionized water as stock solution. Then, 69. 2 mg of $HAuCl_4$ (Gold(III) chloride hydrate, Sigma Aldrich) and 89.1 mL of deionized water were heated to boiling and prepared citrate solution was added. After 15 min of boiling, the solution was cooled to room temperature. The as-prepared APTES1@$TiO_2$ nanoparticles solution was added and stirred for 24 hours at room temperature. The resulting particles were finally precipitated by centrifugation and washed with deionized water (2×). This solution named as Au@$TiO_2$ and re-dispersed in DDI water for further usage.

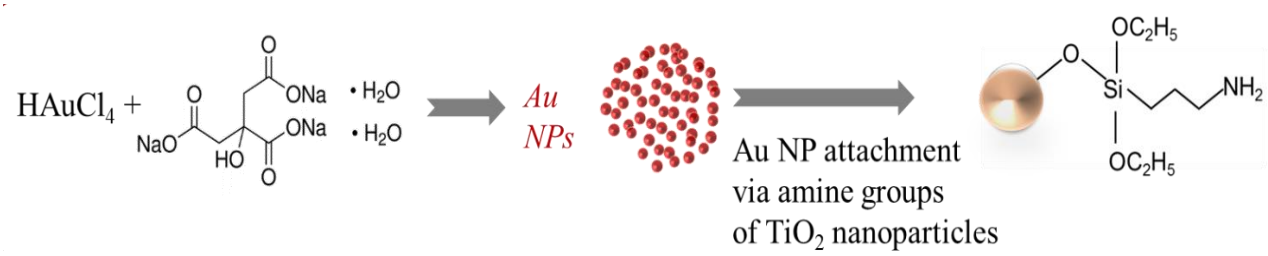


**Figure 3.2** Au Attachment Procedure of $TiO_2$ Nano-particles

#### *3.1.2.2 Synthesis of Ag@Au@$TiO_2$ Nanoparticles*

A seed-mediated growth process was employed to synthesize the Ag shell around the Au@$TiO_2$ nanoparticles. Typically, 1065 mg of $AgNO_3$ (Silver nitrate, Sigma Aldrich), 311

mL DDI water, and 887.5 mg of TSC (Trisodium citrate dihydrate, $HOC(COONa)(CH_2COONa)_2 \cdot 2H_2O$) were mixed and the as-prepared $Au@TiO_2$ solution into the reaction mixture under vigorous stirring. The pH of solution was adjusted to pH:10 using $NH_3$ (Ammonia, 1 M). When solution reach the desired pH level, 1775 µl of HCHO (Formaldehyde solution 10%) was added dropwise. The reaction was stirred for 2 hours at room temperature. The resulting particles were finally precipitated by centrifugation using DDI water and dried at 60°C for further usage.

## 3.2 Device Fabrication

Our DSSC device structure is shown in Figure 3. The sandwich- type structure consists of a $I^-/ I_3^-$ electrolyte solution, $TiCl_4$ blocking layer, plasmonic$TiO_2$ photoelectrode, N719 dye sensitizer, and a Pt coated FTO glass are schematically illustrated.

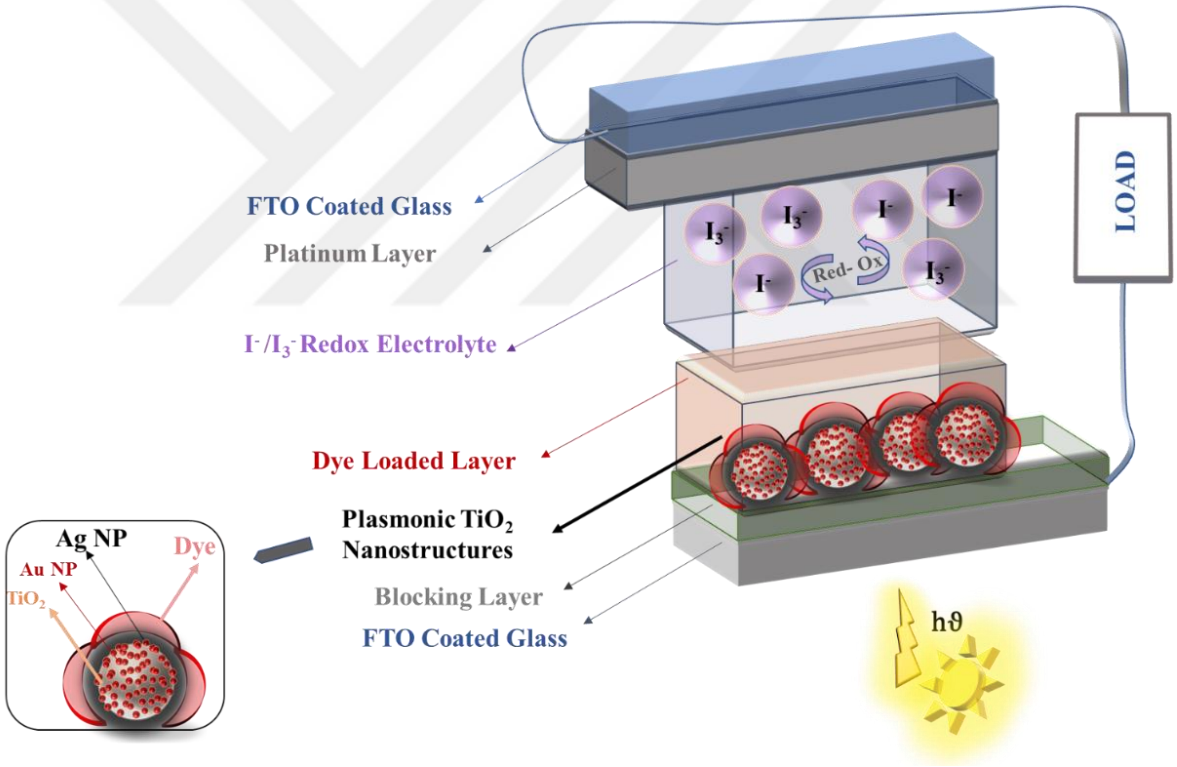


**Figure 3.3** Schematic Representation of the Planned DSSC Structure.

### 3.2.1 Device Fabrication Process

#### *3.2.1.1 FTO Coated Glass Cleaning*

To produce the dye sensitized solar cells, FTO (Fluorine-doped Tin Oxide, Sigma Aldrich) coated substrate was used as a glass plate. The FTO glass was cut into 9 pieces with the help of a glass cutter. The dimensions of each sample are 2.5 cm × 1.5 cm (2.2 mm).

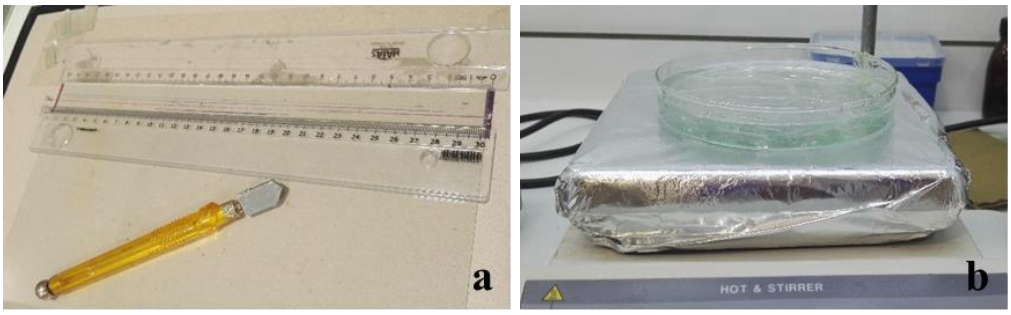


**Figure 3.4 a)** FTO Cutting and **b)** Cleaning Processes

FTO coated glasses were firstly washed with detergent and then rinsed with DDI water in order to eliminate any contaminants. Subsequently, surface cleaning process was started to increase the conductivity on the surface (Figure 3.4). Samples were sonicated for 5 minutes in DDI water (at 70°C) with the addition of 1% Hellmanex III (Sigma Aldrich). After the FTO glasses were dried using filtered compressed gas, the process continued with ultrasonic cleaner bath in isopropyl alcohol bath for 5 minutes. Then, samples were dump-rinsed twice in boiling deionized water and cleaned samples was dried using filtered compressed gas.

To determine the conductive side of glassed, resistance value was controlled using multimeter probes. Finally, samples were placed into the UV Light cabin (254 nm Hg, OSRAM PURITEC HNS UV-C lamps) and irradiated for 10 minutes.

### *3.2.1.2 Preparation of Photoanode Paste*

Preparation of $TiCl_4$ Solution: A stock solution that consist of 2 mL of $TiCl_4$ (Titanium(IV) Chloride, Sigma Aldrich) and 98 mL of deionized water was prepared at 0˚C. 40 mM of the $TiCl_4$ solution was blended and sonicated. Cleaned glass samples was dripped into the prepared solution at 70- 80˚C for 30 minutes. After, samples were annealed at 450˚C for 30 minutes. Then, samples were dump-rinsed twice in boiling deionized water and once in ethanol. Finally, cleaned samples was dried using filtered compressed gas.

Preparation of TTIP Solution: 5.116 g of TTIP (Titanium(IV) isopropoxide, $Ti[OCH(CH_3)_2]_4$), 1.821 g of TEA (Triethylamine, $(C_2H_5)_3N$) and 1.081 g of HAc (Acetic acid, $CH_3CO_2H$) was mixed with 10 mL of ethanol in separate flasks and stirred at room temperature for 15 minutes at 400 rpm. After stirring, solutions were mixed in a single flask and resulting solution was stirred using magnetic stirrer bar at 50˚C for 2 hours at a same rotation speed. The final mixture was aged at room temperature overnight to produce the gel structure. After aging, the mixture was ready to be coated on conductive glass samples. $TiO_2$

layers with varying thickness were coated on cleaned FTO substrates. 50 µL of TTIP sol taken with the aid of adjustable tip ejector and deposited onto glass substrates using a spin coater (2000 rpm, 0 rpm/s, 30 s) and annealed at 450˚C for 30 minutes (Figure 3.5).

Preparation of P25 Paste: 4.24 g of P25 $TiO_2$ powder (Evonik, Degussa, 21 nm), 9.28g of two different EC ( with 56.25 wt % Ethyl Cellulose, Sigma Aldrich and  with 43.75 wt % Ethyl Cellulose, Sigma Aldrich) powders with different viscosities were dissolved together in 18.4 mL of terpineol (Sigma Aldrich) to prepare a homogenous paste according to previous reported study by Atlı et al [248]. Note that, terpineol were used as dispersant, EC were used as thickener, and P25 were used as precursor source.

Spin coating was carried out with FTO glass with $TiO_2$ drop on it (rotates for 30 seconds at 2000 rpm, 1 time) in the spin coater device. Then, samples were taken out of the spin coater and was preheated at 450˚C for 15 minutes inside the furnace to deposit $TiO_2$.

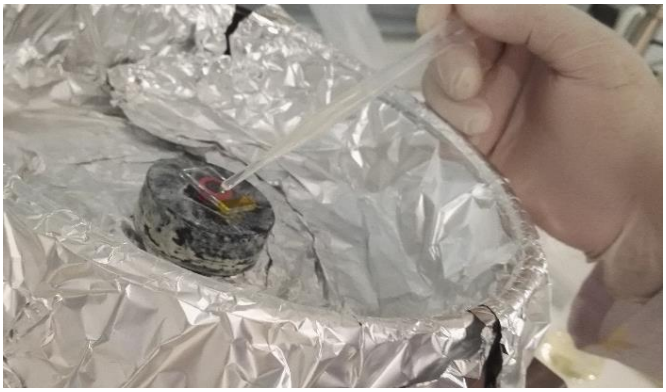

**Figure 3.5** Spin Coating Process.

As a second step, the TTIP solution was coated onto the P25 paste using a spin coater with 3 drop cycles (rotates for 30 seconds at 2000 rpm, 3 times). Subsequently, samples were taken out of the spin coater and was preheated at 450˚C for 5 minutes inside the furnace to deposit TTIP.

The mixing percent of paste and bare & plasmon is given in the Table 3.1.

**Table 3.1** The mixing percent of paste and bare & plasmon

| Label | Nanocomposite concentration (wt %) |
|---|---|
| P 25 paste | - |
| Au@$TiO_2$ | 0.125 |
| Au@ - 2x | 0.25 |
| Au@ - 4x | 0.5 |
| Au@ - 8x | 1 |
| Ag@ - x | 0.125 |
| Ag@ - 2x | 0.25 |
| Ag@- 4x | 0.5 |
| Ag@ - 8x | 1 |

### *3.2.1.3 Anchoring of Dye Sensitizer to Oxide Surface*

To dye anchoring process, N719 (di-tetrabutylammonium cis-bis(isothiocyanato) bis (2,2′-bipyridyl-4,4′-dicarboxylato) ruthenium(II), Sigma Aldrich) was carried out as follows.

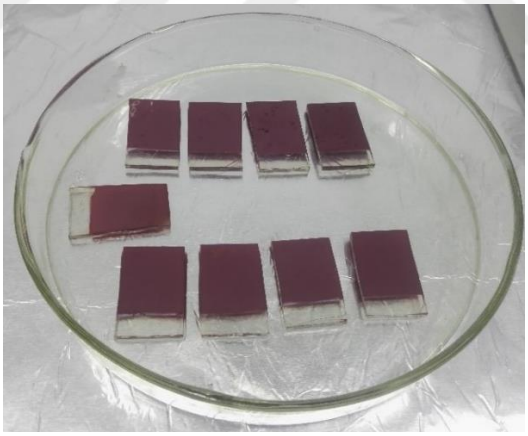

**Figure 3.6** Samples after Dye Loading

A 0.3 mM methanolic dye solution was prepared and the $TiO_2$ thin films produced in the previous step were introduced into the dye sensitizer which was protected from heat and light for 18 hours to perform a molecular bond as well as physical adsorption into the mesoporous structure of the substrates. Finally, the dye-anchored samples were rinsed with ethanol to remove any contaminants (Figure 3.6).

#### *3.2.1.4 Preparation of Electrolyte*

0.6 M of BMII (1-Butyl-3-methylimidazolium iodide, Sigma Aldrich), 0.5M of TBP (4-tert-Butylpyridine, Sigma Aldrich), 0.1M LiI (Lithium Iodide, Merck), 0.05 M $I_2$ (Iodine, Sigma Aldrich) and ACN (Acetonitrile, $CH_3CN$ Sigma Aldrich) were mixed and stirred for 2 hours at 400 rpm.

#### *3.2.1.5 Preparation of Counter Electrode*

Cleaning process of FTO coated conductive glass samples was also done in counter electrode. Typically, 5 mM of Chloroplatinic Acid Hydrate ($H_2PtCl_6 \times H_2O$, Sigma Aldrich) was dissolved in 2-propanol (Sigma Aldrich) was employed to 20 coating cycles onto FTO glass with spin coater (rotates for 30 seconds at 2000 rpm, 5rpm/s, 20 times). Then, the as-prepared counter electrodes were annealed on tube furnace for 30 minutes at 450 ºC.

### 3.2.2 Assembly of DSSC

A metal has a circular hole with a radius of approximately 3 cm was placed on the glass which the $TiO_2$ empty side and all the produced components were combined together in a sandwich-type structure attached with two latches. To form the final structure, the liquid electrolyte solution of the redox reactions (Figure 3.7.a) was poured between the completed photoanode film consists of a dye coated $TiO_2$ working electrode and a Pt coated FTO substrate counter electrode (Figure 3.7.b).

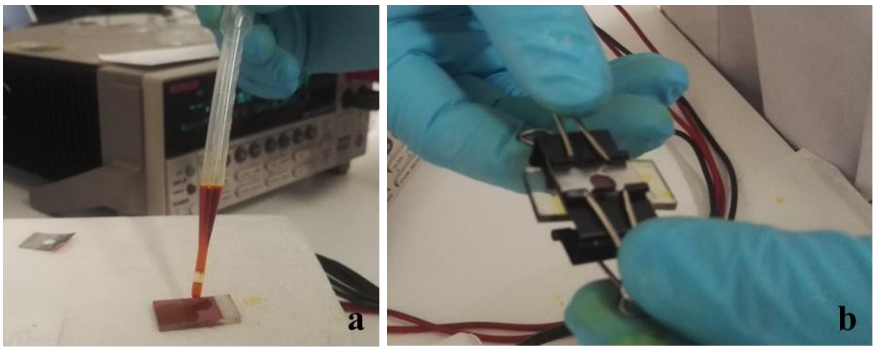


**Figure 3.7** a) Electrolyte Solution applying b) DSSC Assembling

## 3.3 Characterization of the Photoanodes and Devices

### 3.3.1 Characterization Methods Devices of $TiO_2$

Scanning Electron Microscope (SEM): The morphology, composition and structure of the samples were studied using a FEI Quanta 200 FEG Scanning Electron Microscope (SEM).

X-Ray Diffraction Spectroscopy (XRD): In this study, the phase composition of Au and Ag coated mesoporous $TiO_2$ nanoparticles as well as the bare $TiO_2$ was determined by a Rigaku Miniflex 600 Table Top Powder X-ray diffractometer. Cu Kα radiation (λ = 1.54 Å) was used and operated at 40 kV and 15 mA. The diffraction patterns were collected over 20-80 ° with a step size of 0.02 °. Results were analyzed using PDXL software by comparing with the library data [249].

X-Ray Photoelectron Spectroscopy (XPS): To investigate the formation of Au and Ag shell coating on the $TiO_2$ Nano particles, X-ray photoelectron spectroscopy was used by scanning a surface area with a diameter of 400 μm. Analysis was performed using Thermo-K-Alpha-Monochromatic high-performance XPS Spectrometer.

Surface Area Measurement (BET): BET analysis were employed to determine the surface areas of the Au decorated and Ag shell formation of mesoporous $TiO_2$ nanocomposite as well as the bare $TiO_2$ using the Quantachrome Corporation, Autosorb-6 device.

### 3.3.2 Characterization Methods Devices of DSSC

UV- Visible Spectroscopy: Absorption measurements of the films in the dye immersing study were performed with Shimadzu Corporation UV-1700 series. The absorbance properties of UV-visible-infrared regions were determined using reflectance measurements. Thus, the change in absorbance values of the obtained films in the Ultra Violet and Visible regions was observed [250].

Electrochemical Impedance Spectroscopy: The Electrochemical Impedance Spectroscopy (EIS) measurements were performed using a three-electrode configuration in 0.5M $H_2SO_4$. The measurements were done in an Interface 1000E Potenstiostat device at various potentials from 0.0 to -0.3 V versus RHE in the frequency range of 0.05 to $10^5$ Hz with an amplitude of 10 mV.

Current- Voltage Measurements: The performance of a solar cell is determined by its ability to convert the energy they receive from the sun into electrical energy (Figure 3.8).

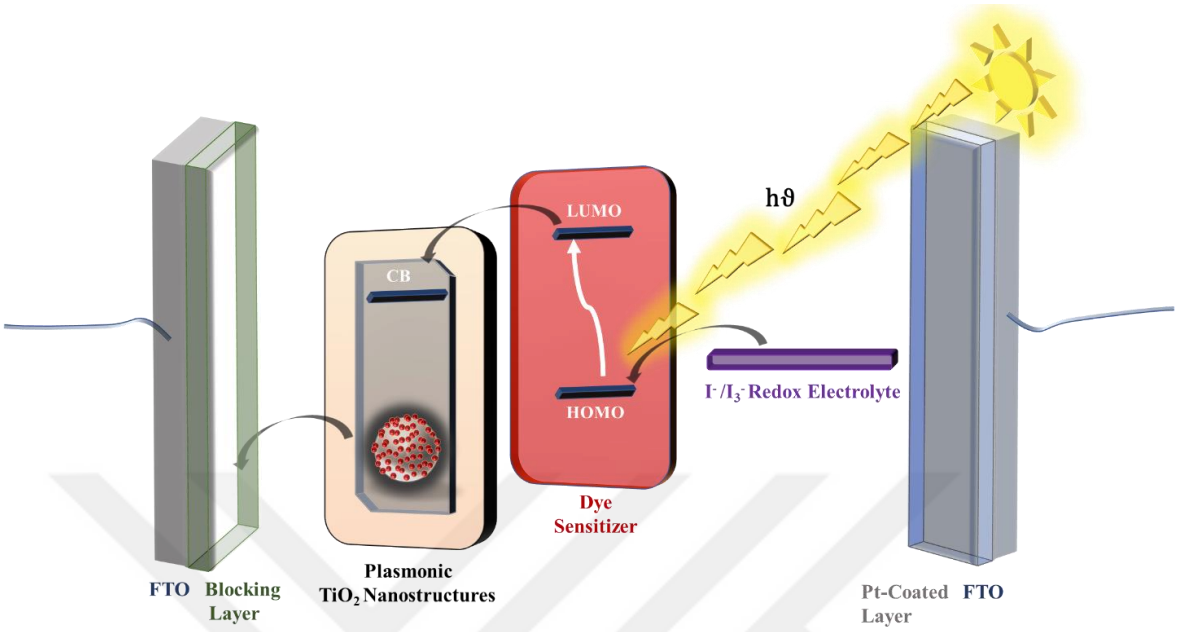


**Figure 3.8** Working Mechanism of Produced DSSC

Thanks to the solar simulator device, measurements were closed to natural sunlight and the performance of the cell were measured by a Abet Technologies device (Keithley 2400 source meter under 0.3 sun illumination, AM 1.5 G 100 mW /cm$^2$, Figure 3.9)

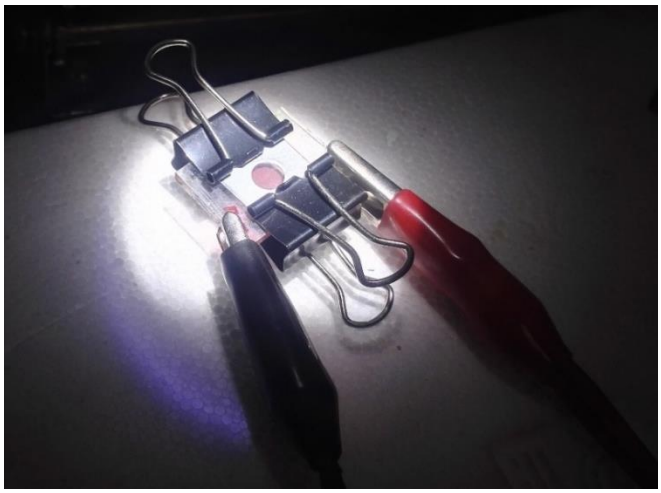

**Figure 3.9** Current- Voltage Measurement Process

# CHAPTER 4

## RESULTS & DISCUSSIONS

### 4.1 Scanning Electron Microscope Results

The SEM images of the plasmonic $TiO_2$ nanoparticles are given in Figure 4.1. All of the nanoparticles were obtained with narrow size distribution and clear morphologies. As seen in Figure 4.1, there is no significant change in both of the mean size distribution and surface morphology of the $TiO_2$ substrate after Au decoration onto bare $TiO_2$ nanoparticles [240, 244]. Figure 4.1-D represents the SEM photographs of Ag shell formation via seed mediated growth of Ag onto Au@$TiO_2$ nanoparticles. The mean size of the Ag@Au@$TiO_2$ nanoparticles slightly changed with no change in the spherical morphology of the main substrate (*i.e.*, bare $TiO_2$).

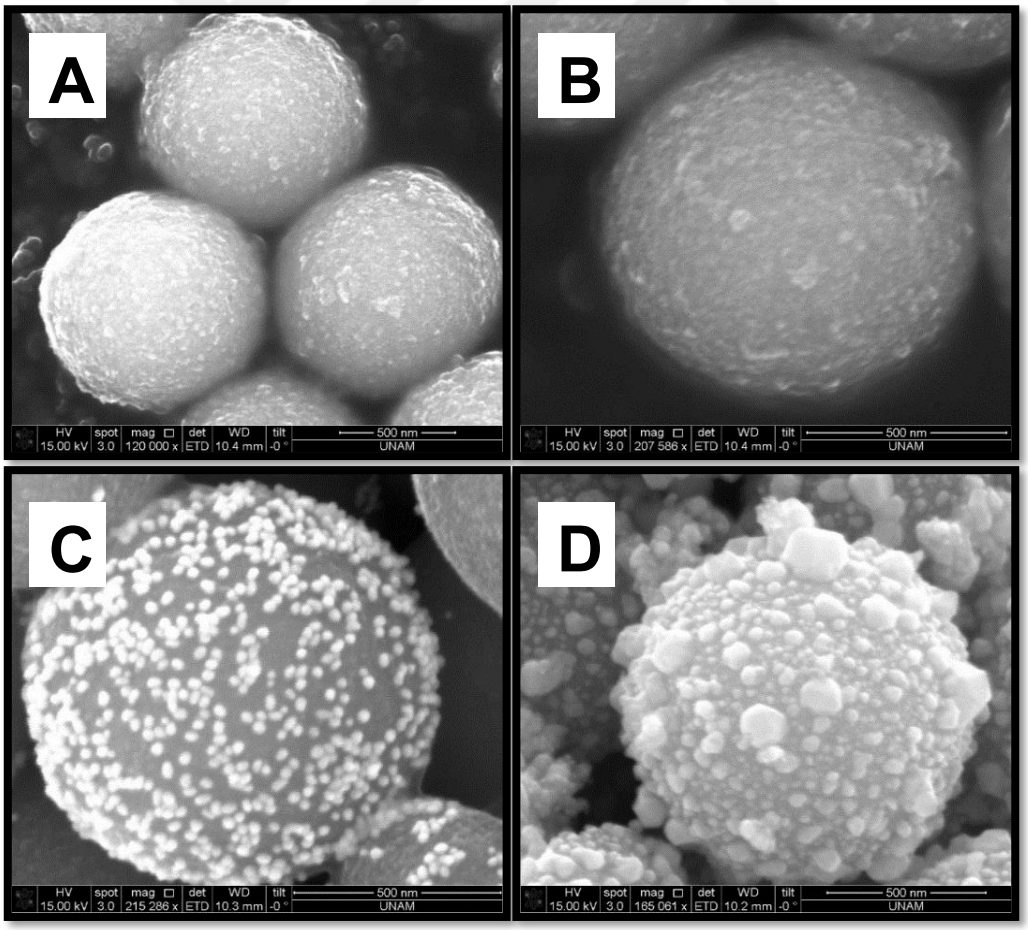


**Figure 4.1.** SEM images of A-B) $TiO_2$ nano-particles, C) Au@$TiO_2$ nano-particles, D) Ag@Au@$TiO_2$ nano-particles.

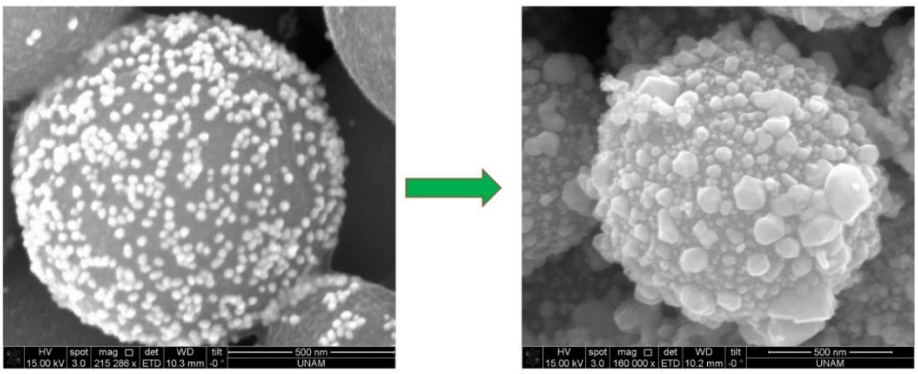

**Figure 4.2** SEM images of Au@TiO2 and Ag@Au@$TiO_2$ nano-particles.

Additionally, Figure 4.2 shows the size distribution of the decorated Au nanoparticles i.e., 15-20 nm) onto primary amine attached $TiO_2$ nanoparticles. Furthermore, the diameter distribution of the Ag shell onto Au@$TiO_2$ nanoparticles was measured using SEM images as well (i.e., 30 nm, 50 nm, and 100 nm)

## 4.2 X-Ray Diffraction Results

XRD measurements were made between 20° and 80° for 2θ value. In the Figure 4.3, the peaks from the crystal structures of the particles can be seen very clearly. The most severe peaks from the XRD graph of the synthesized nanocomposites appears as scattering of approximately 2θ = 25° / 28° (1 0 1) which are shown by green square symbol and shows the formation of anatase $TiO_2$ crystals [250, 251]. It is known that dye-sensitized solar cells demonstrated better light harvesting efficiencies compared to particles with anatase structure [126,127]. The crystal structure of the synthesized particles in the higher anatase phase indicates that more efficiency can be obtained from $TiO_2$ particles, which are commonly used as standard [130].

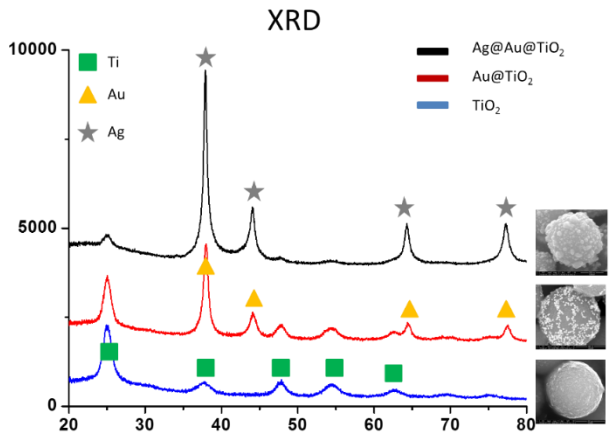


**Figure 4.3** XRD result of Bare $TiO_2$, Au@$TiO_2$ and Ag@Au@$TiO_2$ nano-particles.

Au decorated $TiO_2$ nano-particles and Ag shell formation onto Au@$TiO_2$ nano-particles were also analyzed by XRD (Figure 4.3). The crystalline peaks of Au were indicated by yellow triangle symbols. 2θ =37° peak indicated the Au is decorated onto $TiO_2$ [240]. In the silver doped structure 2θ = 44°, and 2θ = 64° peaks were observed [244]. This peaks strongly are in a good agreement with SEM images and represents the formation of Ag shell. As seen in Figure 4.3., by coating of Ag onto the Au@$TiO_2$ nanoparticles, the specific peaks and related intensities were improved. The increase in the intensity of the plasmonic peaks showed the successful fabrication of plasmonic $TiO_2$ nano-particles.

## 4.3 X-Ray Photoelectron Spectroscopy Results

XPS was used to investigate the attachment of Au and Ag shell formation onto $TiO_2$ nanoparticles by scanning a surface area with a diameter of 400 μm (Figure 4.4)

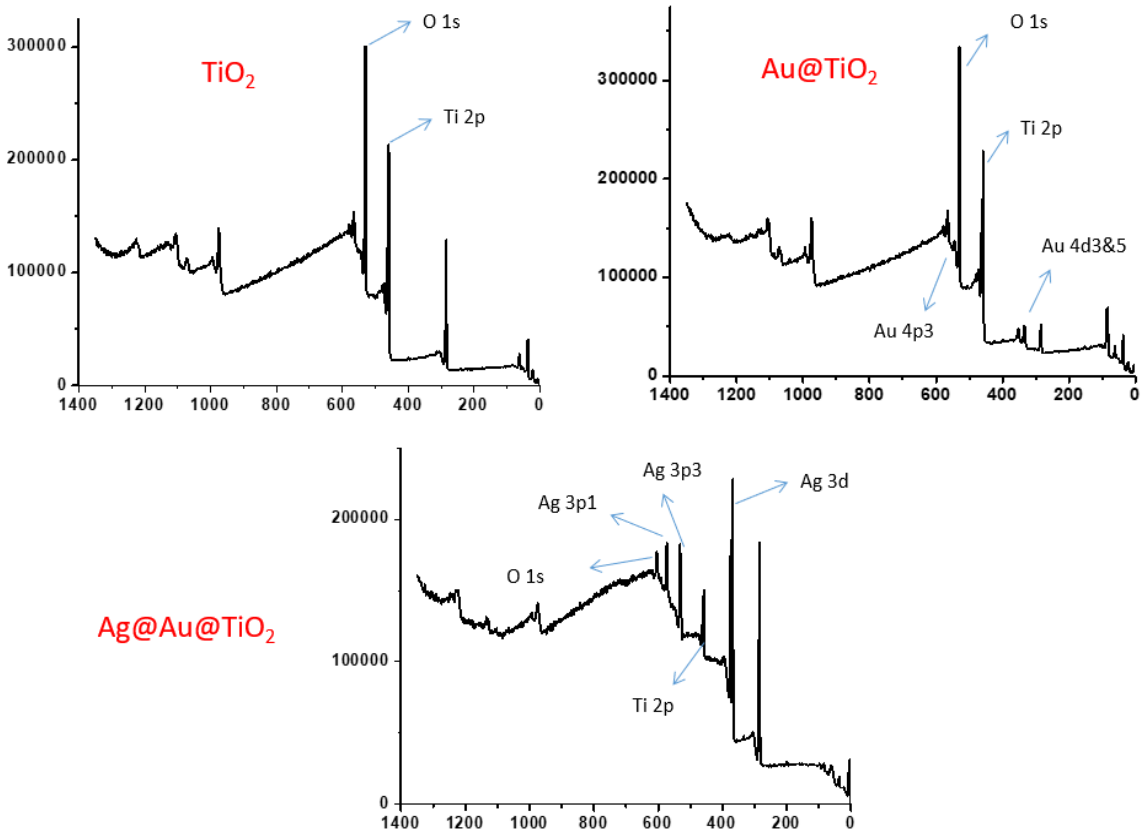


**Figure 4.4** XPS images of Bare $TiO_2$, Au@$TiO_2$ and Ag@Au@$TiO_2$ Nano-particles

Ti 2p, O 1s, Au 4f, and Ag 3d bands obtained for plasmonic nano-particles clearly demonstrated the successful formation of Au@$TiO_2$ and Ag@Au@$TiO_2$ nanoparticles. Finally, the presence of Ti 2p band in all of the results can be evaluated as a critic point

showing the deposition of Au and Ag@Au onto $TiO_2$ nanoparticles in good agreement with SEM and XRD results.

## 4.4 Surface Area Measurement (BET) Results

The surface areas of the synthesized bare $TiO_2$, Au@$TiO_2$ and Ag@Au@$TiO_2$ nanoparticles were evaluated according to the BET model and the obtained results are given in Table 4.1. From the 7-point BET analysis, the specific surface area of the anatase $TiO_2$ powders was increased after the attachment of Au nanoparticles. Additionally, the specific surface area of Ag@Au@$TiO_2$ nanoparticles was markedly lower compared to the Au@$TiO_2$ with respect to the Ag shell layer. It could be noted that, high surface is one of the crucial points that will improved the highly amount dye molecule adsorption, filling of mesopores, as well as efficient light harvesting efficiency for newly synthesized photoanodes [205,234].

**Table 4.1** Area-Volume-Pore Size Summary of Synthesized Materials

| **Area-Volume-Pore Size Summary- $TiO_2$** | | |
|---|---|---|
| Surface Area Data | Multipoint BET | 144.7 m²/g |
| | BJH Method Cumulative Adsorption Surface Area | 192.1 m²/g |
| | BJH Method Cumulative Desorption Surface Area | 209.8 m²/g |
| Pore Volume Data | BJH Method Cumulative Adsorption Pore Volume | 0.2924 cc/g |
| | BJH Method Cumulative Desorption Pore Volume | 0.2982 cc/g |
| Pore Size Data | BJH Method Adsorption Pore Diameter (Mode). | 7.78 nm |
| | BJH Method Desorption Pore Diameter (Mode) | 5.67 nm |
| **Area-Volume-Pore Size Summary - Au@$TiO_2$** | | |
| Surface Area Data | Multipoint BET | 157.2 m²/g |
| | BJH Method Cumulative Adsorption Surface Area | 208.7 m²/g |
| | BJH Method Cumulative Desorption Surface Area | 214.8 m²/g |
| Pore Volume Data | BJH Method Cumulative Adsorption Pore Volume | 0.2524 cc/g |
| | BJH Method Cumulative Desorption Pore Volume | 0.2530 cc/g |
| | BJH Method Adsorption Pore Diameter (Mode). | 5.60 nm |

| | | |
|---|---|---|
| Pore Size Data | BJH Method Desorption Pore Diameter (Mode) | 4.92 nm |
| **Area-Volume-Pore Size Summary - Ag@Au@TiO$_2$** | | |
| Surface Area Data | Multipoint BET | 52.85 m²/g |
| | BJH Method Cumulative Adsorption Surface Area | 68.80 m²/g |
| | BJH Method Cumulative Desorption Surface Area | 73.61 m²/g |
| Pore Volume Data | BJH Method Cumulative Adsorption Pore Volume | 0.1087 cc/g |
| | BJH Method Cumulative Desorption Pore Volume | 0.1105 cc/g |
| Pore Size Data | BJH Method Adsorption Pore Diameter (Mode). | 6.68 nm |
| | BJH Method Desorption Pore Diameter (Mode) | 5.63 nm |

Figure 4.5 shows the comparison of the pore size distribution of bare $TiO_2$, Au@$TiO_2$ and Ag@Au@$TiO_2$ nanoparticles, respectively. All of the nanoparticles demonstrated sharp peaks related to the mesopore fraction ranging between 4.8-7 nm. The marked decrease of the mesopore fraction from 4.8 nm (*i.e.*, Au@$TiO_2$) to 6 nm (Ag@Au@$TiO_2$) should be explained by the filling of the mesopores of the Au@$TiO_2$ nanoparticles after the Ag shell formed.

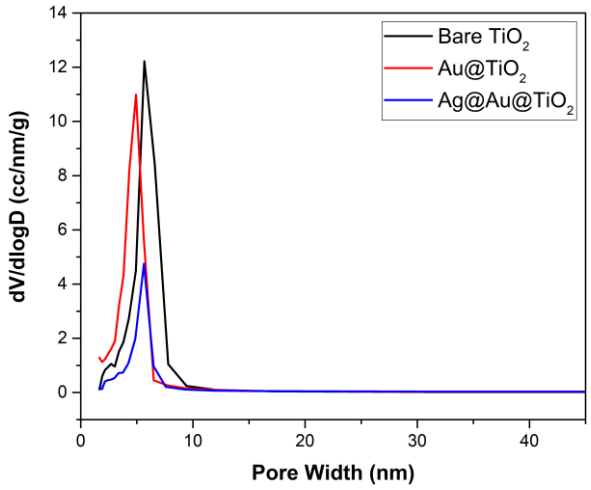


**Figure 4.5** BET Pore Volume Results

To visualize the adsorption isotherm, Relative Pressure against Volume graph was plotted for each sample (Figure 4.6). Isotherm graphs are given information about the porosity in particular regarding the shape, type and depth of porosity of the existing pores.

Basically, isotherm indication divided into three regions. First of from 0 to 0.3 P/P0 is derived from the relative pressure, the second from 0.3 to 0.75 P/P0 and the third of 0.75 – 1.0 is P/P0 range. The graphs are consistent with Type 4 isotherm graphs and strongly proves that the newly synthesized photoanodes bears mesoporous structure.

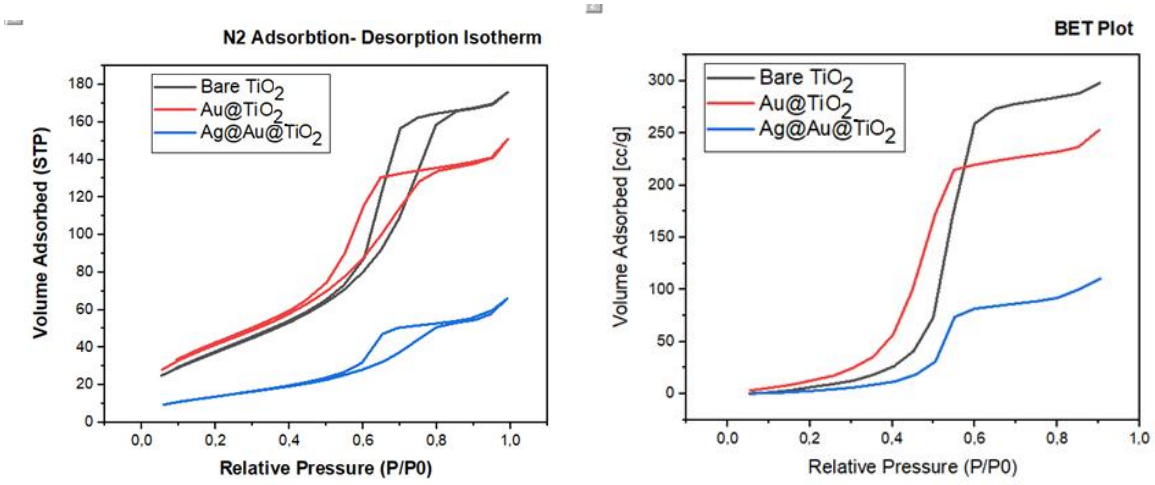


**Figure 4.6 A)**$N_2$ Adsorption/ Desorption Isotherm of Synthesized Materials,
**B)**BET Plot of Synthesized Materials

## 4.5 Device Characterization Results

Figure 4.7 shows the UV-Visible results of the prepared devices. Considering the spectrum between 400 and 800 nm, an absorption peak of $TiO_2$ can be seen in all samples before dye doping. Presence of Au and Ag particles is also seen from the pre-dye absorption analysis results. From the UV-Visible data, the intensity of the absorbance increased as the coating cycle increased.

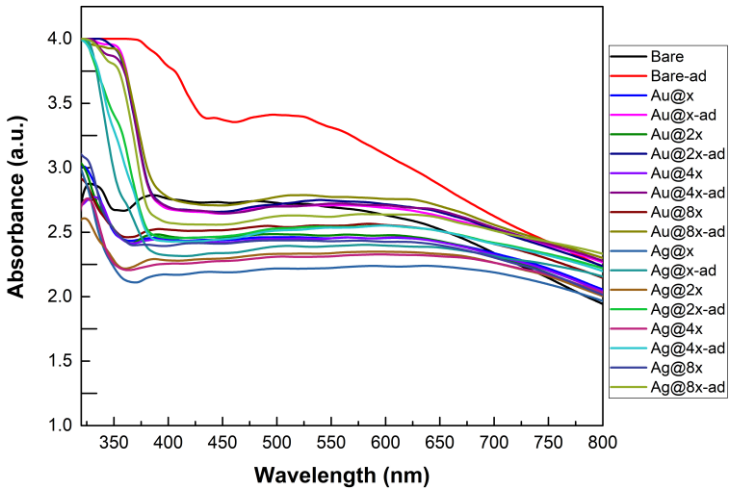


**Figure 4.7** Absorption Spectra of All Samples

In the figures 4.8, 4.9 and 4.10, devices before and after dye loading are compared, respectively. After dye loading, new peaks of absorbance at long wavelengths are formed. The adsorption of dye molecules resulted in a considerable increase in the absorption of sunlight in the visible region for all samples. By considering the absorbance value of the samples before dye adsorption first sample as a reference, light absorption is improved in the visible and NIR region when the Au and Ag layer was applied (Figure 4.9 and Figure 4.10). As a noticeable conclusion, the formation of Ag shell using a seed mediated growth leads to the better absorbing quality compared to bare and Au@$TiO_2$ added devices (range up to NIR field).

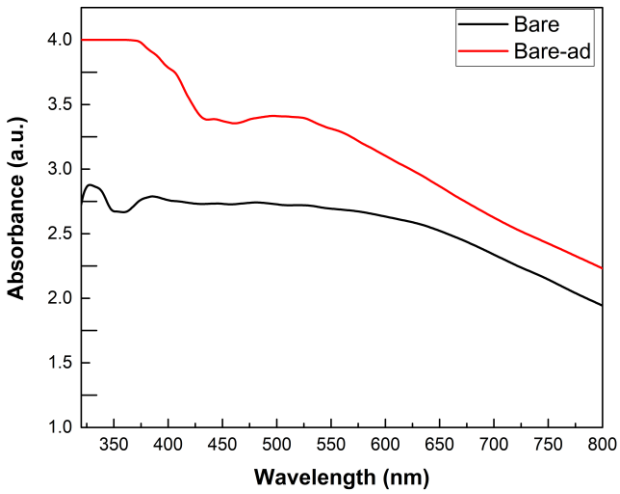


**Figure 4.8** Absorption Spectra of Before and After Dye Loading of Bare $TiO_2$

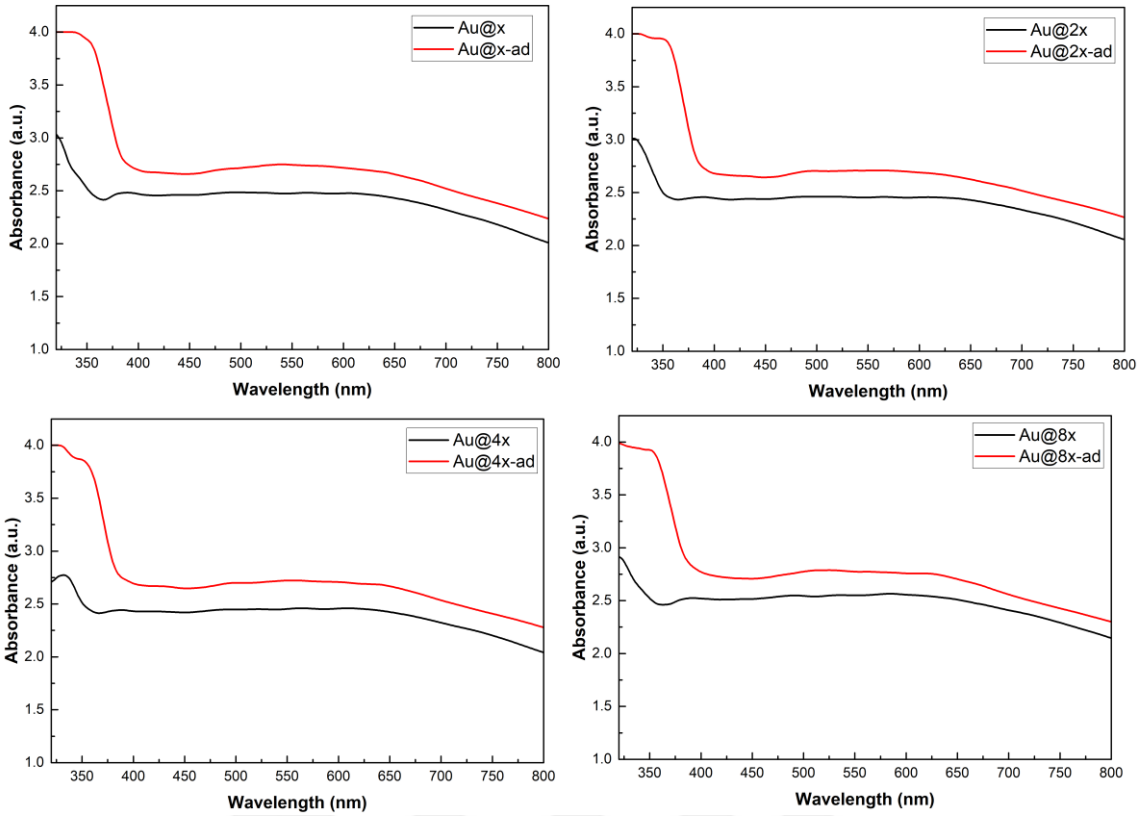


**Figure 4.9** Absorption Spectra of Before and After Dye Loading of Au@$TiO_2$ nano-particles

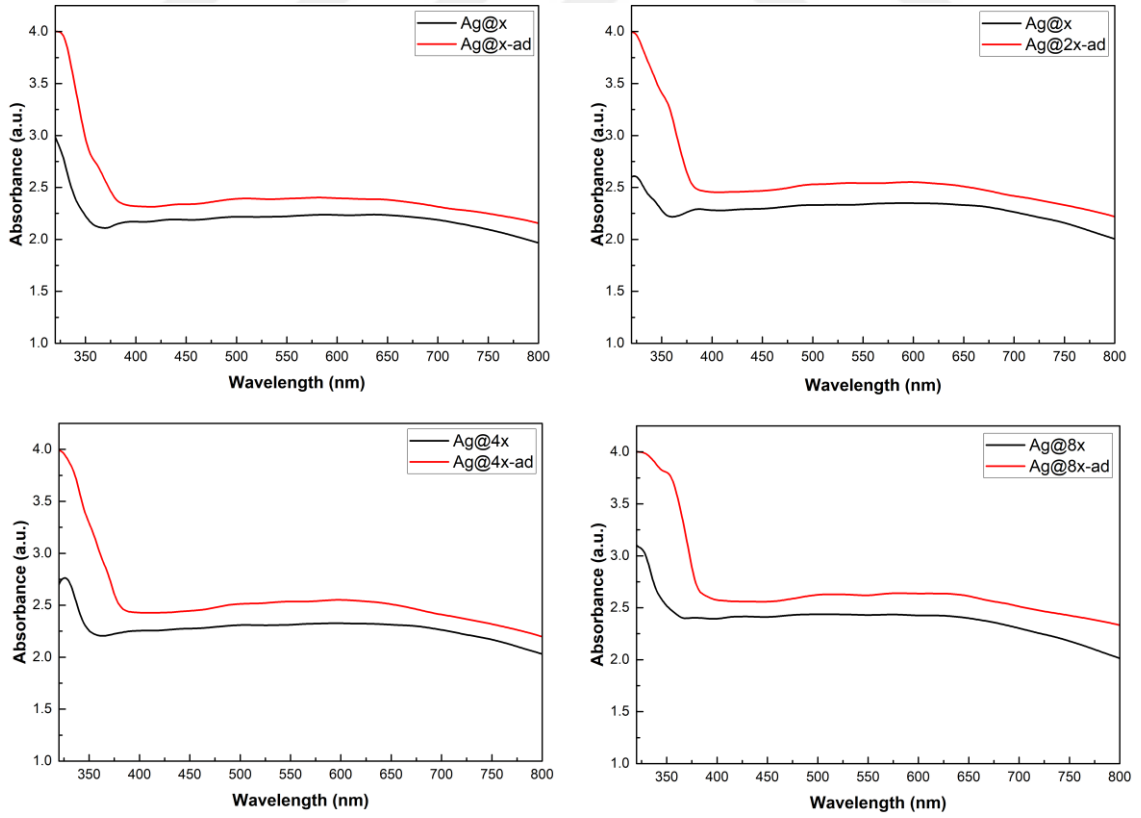


**Figure 4.10** Absorption Spectra of Before and After Dye Loading of Ag@Au@$TiO_2$ nano-particles

## 4.6 Current-Voltage Measurements Results

To investigate the photovoltaic performance of plasmonic DSSC, current-voltage (J-V) properties were obtained. Active area for all of the measurements is given as 0.27 $cm^2$. Jsc, Voc, FF and Ƞ values and the photovoltaic performance of the cells is summarized in Table 4.2.

**Table 4.2** JV Characteristics for Different Sample Ratios

| **NP (w 2 gr P25 paste)** | **Sample** | **Rs (Ω)** | **RCT (Ω)** | **Rr (Ω)** | **Jsc ($mA/cm^2$)** | **Voc (V)** | **FF** | **Ƞ (%)** |
|---|---|---|---|---|---|---|---|---|
| 0 g | Bare | 29.09 | 324.00 | 241.10 | 13.41 | 0.68 | 0.65 | 5.91 |
| 2.5 mg | Au@-x | 19.29 | 94.66 | 121.8 | 17.20 | 0.64 | 0.62 | 6.86 |
| 5.0 mg | Au@-2x | 22.7 | 350.6 | 10.63 | 18.36 | 0.65 | 0.64 | 7.62 |
| 10.0 mg | Au@-4x | 17.76 | 637.9 | 18.11 | 14.13 | 0.66 | 0.65 | 6.08 |
| 20.0 mg | Au@-8x | 16.61 | 261.8 | 235.3 | 14.59 | 0.63 | 0.63 | 5.85 |
| 2.5 mg | Ag@-x | 23.44 | 513.00 | 600.00 | 17.18 | 0.66 | 0.66 | 7.41 |
| 5.0 mg | Ag@-2x | 22.14 | 1005.00 | 1017.00 | 17.30 | 0.64 | 0.61 | 6.76 |
| 10.0 mg | Ag@-4x | 19.15 | 125.30 | 133.10 | 14.98 | 0.67 | 0.63 | 6.35 |
| 20.0 mg | Ag@-8x | 17.66 | 54.54 | 136.00 | 12.97 | 0.71 | 0.66 | 6.07 |

The highest open-circuit voltage (Voc) was taken as 0.71 V from the cell using 20 mg Ag@Au@$TiO_2$ nanoparticles. The highest value of the short circuit current per $cm^2$ (Jsc) was taken from the cell containing 5 mg Au@$TiO_2$ nanoparticles as 18.36 $mA/cm^2$. Based on these values it is clear that the plasmonic particles directly affects the efficiency of the solar cell (Figure 4.11).

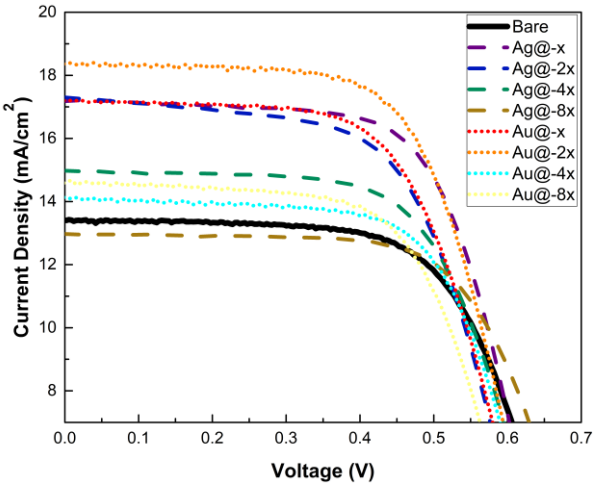


**Figure 4.11** JV Characteristics of all synthesized nano-particles

The presence of plasmonic photoanodes affected directly the Jsc value of the devices as (Figure 4.11). By increasing the amount of the plasmonic photoanodes, a decrease in the Jsc value was observed (Figure 4.11). Additionally, the maximum Jsc value was found around 17.30 using Ag-2x particles. Furthermore, from Table 4.3, as the amount of current increases, the voltage value also increased for both particle types (*i.e.*, Au@$TiO_2$ and Ag@Au@$TiO_2$ nanoparticles, Figure 4.12) [253].

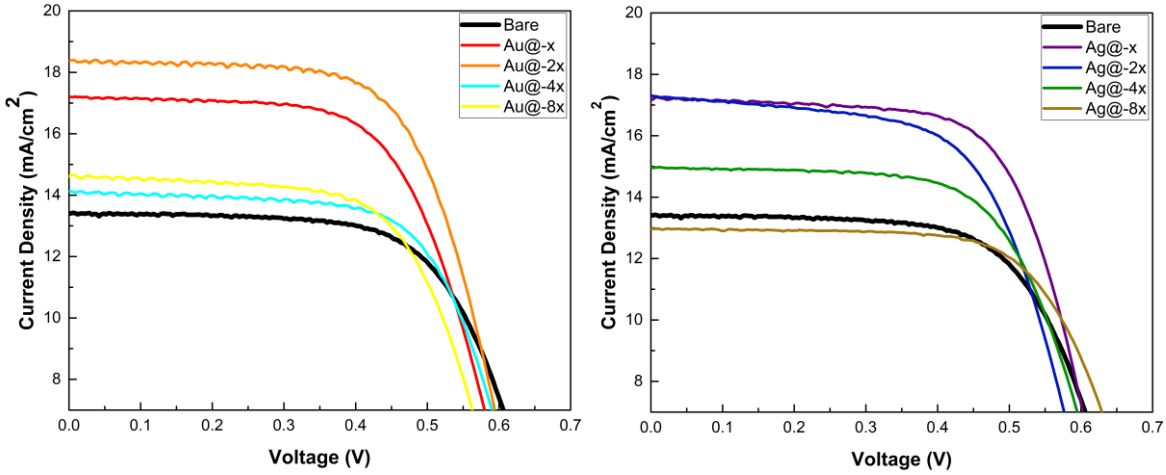


**Figure 4.12** JV Characteristics of A) Au@$TiO_2$ and B) Ag@Au@$TiO_2$ nano-particles

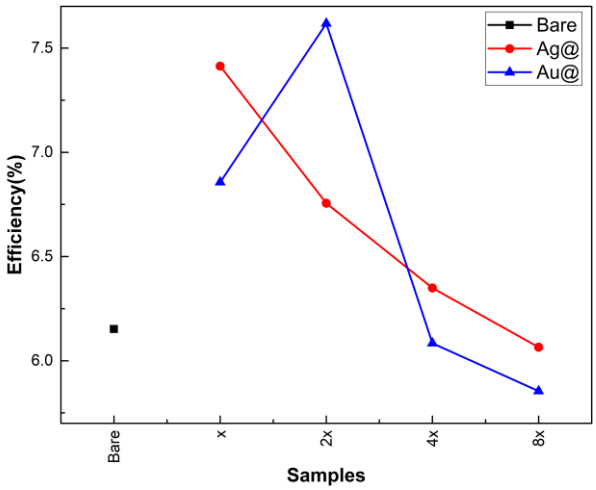


**Figure 4.13** Efficiency curve of Bare $TiO_2$, Au@$TiO_2$ and Ag@Au@$TiO_2$ nano-particles

The device efficiency values using different plasmonic nanoparticles are given in Figure 4.13. As seen here, while the efficiency of the cell using only bare $TiO_2$ nanoparticles reached to 5.91%, DSSCs with Au@$TiO_2$ and Ag@Au@$TiO_2$ nanoparticles demonstrated 6.86% and 7.41% efficiencies, respectively. These results clearly proved that the addition of plasmonic nanostructures directly affected the cell efficiency even at low concentrations. However, by increasing the amount of nanoparticles (*i.e.*, 2x, 5 mg), the efficiency related to the Ag@Au@$TiO_2$ nanoparticles decreased due to the reduced surface area compared to Au@$TiO_2$ nanoparticles. The highest efficiency obtained after the measurement are established as the seventh sample with 7.62 % that is doped using 5 mg of Au particles (Figure 4.13). On the other hand, solar cells with 2x amount of plasmonic nanoparticles (*i.e.*, 5 mg) showed smaller Voc value (0.64 V and 0.63 V for Ag@Au@$TiO_2$ and Au@$TiO_2$ nanoparticles, respectively) and maximum resistivity (1017 Ω and 253 Ω for Ag@Au@$TiO_2$ and Au@$TiO_2$ nanoparticles, respectively) for two kinds of photoanodes.

The generation of photoelectrons is closely related to the dye molecules. The surface area of $TiO_2$ determines the amount of adsorption of dye molecules. Therefore, the design and preparation of $TiO_2$ with a high specific surface area plays an important role in the generation of photoelectrons. We can compare the results from the literature in two different categories. The first group is the application of bare $TiO_2$ micro/nanoparticles for dye sensitized solar cell: for example, $TiO_2$ microspheres and uniform $TiO_2$ submicrospheres were synthesized for dye sensitized solar cells application with high PCE value [254, 255]. Zhao-Qian Li *et. al.* reported the hierarchical $TiO_2$ microstructures with the 9.79% PCE value [256]. In another work, mesoporous $TiO_2$ (mp-$TiO_2$) with a compact $TiO_2$ blocking layer (bl-$TiO_2$) were utilized for enhanced dye sensitized solar cells applications [257]. Yuewu Huang *et.*

*al.* employed the commercial P25 nanoparticles and achieved an efficiency of 10.3% [258]. Additionally, mesoporous $TiO_2$ microspheres with P25 were applied with double-layer P25 film and they achieved 5.61% PCE value [259]. Weiguo Zhang *et. al.* synthesized mesoporous anatase or rutile phase microspheres for efficient dye sensitized solar cell applications with 5.9- 6.3 % PCE value [260]. Furthermore, hollow $TiO_2$ spheres (HSs) and $TiO_2$ nanorods (NRs), and hierarchical $SnO_2/TiO_2$ composite hollow microspheres were utilized for DSSCs with 9.6 % and 8.70% PCE values, respectively [261, 262].

The second group is the application of metal doped $TiO_2$ nanocomposites for dye sensitized solar cell: for example, W-$TiO_2$ and Cu-doped $TiO_2$ nanostructures were employed for DSSCs applications and they achieved 7.76% and 6.71% PCE values, respectively [263, 264]. It should be noted that, metal doped $TiO_2$ nanocomposites demonstrated similar results in the term of PCE values [265, 266]

The most preferred metal nanoparticles are noble materials including Au and Ag. For example, Au@$SiO_2$, Ag@$SiO_2$, and Au/$TiO_2$ nanocomposites with different noble metal morphologies (i.e., sphere, nanorod, and etc.) are the frequent structures for DSSCs applications [267-270]. Note that, our reported plasmonic $TiO_2$ nanocomposites demonstrate the same results in the case of photovoltaic performance with plasmonic metal nanoparticles doped $TiO_2$ nanocomposites in the literature. Similar examples are: Au-decorated $TiO_2$ hollow spheres synthesized with 7.3% efficiency, Au@$TiO_2$ hollow spheres with 8.31% PCE, Au@TNTs with 5.63% PCE, Au@TNTs with 6.94% performance, Ag-doped TNPs with 5.74% PCES, Ag-doped anatase-$TiO_2$ with 9.45% PCE, Au/Ag/$SiO_2$ nanostructures with 7.51% efficiency, Au/Ag $TiO_2$ nanospheres/perovskite with 8.30 % PCE, $SiO_2$@$TiO_2$ Core Shell to $TiO_2$ hollow and Au@Ag/$TiO_2$ Hollow nanoparticles with 9.7% PCE values [271-275].

## 4.7 Electrochemical Impedance Spectroscopy Results

Characterization of the surface modifications is essential in the energy related studies. Electrochemical impedance spectroscopy is a powerful method to analyses the complex electrical resistance of a system and is sensitive to surface phenomena and changes of bulk properties. This technique is interested in the interaction between the interface, surface, and reactive media.

In DSSCs, electrochemical impedance spectroscopy is used to characterize the interface load transfer process and the reaction performance on the electrode surface. Such measurements (*i.e.,* EIS) are used to monitor the resistances between the electrolyte and the opposite electrode.

Electrochemical impedance spectroscopy is usually measured by applying an electrical potential to an electrochemical cell and measuring the current. If one were to apply a sinusoidal potential to the cell the response would be the ac current signal. EIS is normally measured using an excitation signal that makes the cell respond pseudo-linearly. With this linear system, the current response of the sinusoidal potential will be a sinusoid at the same frequency but with a shift in phase. The two lines represent the current and voltage of the electrochemical cell. A value of resistance and capacitance for the coating can be determined through modeling of the electrochemical data. The modeling procedure uses electrical circuits built from components such as resistors and capacitors to represent the electrochemical behavior of the coating and the metal substrate.

The charge transfer resistance between the $TiO_2$/electrolyte interface electrode must be independent of that of the opposite electrode. Impedance frequencies around 100 kHz are dominant by the Ohmic Series Resistor (Rs) of the conductive surfaces. By scanning a range between 0.1 Hz and 1 MHz, the load transfer resistance between the Pt/electrolyte interface were reported as Rct and its values are summarized in Table 4.4.

For the situation of an electrode in contact with an electrolyte, the so-called Randles circuit is, comprising the solution resistance Rs, the charge transfers resistance Rct, the double layer capacitance Cd and the Warburg impedance W. The resistivity values that related with the frequency are given in Table 4.4 and $\tau_e$ values are calculated as followed equation:

$$\boldsymbol{\tau_e = \frac{1}{2\pi f_{max}}} \qquad \textbf{(4.1)}$$

The comparison results of EIS show that the Rct values as expected are higher for the dye absorbed electrodes compared to the bare $TiO_2$ electrodes. As seen here, the surface modification changes the value of electrical elements in the circuit (Table 4.4). The most significant increase occurred to the electron transfer resistance. The Au and Ag plasmonic nanostructures formed a barrier that prevented direct approach of the redox specious to the electrical surface (Table 4.3).

**Table 4.3** EIS Characteristics for Different Sample Ratios

| Label | Rs | Rt | Rct | fmax (Hz) | $\tau_e$ (ms) |
|---|---|---|---|---|---|
| Bare | 29.09 | 324 | 241.1 | 110.32 | 1.44 |
| Ag@-x | 23.44 | 513 | 600 | 153 | 1.04 |
| Ag@-2x | 22.14 | 1005 | 1017 | 47.9 | 3.32 |
| Ag@-4x | 19.15 | 125.3 | 133.1 | 308.68 | 0.52 |
| Ag@-8x | 17.66 | 54.54 | 136 | 415.71 | 0.38 |
| Au@-x | 19.29 | 94.66 | 121.8 | 324.62 | 0.49 |
| *Au@-2x* | *22.7* | *350.6* | *10.63* | *47.72* | *3.33* |
| Au@-4x | 17.76 | 637.9 | 18.11 | 68.79 | 2.31 |
| Au@-8x | 16.61 | 261.8 | 235.3 | 155.06 | 1.03 |

Figure 4.14 depicts the resistance of the all prepared devices. The decrease of charge transfer resistance (Rct) with the increasing of applied bias voltage was achieved. Because of carrier transfer resistance is defined by the interaction between Platinum ad electrode, lower values were obtained. In this results the Rr defines the resistivity between $TiO_2$ and electrode as well. From the literature, the carrier transfer resonance (Rct) should be smaller while the Rr is higher to prevent the recombination problem [253]. Additionally, solution resistance Rs values ranging between 15-20 ohm are favorable for DSSCs.

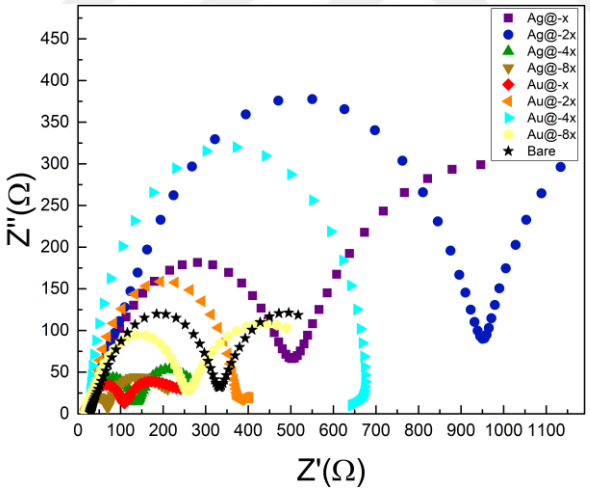


**Figure 4.14** Impedance Graph of all Devices

The impedance results of the devices including $Au@TiO_2$ and $Ag@Au@TiO_2$ nanoparticles are given in Figure 4.15. As seen here, the first semi-circle corresponds to the decoration of plasmonic nanoparticles onto the electrode. By introduction of the plasmonic nanoparticles into device, the second semi-circle was increased compared to the bare one. Thus, an increase in impedance was obtained which confirms the recognition between $TiO_2$/plasmonic nanoparticles interface. Therefore, by increasing the concentration of

plasmonic $TiO_2$ nanoparticles the semi-circles were increased which highlighted the good sensitivity of the solar cell.

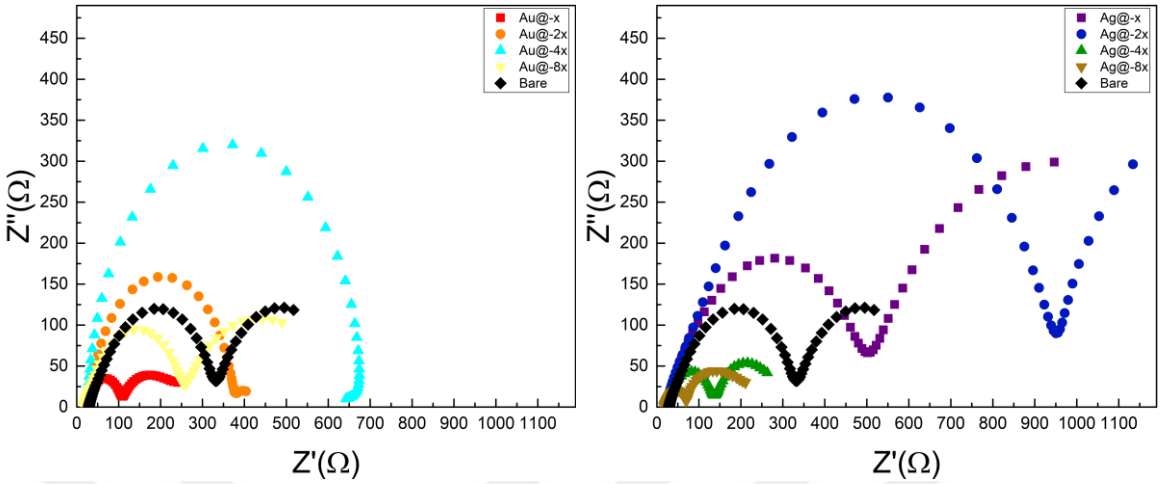


**Figure 4.15** Impedance graph of A) Au@$TiO_2$ and B) Ag@Au@$TiO_2$ nanoparticles

Moreover, the life time of an electron and recombination time values for all of the devices were calculated from impedance parameters and is shown with $\tau_e$ value (Figure 4.14). From the obtained results, it could be noted that the higher life time demonstrates lower recombination rate so it effects the performance of solar cells. So, the maximum $\tau_e$ value was achieved for Ag-2x containing device (i.e., 5 mg Ag@Au@$TiO_2$) and is in a good agreement with obtained efficiency values for this device.

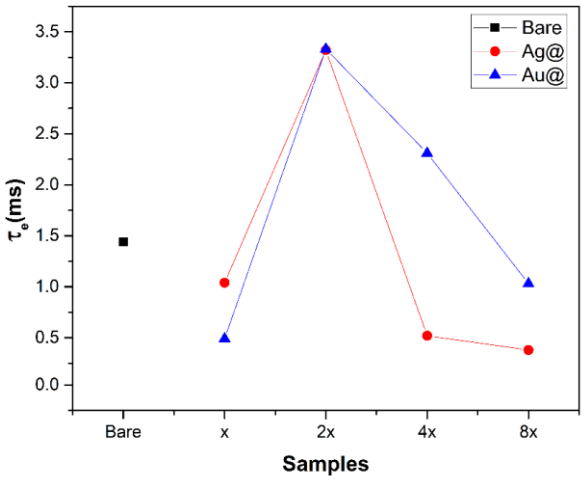


**Figure 4.16** $\tau_e$ coefficient comparison of all synthesized nano-particles

# CHAPTER 5

## CONCLUSION

Producing environmentally friendly materials and protecting nature is an important responsibility of human beings. For this purpose, in this master thesis, an alternative technique was employed to produce renewable energy. In this thesis, a photovoltaic performance of 7.62% was achieved using plasmonic particles doped nanocomposite.

In summary, $TiO_2$ powder sample was produced using two-step synthesis method and two different doping methods. The morphology and optical properties of the produced gold and silver plasmonic nanostructures were analyzed by different characterization methods. The results obtained from XRD, XPS, SEM and BET were well matched with each other, and the findings obtained from UV-Vis, Solar Simulator and EIS in DSSC characterization supported the finding of the thesis as well.

- The crystal structures of the produced powders were analyzed by X-ray Diffraction (XRD). The presence of metal particles in Au and Ag coated nanocomposites was supported by peaks, while the structure was clearly in anatase form.
- The elements found on the surface of the produced powders were examined by X-ray Photoelectron Spectroscope (XPS) and plasmon structures were found to support other structure characterizations.
- The surface morphology was investigated by Scanning Electron Microscope (SEM) images. With the addition of metal nanoparticles, metal particles on the surface of the material were more clearly seen.
- The specific surface area, mean pore size, and pore size distribution values of the plasmonic $TiO_2$ nanoparticles were examined according to the Brunauer-Emmett-Teller (BET) method. No significant change in the mesoporous structure of the plasmonic nanoparticles were achieved via novel seed mediated growth of the Ag shell.
- UV-Vis results of plasmonic demonstrated $TiO_2$ nanoparticles was achieved and demonstrated the high absorption capability for both of the $Ag@Au@TiO_2$ and $Au@TiO_2$ even in the NIR region.
- From the current voltage measurements, it was determined that the highest PCE value was obtained (*i.e.*, 7.62%) using $Ag@Au@TiO_2$ containing devices.

- As a conclusion, an efficient cell performance values were obtained by a some pre/post treatment layers to overcome the poor efficiency issues.

To sum up of all the findings, it will be inevitable that plasmonic nanocomposite materials obtained by mixing $TiO_2$ nano-particle with different metal oxides in future will be preferred due to their superior properties in photocatalytic and energy applications.

# REFERENCES


[1] R. Noack, Human Energy Requirements. A Manual for Planners and Nutritionists, 45th ed., Oxford, New York: Oxford University Press, 1991.

[2] X. Zhan, Z. Chen, and Q. Zhang, Recent Progress in Two-Dimensional COFs for Energy-Related Applications, J. Mater. Chem. A, vol. 5, no. 28, pp. 14463–14479, 2017.

[3] BP, BP Energy Outlook 2019 edition, Retrieved March 20, 2019 from /www.bp.com/, February 14 2019.

[4] Oğuz Türkyılmaz, Turkey Energy Outlook And Renewable Energy, Retrieved March 21, 2019 from //www.eppen.org/, June 2019.

[5] W. Energy, C. Turkish, N. Committee, and Q. W. Group, Turkish Energy Demand Prediction for 2017, no. June, pp. 2017–2019, 2018.

[6] W. Li, J. Liu, and D. Zhao, Mesoporous Materials for Energy Conversion and Storage Devices, Nat. Rev. Mater., vol. 1, no. 6, 2016.

[7] A. E. I.B. Cohen, An Interview with Einstein, 193rd ed. 1955.

[8] W. Tress, Device Physics of Organic Solar Cells, Master's Thesis, Dresden, 2011.

[9] V. Gusak, Nanoplasmonics for Solar Cells, Master's Thesis, 2014.

[10] H. Ellis, Characterization of Dye-Sensitized Solar Cells Components for Environmentally Fiendly Photovoltaics, 063, 2014.

[11] P. W¨urfel, Physics of Solar Cells: From Basic Principles to Advanced Concepts, Weinheim: WileyVCH, 2009.

[12] S. Suhaimi, M. M. Shahimin, Z. A. Alahmed, J. Chyský, and A. H. Reshak, Materials for Enhanced Dye-Sensitized Solar Cell Performance: Electrochemical Application, Int. J. Electrochem. Sci., vol. 10, no. 4, pp. 2859–2871, 2015.

[13] S. Esiner, R. E. M. Willems, A. Furlan, W. Li, M. M. Wienk, and R. A. J. Janssen, Photoelectrochemical Water Splitting in an Organic Artificial Leaf, J. Mater. Chem. A, vol. 3, no. 47, pp. 23936–23945, 2015.

[14] N. S. Lewis, Solar Energy Use, Science, vol. 798, no. 2007, pp. 798–801, 2012.

[15] B. Minnaert and M. Burgelman, Influence of the Energy Levels on the Efficiency of Organic Bulk Heterojunction Solar Cells, Proc. 22nd European Photovolt. Sol. Energy Conf. Milano, September, pp. 498–501, 2007.

[16] J. Kim, J. H. Kim, and K. Ariga, Redox-Active Polymers for Energy Storage Nanoarchitectonics, Joule, vol. 1, no. 4, pp. 739–768, 2017.

[17] H. J. Hwang, S. J. Joo, S. A. Patil, and H. S. Kim, Efficiency Enhancement in Dye-

Sensitized Solar Cells Using the Shape/Size-Dependent Plasmonic Nanocomposite Photoanodes İncorporating Silver Nanoplates, Nanoscale, vol. 9, no. 23, pp. 7960–7969, 2017.

[18] W. McCartney, H. A., Unsworth, Spectral Distribution of Solar Radiation. I: Direct Radiation, Quart. J. R. Met. Soc., vol. 204, pp. 699–718, 1978.

[19] D. M. E. Ocak, Güneş Enerjisinin Kaynağı Nedir?, Retrieved March 20, 2019 from http://www.bilimgenc.tubitak.gov.tr/makale/gunes-enerjisinin-kaynagi-nedir., June 2019.

[20] NREL, Solar Spectra: Air Mass Zero, Retrieved March 21, 2019 from https://rredc.nrel.gov/solar//spectra/am0/, June 2019.

[21] J. Fröhlich, C. , Lean, Solar Radiative Output and Its Variability: Evidence And Mechanisms, Astron. Astrophys. Rev., vol. 12, pp. 273–320, 2004.

[22] Yuri Mun, Overview of Earth Radiation Budget, Retrieved March 24, 2019 from https://marine.rutgers.edu/cool/education/class/yuri/erb.html., 1998.

[23] NREL, Solar Radiation Research Laboratory, Retrieved March 26, 2019 from https://www.nrel.gov/esif/solar-radiation-research-laboratory.html., June 2019.

[24] G. Oliveti, L. Marletta, N. Arcuri, M. De Simone, R. Bruno, and G. Evola, Solar Energy, pp. 159–214, 2014.

[25] S. Dagher, PbS Quantum Dot-Based Hetrojunction Solar Cells, Master's Thesis, 2014.

[26] P. Kadar, Solar Belt Supplies Electricity for the World, vol. 1. 2017.

[27] K. Ranabhat, L. Patrikeev, A. A. Revina, K. Andrianov, V. Lapshinsky, and E. Sofronova, An Introduction to Solar Cell Technology, vol. 14. 2016.

[28] S. Öksüz, Güneş Enerjisi Sistemleri Temel Prensipler, TMMOB Makina Mühendisleri Odası, 2014.

[29] U. Gürsoy, Dikensiz Gül: Temiz Enerji, 1999.

[30] K. S. El-Refı, Dye-Sensitized Solar Cells Using $TiO_2$ as a Semiconducting Layer, 023, pp. 7–12, 2013.

[31] ABC Solar Enerji Elektrik Üretim Sistemleri San.Ve Tic.Ltd.Şti., Solar Enerji Sistemleri, Retrieved March 27, 2019 from //www.abcsolarenerji.com/, June 2019.

[32] J. M. Nunzi, Organic Photovoltaic Materials and Devices, Comptes Rendus Phys., vol. 3, no. 4, pp. 523–542, 2002.

[33] E. Becquerél, Mémoire Sure les Effets Électriques Produits Ous L'influence des Rayons Solaires, Comptes Rendues, vol. 6, p. 561, 1839.

[34] R. E. Adams, W.G., Day, On the Action of Light on Selenium, Proc. R. Soc.

London, vol. 25, pp. 113–117, 1876.

[35] R. S. Ohl, Light-Sensitive Electric Device, 1941.

[36] Chapin et al, A New Silicon p-n Junction Photocell for Converting Solar Radiation into Electrical Power, J. Appl. Phys., vol. 25, pp. 676–677, 1954.

[37] R. L. Easton and M. J. Votaw, Vanguard I IGY satellite (1958 beta), vol. 30. 1959.

[38] L. L. Kazmerski, Solar Photovoltaics R&D at the Tipping Point: A 2005 Technology Overview, vol. 150. 2006.

[39] The National Renewable Energy Laboratory, Best Research- Cell Efficiencies, 2014.

[40] B. O'Regan and M. Grätzel, A Low-Cost, High-Efficiency Solar Cell Based on Dye-Sensitized Colloidal $TiO_2$ Films, Nature, vol. 353, no. 6346, pp. 737–740, 1991.

[41] A. Goetzberger and C. Hebling, Photovoltaic Materials, Past, Present, Future, vol. 62. 2000.

[42] H. Cotal et al., III-V Multijunction Solar Cells for Concentrating Photovoltaics, vol. 2. 2009.

[43] J. Halme, Dye-Sensitized Nanostructured and Organic Photovoltaic ,Cells: Technical Review and Preliminary Tests, Helsinki University Of Technology, 2002.

[44] H. Jun, M. Careem, and A. K. Arof, Quantum Dot-Sensitized Solar Cells—Perspective and Recent Developments: A Review of Cd Chalcogenide Quantum Dots as Sensitizers, vol. 22. 2013.

[45] N. S. Sarıçiftçi, L. Smilowitz, A. J. Heeger, and F. A. Wudl, Photoinduced Electron Transfer from a Conducting Polymer to Buckminsterfullerene, vol. 258. 1992.

[46] N. S. Lewis, Solar Energy Use, Science, vol. 798, no. 2007, pp. 798–801, 2012.

[47] B. Minnaert and P. Veelaert, Guidelines for the Bandgap Combinations and Absorption Windows for Organic Tandem and Triple-Junction Solar Cells, Materials (Basel), vol. 5, no. 10, pp. 1933–1953, 2012.

[48] J. Weickert, R. B. Dunbar, H. C. Hesse, W. Wiedemann, and L. Schmidt-Mende, Nanostructured Organic and Hybrid Solar Cells, Adv. Mater., vol. 23, no. 16, pp. 1810–1828, Apr. 2011.

[49] G. Teran-Escobar et al., On the Stability of a Variety of Organic Photovoltaic Devices by IPCE and in situ IPCE analyses – the ISOS-3 Inter-Laboratory Collaboration, Phys. Chem. Chem. Phys., vol. 14, no. 33, pp. 11824–11845, 2012.

[50] X. Zhan and D. Zhu, Conjugated Polymers for High-Efficiency Organic Photovoltaics, Polym. Chem., vol. 1, no. 4, pp. 409–419, 2010.

[51] Y. Zhou et al., Recyclable Organic Solar Cells on Cellulose Nanocrystal Substrates, Sci. Rep., vol. 3, p. 1536, Mar. 2013.

[52] J. Burschka et al., Sequential Deposition as a Route to High-Performance Perovskite-Sensitized Solar Cells, Nature, vol. 499, p. 316, Jul. 2013.

[53] M. M. Lee, J. Teuscher, T. Miyasaka, T. N. Murakami, and H. J. Snaith, Efficient Hybrid Solar Cells Based on Meso-Superstructured Organometal Halide Perovskites, Science, vol. 338, no. 6107, p. 643 LP-647, Nov. 2012.

[54] P. Docampo, J. M. Ball, M. Darwich, G. E. Eperon, and H. J. Snaith, Efficient Organometal Trihalide Perovskite Planar-Heterojunction Solar Cells On Flexible Polymer Substrates, Nat. Commun., vol. 4, pp. 1–6, 2013.

[55] N.-G. Park, Organometal Perovskite Light Absorbers Toward a 20% Efficiency Low-Cost Solid-State Mesoscopic Solar Cell, J. Phys. Chem. Lett., vol. 4, no. 15, pp. 2423–2429, Aug. 2013.

[56] N. J. Jeon et al., Compositional Engineering of Perovskite Materials for High-Performance Solar Cells, Nature, vol. 517, p. 476, Jan. 2015.

[57] L. Yang, A. Barrows, D. Lidzey, and T. Wang, Recent Progress and Challenges Of Organometal Halide Perovskite Solar Cells, vol. 79. 2016.

[58] B. E. Hardin, H. J. Snaith, and M. D. McGehee, The renaissance of dye-sensitized solar cells, Nat. Photonics, vol. 6, p. 162, Feb. 2012.

[59] V. Sugathan, E. John, and K. Sudhakar, Recent Improvements in Dye Sensitized Solar Cells: A review, vol. 52. 2015.

[60] A. Hagfeldt, G. Boschloo, L. Sun, L. Kloo, and H. Pettersson, Dye-Sensitized Solar Cells, Chem. Rev., vol. 110, no. 11, pp. 6595–6663, Nov. 2010.

[61] G. H. Carey, A. L. Abdelhady, Z. Ning, S. M. Thon, O. M. Bakr, and E. H. Sargent, Colloidal Quantum Dot Solar Cells, Chem. Rev., vol. 115, no. 23, pp. 12732–12763, Dec. 2015.

[62] P. V Kamat, Quantum Dot Solar Cells. Semiconductor Nanocrystals as Light Harvesters, J. Phys. Chem. C, vol. 112, no. 48, pp. 18737–18753, Dec. 2008.

[63] J. Duan, H. Zhang, Q. Tang, B. He, and L. Yu, Recent Advances in Critical Materials for Quantum Dot-Sensitized Solar Cells: A Review, J. Mater. Chem. A, vol. 3, no. 34, pp. 17497–17510, 2015.

[64] K. Ebrahim, Dye Sensitized Solar Cells - Working Principles, Challenges and Opportunities, Sol. Cells - Dye. Devices, 2012.

[65] D. J. Coyle et al., Life Prediction for CIGS Solar Modules Part 2, Prog. Photovoltaics, no. October 2011, pp. 156–172, 2013.

[66] M. K. Nazeeruddin et al., Engineering of Efficient Panchromatic Sensitizers for Nanocrystalline $TiO_2$-Based Solar Cells, J. Am. Chem. Soc., vol. 123, no. 8, pp.

1613–1624, Feb. 2001.

[67] LPI Laboratory of Photonics and Interfaces, Prof. Michael Graetzel, Retrieved April 5, 2019 from https://www.epfl.ch/labs/lpi/graetzel/, June 2019.

[68] R. Ameta, S. Benjamin, S. Sharma, and M. Trivedi, Dye-Sensitized Solar Cells, Sol. Energy Convers. Storage Photochem. Modes, vol. 4, pp. 85–113, 2015.

[69] R. Sastrawan, Photovoltaic Modules of Dye Solar Cells, 2006.

[70] C. Granqvist, Transparent Conductors as Solar Energy Materials: A Panoramic Review, vol. 91. 2007.

[71] T. Stergiopoulos, I. Arabatzis, H. Cachet, and P. Falaras, Photoelectrochemistry at $SnO_2$ Particulate Fractal Electrodes Sensitized by a Ruthenium Complex: Solid-State Solar Cell Assembling vy İncorporating a Composite Polymer Electrolyte, vol. 155. 2003.

[72] H. Rensmo et al., High Light-to-Energy Conversion Efficiencies for Solar Cells Based on Nanostructured ZnO Electrodes, vol. 101. 1997.

[73] I. K. Konstantinou and T. A. Albanis, $TiO_2$-Assisted Photocatalytic Degradation of Azo Dyes in Aqueous Solution: Kinetic and Mechanistic Investigations: A Review, Appl. Catal. B Environ., vol. 49, no. 1, pp. 1–14, 2004.

[74] M. Grätzel, Dye-Sensitized Solar Cells, J. Photochem. Photobiol. C Photochem. Rev., vol. 4, no. 2, pp. 145–153, 2003.

[75] S. Hao, J. Wu, Y. Huang, and J. Lin, Natural Dyes as Photosensitizers for Dye-Sensitized Solar Cell, vol. 80. 2006.

[76] M. Zayat, P. Garcia-Parejo, and D. Levy, Preventing UV-Light Damage of Light Sensitive Materials Using a Highly Protective UV-Absorbing Coating, Chem. Soc. Rev., vol. 36, no. 8, pp. 1270–1281, 2007.

[77] J. Mikroyannidis, P. Suresh, M. S. Roy, and G. Sharma, Triphenylamine- and Benzothiadiazole-Based Dyes With Multiple Acceptors for Application in Dye-Sensitized Solar Cells, vol. 195. 2010.

[78] M. Grätzel, Solar Energy Conversion by Dye-Sensitized Photovoltaic Cells, Inorg. Chem., vol. 44, no. 20, pp. 6841–6851, 2005.

[79] M. Wang et al., An Organic Redox Electrolyte to Rival Triiodide/Iodide in Dye-Sensitized Solar Cells, Nat. Chem., vol. 2, p. 385, Apr. 2010.

[80] I. Chung, B. Lee, J. He, R. P. H. Chang, and M. G. Kanatzidis, All-Solid-State Dye-Sensitized Solar Cells with High Efficiency, Nature, vol. 485, p. 486, May 2012.

[81] G. Wolfbauer, A. M. Bond, J. C. Eklund, and D. R. MacFarlane, A Channel Flow Cell System Specifically Designed to Test the Efficiency of Redox Shuttles in Dye Sensitized Solar Cells, vol. 70. 2001.

[82] S. Nakade, Y. Makimoto, W. Kubo, T. Kitamura, Y. Wada, and S. Yanagida, Roles of Electrolytes on Charge Recombination in Dye-Sensitized $TiO_2$ Solar Cells (2): The Case of Solar Cells Using Cobalt Complex Redox Couples, J. Phys. Chem. B, vol. 109, no. 8, pp. 3488–3493, Mar. 2005.

[83] H. Pettersson et al., The Monolithic Multicell: A Tool for Testing Material Components in Dye-Sensitized Solar Cells, vol. 15. 2007.

[84] Y. Saito, W. Kubo, T. Kitamura, Y. Wada, and S. Yanagida, I-/$I_3$- Redox Reaction Behavior on Poly (3,4-Ethylenedioxythiophene) Counter Electrode in Dye-Sensitized Solar Cells, vol. 164. 2004.

[85] X. Fang, T. Ma, G. Guan, M. Akiyama, T. Kida, and E. Abe, Eff ect of the Thickness of the Pt film Coated on a Counter Electrode on the Performance of a Dye-Sensitized Solar Cell, vol. 570. 2004.

[86] N. Papageorgiou, W. F. Maier, and M. Gratzel, An Iodine/Triiodide Reduction Electrocatalyst for Aqueous and Organic Media, vol. 144. 1997.

[87] P. E. F. J. Himpsel, New Materials for Solar Cells. Retrieved From: http://uw.physics.wisc.edu/~himpsel/solar.html.

[88] S. Sakka, Handbook of Sol-Gel Science and Technology, 3rd ed. Springer Science & Business Media, 2005.

[89] G. K. Mor, O. Varghese, M. Paulose, K. Shankar, and C. A. Grimes, A Review on Highly Ordered, Vertically Oriented $TiO_2$ Nanotube Arrays: Fabrication, Material Properties, and Solar Energy Applications, vol. 90. 2006.

[90] Dyenamo AB, Metal-Organic Sensitizing Dyes, Retrieved April 16, 2019 from https://dyenamo.se/dyenamo_metal-organic-dyes.php, June 2019.

[91] D.-B. Kuang et al., High- Efficiency and Stable Mesoscopic Dye- Sensitized Solar Cells Based on a High Molar Extinction Coefficient Ruthenium Sensitizer and Nonvolatile Electrolyte, vol. 19. 2007.

[92] M. Nazeeruddin, E. Baranoff, and M. Grätzel, Dye-Sensitized Solar Cells: A Brief Overview, vol. 85. 2011.

[93] M. Junghänel, Novel Aqueous Electrolyte Films for Hole Conduction in Dye Sensitized Solar Cells And Development Of An Electron Transport Model, Pharmazie, no. September, 2007.

[94] C. Bauer, G. Boschloo, E. Mukhtar, and A. Hagfeldt, Interfacial Electron-Transfer Dynamics in Ru(tcterpy)$(NCS)_3$-Sensitized $TiO_2$ Nanocrystalline Solar Cells, J. Phys. Chem. B, vol. 106, no. 49, pp. 12693–12704, Dec. 2002.

[95] Z. Kebede and S.-E. Lindquist, Donor–Acceptor Interaction Between Non-Aqueous Solvents and $I_2$ To Generate $I_3$, And Its Implication in Dye Sensitized Solar Cells, vol. 57. 1999.

[96] Y. Tachibana, J.-E. Moser, M. Graetzel, D. Klug, and J. R Durrant, Subpicosecond

Interfacial Charge Separation in Dye-Sensitized Nanocrystalline Titanium Dioxide Films, vol. 100. 1996.

[97] J. B. Asbury, R. Ellingson, H. Ghosh, S. Ferrere, A. Nozik, and T. Lian, Femtosecond IR Study of Excited-State Relaxation and Electron-Injection Dynamics of $Ru(dcbpy)_2(NCS)_2$ in Solution and on Nanocrystalline $TiO_2$ and $Al_2O_3$ Thin Films, vol. 103. 1999.

[98] G. Benkö, J. Kallioinen, J. Korppi-Tommola, A. Yartsev, and V. Sundström, Photoinduced Ultrafast Dye-to-Semiconductor Electron Injection from Nonthermalized and Thermalized Donor States, vol. 124. 2002.

[99] H. D. Holland, K. K. Turekian, and B. S. Lollar, Treatise on Geochemistry Volume 9: Environmental Geochemistry. Elsevier, 2004.

[100] A. J. Frank, N. Kopidakis, and J. van de Lagemaat, Electrons in Nanostructured $TiO_2$ Solar Cells: Transport, Recombination and Photovoltaic Properties, vol. 248. 2004.

[101] J. Krüger, Interface Engineering In Solid-State Dye-Sensitized Solar Cells, École Polytech. Fédérale Lausanne, vol. 2793, p. 153, 2003.

[102] H. Hafez, Z. Lan, Q. Li, and J. Wu, High Efficiency Dye-Sensitized Solar Cell Based on Novel $TiO_2$ Nanorod/Nano-particle Bilayer Electrode, Nanotechnol. Sci. Appl., vol. 3, no. 1, pp. 45–51, 2010.

[103] S. J. Fonash, Solar Cell Device Physics - Acknoledgements, p. 309, 2010.

[104] C. Julian Chen, Physics of Solar Energy. Hoboken, New Jersey: John Wiley & Sons, Inc., 2011.

[105] Z. K. Yıldız, $TiO_2$ Based Dye Sensitized Solar Cells Obtained by Sol-Gel Method, Master's Thesis, Ankara Yıldırım Beyazıt University, 2018.

[106] A. Hagfeldt and M. Graetzel, Light-Induced Redox Reactions in Nanocrystalline Systems, Chem. Rev., vol. 95, no. 1, pp. 49–68, Jan. 1995.

[107] M. Grätzel, Photoelectrochemical Cells, Nature, vol. 414, no. 6861, pp. 338–344, 2001.

[108] J. Taylor, Modern Physics for Scientists and Engineers, second edition. Upper Saddle River, N.J.: Pearson/Prentice Hall., 2004.

[109] B. Sernelius, K. Berggren, Z.-C. Jin, I. Hamberg, and C. Granqvist, Band-Gap Tailoring of ZnO by Means of Heavy Al Doping, vol. 37. 1988.

[110] A. W. Bott and D. Ph, Cs-17-3D, vol. 3, pp. 1–5, 2000.

[111] Krishnan Rajeshwar, Fundamentals of Semiconductor Electrochemistry and Photoelectrochemistry, Encycl. Electrochem., 2007.

[112] Chenming Hu, Modern SemiconIductor Devices for Integrated Circuits - Chapter 5

MOS Capacitor, p. 38, 2009.

[113] R. Melikov, Protein Integrated Light-Emitting Diodes, 2016.

[114] N. M. Gao, W., & Sammes, An Introduction to Electronic and Ionic Materials, River Edge: N.J: World Scientific, 1999.

[115] E. Burstein, Anomalous Optical Absorption Limit in InSb, Phys. Rev., vol. 93, no. 3, pp. 632–633, Feb. 1954.

[116] K. Kalyanasundaram and M. Grätzel, aChemInform Abstract: Applications of Functionalized Transition Metal Complexes in Photonic and Optoelectronic Devices, vol. 177. 1998.

[117] S. Ito et al., High-Efficiency (7.2%) Flexible Dye-Sensitized Solar Cells With Ti-Metal Substrate for Nanocrystalline-$TiO_2$ Photoanode, vol. 38. 2006.

[118] S. P. Lim, H. Ming, H. Lim, and M. Mazhar, Aerosol Assisted Chemical Vapour Deposited (AACVD) Of $TiO_2$ Thin Film as Compact Layer For Dye-Sensitised Solar Cell, vol. 40. 2014.

[119] E. E. Gökgöz, Renklendirilmiş Organik-$TiO_2$ ile Kaplanmış Camların Yapısal, Optik ve Elektriksel Özelliklerinin İncelenmesi, Süleyman Demirel Üniversitesi, 2010.

[120] C. P. Richter, Titania Nanotubes for Solar Energy and Catalysis, Doctor of Philosophy in Chemical Engineering, Northeastern University., 2008.

[121] A. Fujishima, T. N. Rao, and D. A. Tryk, Titanium Dioxide Photocatalysis, J. Photochem. Photobiol. C Photochem. Rev., vol. 1, no. 1, pp. 1–21, 2000.

[122] Z. Çolak, Anodik Oksidasyon Yöntemi İle Üretilen Titanyum OksitNanotüplerin Hidrojen Algılama Özelliklerinin İncelenmesi, Gebze İleri Teknoloji Enstitüsü., 2008.

[123] A. Fujıshıma and K. Honda, Electrochemical Photolysis of Water at a Semiconductor Electrode, Nature, vol. 238, no. 5358, pp. 37–38, 1972.

[124] J. Rino and N. Studart, Structural Correlations in Titanium Dioxide, vol. 59. 1999.

[125] L. Kavan, M. Grätzel, S. E. Gilbert, C. Klemenz, and H. J. Scheel, Electrochemical and Photoelectrochemical Investigation of Single-Crystal Anatase, J. Am. Chem. Soc., vol. 118, no. 28, pp. 6716–6723, Jan. 1996.

[126] U. Diebold, The Surface Science of Titanium Dioxide, vol. 48. 2003.

[127] S. mo and W. Ching, Electronic and Optical Properties of Three Phases of Titanium Dioxide: Rutile, Anatase, and Brookite, vol. 51. 1995.

[128] Y. Chang, Supported $TiO_2$ Photocatalysts Synthesis and Some Applications to Water Purification, University of Calgary, 2004.

[129] R. M. and Ana Pimentel, Daniela Nunes, Sónia Pereira and E. Fortunato, Photocatalytic Activity of $TiO_2$ Nanostructured Arrays Prepared by Microwave-Assisted Solvothermal Method, Semiconductor Photocatalysis - Materials, Mechanisms and Applications, 2016.

[130] O. Caep, C. L. Huisman, and A. Reller, Photoinduced Reactivity of Titanium Dioxide, vol. 32. 2004.

[131] A. Erdem, Short-Term Toxicity of Photocatalytic Titanium Dioxide to Bacteria Under Ambient Conditions, Delaware University, 2008.

[132] G. M. Murphy, Sunblocks : Mechanisms of Action, pp. 34–36, 1999.

[133] Photocatalysis and Water Purification. From Fundamentals to Recent Applications, Retrieved April 19, 2019 from https://download.e-bookshelf.de/download/0003/7378/11/L-X-0003737811-0002059926.XHTML/index.xhtml, June 2019.

[134] K. Nakata and A. Fujishima, $TiO_2$ Photocatalysis: Design and Applications, J. Photochem. Photobiol. C Photochem. Rev., vol. 13, no. 3, pp. 169–189, 2012.

[135] B. Ohtani, K. Iwai, H. Kominami, T. Matsuura, Y. Kera, and S. ichi Nishimoto, Titanium-Oxide Photocatalyst, Three Bond Tech. News, vol. 62, pp. 1–3, 2004.

[136] K. Michael. Schindler and M. Kunst, Charge-Carrier Dynamics in $TiO_2$ Powders, vol. 94. 1990.

[137] X. Chen, Titanium Dioxide Nanomaterials and Their Energy Applications, vol. 30. 2009.

[138] A. Fujishima, X. Zhang, and D. Tryk, $TiO_2$ Photocatalysis and Related Surface Phenomena, vol. 63. 2008.

[139] N. Hafizah and I. Sopyan, Nanosized $TiO_2$ Photocatalyst Powder via Sol-Gel Method: Effect of Hydrolysis Degree on Powder Properties. 2009.

[140] W. Zhang, T. Zhang, W. Yin, and G. Cao, Relationship Between Photocatalytic Activity and Structure of $TiO_2$ Thin Film, vol. 20. 2007.

[141] T. Luttrell, S. Halpegamage, J. Tao, A. Kramer, E. Sutter, and M. Batzill, Why is Anatase a Better Photocatalyst Than Rutile? - Model Studies on Epitaxial $TiO_2$ Films, Sci. Rep., vol. 4, p. 4043, Feb. 2014.

[142] Y. Kakuma, A. Y. Nosaka, and Y. Nosaka, Difference in $TiO_2$ Photocatalytic Mechanism Between Rutile and Anatase Studied by the Detection of Active Oxygen and Surface Species in Water, Phys. Chem. Chem. Phys., vol. 17, no. 28, pp. 18691–18698, 2015.

[143] S. K. Deb, Dye-Sensitized $TiO_2$ Thin-Film Solar Cell Research at the National Renewable Energy Laboratory (NREL), vol. 88. 2005.

[144] M. Dürr, S. Rosselli, A. Yasuda, and G. Nelles, Band-Gap Engineering of Metal

Oxides for Dye-Sensitized Solar Cells, J. Phys. Chem. B, vol. 110, no. 43, pp. 21899–21902,. 2006.

[145] S. Nakade, Y. Saito, W. Kubo, T. Kitamura, Y. Wada, and S. Yanagida, Influence of $TiO_2$ Nano-particle Size on Electron Diffusion and Recombination in Dye-Sensitized $TiO_2$ Solar Cells, vol. 107. 2003.

[146] J. Zhang, P. Zhou, J. Liu, and J. Yu, New Understanding of the Difference of Photocatalytic Activity Among Anatase, Rutile and Brookite $TiO_2$, Phys. Chem. Chem. Phys., vol. 16, no. 38, pp. 20382–20386, 2014.

[147] J. Macak et al., $TiO_2$ Nanotubes: Self-Organized Electrochemical Formation, Properties and Applications, vol. 11. 2007.

[148] S. Caillol, Fighting global warming: The Potential of Photocatalysis Against $CO_2$, $CH_4$, $N_2O$, CFCs, Tropospheric $O_3$, BC and Other Major Contributors to Climate Change, vol. 12. 2011.

[149] S. Banerjee, J. Gopal, P. Muraleedharan, A. K. Tyagi, and B. Raj, Physics and Chemistry of Photocatalytic Titanium Dioxide: Visualization of Bactericidal Activity Using Atomic Force Microscopy, vol. 90. 2006.

[150] X. Feng, Q. Wang, G. Wang, And F. Qıu, Preparation of Nano-$TiO_2$ by Ethanol-Thermal Method and Its Catalytic Performance for Synthesis of Dibutyl Carbonate by Transesterification, Chinese J. Catal., vol. 27, no. 3, pp. 195–196, 2006.

[151] Z. A. Shah, K. Zaib, and A. Khan, Fundamentals of Renewable Energy and Applications Dye Sensitized Solar Cells Based on Different Solvents : Comparative Study, vol. 7, no. 4, pp. 4–6, 2017.

[152] G. Niu, W. Li, J. Li, X. Liang, and L. Wang, Enhancement of Thermal Stability for Perovskite Solar Cells Through Cesium Doping, RSC Adv., vol. 7, no. 28, pp. 17473–17479, 2017.

[153] A. Kogo, Y. Sanehira, M. Ikegami, and T. Miyasaka, Brookite $TiO_2$ as a Low-Temperature Solution-Processed Mesoporous Layer for Hybrid Perovskite Solar Cells, J. Mater. Chem. A, vol. 3, no. 42, pp. 20952–20957, 2015.

[154] D. P. MacWan, P. N. Dave, and S. Chaturvedi, A Review on Nano-$TiO_2$ Sol-Gel Type Syntheses and Its Applications, J. Mater. Sci., vol. 46, no. 11, pp. 3669–3686, 2011.

[155] P. Nyamukamba, O. Okoh, H. Mungondori, R. Taziwa, and S. Zinya, Synthetic Methods for Titanium Dioxide Nano-particles: A Review, Titan. Dioxide - Mater. a Sustain. Environ., no. June 2018, 2018.

[156] M. T. Noman, M. A. Ashraf, and A. Ali, Synthesis and Applications of Nano-$TiO_2$: a Review, Environ. Sci. Pollut. Res., vol. 26, no. 4, pp. 3262–3291, 2019.

[157] X. Chen and S. S. Mao, Titanium Dioxide Nanomaterials: Synthesis, Properties, Modifications, and Applications, Chem. Rev., vol. 107, no. 7, pp. 2891–2959, Jul. 2007.

[158] C.-C. Wang and J. Y. Ying, Sol−Gel Synthesis and Hydrothermal Processing of Anatase and Rutile Titania Nanocrystals, Chem. Mater., vol. 11, no. 11, pp. 3113–3120, Nov. 1999.

[159] K. Sahu and V. V. S. Murty, Novel Sol Gel Method of Synthesis of Pure and Aluminium Doped $TiO_2$ Nano Particles Useful for Dye Sensitized Solar Cell Applications, vol. 2, pp. 567–571, 2015.

[160] M. Geetha, K. Suguna, and P. M. Anbarasan, Photoanode Modification in DSSC Using Chromium Doped $TiO_2$ Nano-particles by Sol-Gel Method, Arch. Phys. Res., vol. 3, no. 4, pp. 303–308, 2012.

[161] E. M. Jin, S. M. Jeong, H.-C. Kang, and H.-B. Gu, Photovoltaic Effect of Metal-Doped $TiO_2$ Nano-particles for Dye-Sensitized Solar Cells, ECS J. Solid State Sci. Technol., vol. 5, no. 5, pp. Q109–Q114, 2016.

[162] E. M. Jin et al., Sol–Gel Synthesized Mesoporous Anatase Titanium Dioxide Nano-particles for Dye Sensitized Solar Cell (DSSC) Applications, J. Mater. Sci. Mater. Electron., vol. 38, no. 37, pp. 16380–16386, Aug. 2018.

[163] I. Chan Baek et al., Facile Preparation of Large Aspect Ratio Ellipsoidal Anatase $TiO_2$ Nano-Particles and Their Application to Dye-Sensitized Solar Cell, vol. 11. 2009.

[164] C. Wook Oh, G. D. Lee, S. Park, C.-S. Ju, and S.-S. Hong, Synthesis of Nanosized $TiO_2$ Particles via Ultrasonic Irradiation and Their Photocatalytic Activity, vol. 85. 2005.

[165] J. Cai et al., Hydrogen Production: Light-Driven Sustainable Hydrogen Production Utilizing $TiO_2$ Nanostructures: A Review, Small Methods, vol. 3, no. 1, p. 1800053, 2019.

[166] J. Jiu, S. Isoda, M. Adachi, and F. Wang, Preparation of $TiO_2$ Nanocrystalline with 3-5 nm and Application for Dye-Sensitized Solar Cell, J. Photochem. Photobiol. A Chem., vol. 189, no. 2–3, pp. 314–321, 2007.

[167] S. Chang and R. Doong, Characterization of Zr-Doped $TiO_2$ Nanocrystals Prepared by a Nonhydrolytic Sol−Gel Method at High Temperatures, J. Phys. Chem. B, vol. 110, no. 42, pp. 20808–20814, Oct. 2006.

[168] T. Trentler, T. E. Denler, J. F. Bertone, and Aarti Agrawal, and V. Colvin, Synthesis of $TiO_2$ Nanocrystals by Nonhydrolytic Solution-Based Reactions, vol. 121. 1999.

[169] P. Arnal, R. J. P. Corriu, D. Leclercq, P. Mutin, and A. Vioux, A Solution Chemistry Study of Nonhydrolytic Sol−Gel Routes to Titania, vol. 9. 1997.

[170] H. Parala, A. Devi, R. Bhakta, and R. A. Fischer, Synthesis of Nano-Scale $TiO_2$ Particles by a Nonhydrolytic Approach, vol. 12. 2002.

[171] P. Arnal, R. J. P. Corriu, D. Leclercq, P. Mutin, and A. Vioux, Preparation of Anatase, Brookite and Rutile at Low Temperature By Non-Hydrolytic Sol-Gel Methods, vol. 6. 1996.

[172] A. Arkhireeva et al., Synthesis of Organic-Inorganic Hybrid Particles by Sol-Gel Chemistry, J. Sol-Gel Sci. Technol., vol. 31, no. 1, pp. 31–36, 2004.

[173] D. V Bavykin, V. N. Parmon, A. A. Lapkin, and F. C. Walsh, The effect of hydrothermal conditions on the mesoporous structure of $TiO_2$ nanotubes, J. Mater. Chem., vol. 14, no. 22, pp. 3370–3377, 2004.

[174] M. Qamar et al., Preparation of Titanium Oxide Nanotube by Hydrothermal Process, vol. 124–126. 2007.

[175] Y. Q. Wang, G. Q. Hu, X. F. Duan, H. L. Sun, and Q. K. Xue, Microstructure and Formation Mechanism of Titanium Dioxide Nanotubes, Chem. Phys. Lett., vol. 365, no. 5, pp. 427–431, 2002.

[176] A. Hegazy, N. Kinadjian, B. Sadeghimakki, S. Sivoththaman, N. K. Allam, and E. Prouzet, $TiO_2$ Nano-particles Optimized for Photoanodes Tested in Large Area Dye-Sensitized Solar Cells (DSSC), vol. 153. 2016.

[177] F. Xie, J. Wang, Y. Li, J. Dou, and M. Wei, One-Step Synthesis of Hierarchical $SnO_2$ /$TiO_2$ Composite Hollow Microspheres As An Efficient Scattering Layer For Dye-Sensitized Solar Cells, Electrochim. Acta, vol. 296, pp. 142–148, 2019.

[178] J. Xue et al., Controlling Self-Assembly of Cellulose Nanocrystal to Synergistically Regulate (001) Reactive Facets and Hierarchical Pore Structure of Anatase Nano-$TiO_2$ for High Photocatalytic Activity, ACS Sustain. Chem. Eng., vol. 7, no. 2, pp. 1973–1979, 2019.

[179] V. M. Ramakrishnan, M. Natarajan, A. Santhanam, V. Asokan, and D. Velauthapillai, Size Controlled Synthesis of $TiO_2$ Nano-particles by Modified Solvothermal Method Towards Effective Photo Catalytic and Photovoltaic Applications, Mater. Res. Bull., vol. 97, pp. 351–360, 2018.

[180] X. Wang, J. Zhuang, Q. Peng, and Y. Li, A General Strategy for Nanocrystal Synthesis, Nature, vol. 437, no. 7055, pp. 121–124, 2005.

[181] K. Kalaga, V. A. Pai, V. R. Marathe, M. Sharon, and M. Mishra, A Theoretical Approach to the Design of Reduced Band Gap Noncorrosive Electrodes for Photoelectrochemical Solar Cells, vol. 38. 1990.

[182] E. Bayraktar, Nano Yapıda Demir Bileşiklerinin Üretimi, Master's Thesis, 2006.

[183] D. Zhang, L. Qi, J. Ma, and H. Cheng, Formation of Crystalline Nanosized Titania in Reverse Micelles at Room Temperature, vol. 12. 2002.

[184] S. Pratsinis, Flame Aerosol Synthesis of Ceramic Powders, vol. 24. 1998.

[185] A. Kumar, Different Methods Used for the Synthesis of $TiO_2$ Based Nanomaterials: A Review, vol. 6. 2018.

[186] J. Deng, M. Wang, J. Fang, X. Song, Z. Yang, and Z. Yuan, Synthesis of Zn-Doped $TiO_2$ Nano-Particles Using Metal Ti and Zn as Raw Materials and Application in Quantum Dot Sensitized Solar Cells, J. Alloys Compd., vol. 791, pp. 371–379,

2019.

[187] A. Gardecka et al., High Efficiency Water Splitting Photoanodes Composed of Nano-Structured Anatase-Rutile $TiO_2$ Heterojunctions by Pulsed-Pressure MOCVD, vol. 224. 2017.

[188] Y. Cao, W. Yang, W. Zhang, G. Liu, and P. Yue, Improved Photocatalytic Activity Of $Sn_4^+$ Doped $TiO_2$ Nanoparticulate Films Prepared by Plasma-Enhanced Chemical Vapor Deposition, New J. Chem., vol. 28, no. 2, pp. 218–222, 2004.

[189] J. Kim, J. W. Lee, T. Gyu Lee, S. Woo Nam, and J. Han, Nanostructured Titania Membranes with Improved Thermal Stability, vol. 40. 2005.

[190] M. E. Stewart et al., Nanostructured Plasmonic Sensors, Chem. Rev., vol. 108, no. 2, pp. 494–521, 2008.

[191] H. A. Atwater, S. Maier, A. Polman, J. A. Dionne, and L. Sweatlock, The New 'p–n Junction': Plasmonics Enables Photonic Access to the Nanoworld, MRS Bull., vol. 30, no. 5, pp. 385–389, 2005.

[192] C. F. Bohren, How Can a Particle Absorb More Than the Light Incident on it?, vol. 51. 1983.

[193] S. Maier, P. Barclay, T. J. Johnson, M. D. Friedman, and O. Painter, Low-Loss Fiber Accessible Plasmon Waveguide for Planar Energy Guiding and Sensing, vol. 84. 2004.

[194] M. Cortie, X. Xu, H. Chowdhury, H. Zareie, and G. Smith, Plasmonic heating of gold nano-particles and its exploitation, vol. 5649. 2004.

[195] W. L. Barnes, A. Dereux, and T. W. Ebbesen, Surface Plasmon Subwavelength Optics, Nature, vol. 424, no. 6950, pp. 824–830, 2003.

[196] S. A. Maier et al., Local Detection of Electromagnetic Energy Transport Below the Diffraction Limit in Metal Nano-particle Plasmon Waveguides, Nat. Mater., vol. 2, no. 4, pp. 229–232, 2003.

[197] B. Pettinger, B. Ren, G. Picardi, R. Schuster, and G. Ertl, Nanoscale Probing of Adsorbed Species by Tip-Enhanced Raman Spectroscopy, Phys. Rev. Lett., vol. 92, no. 9, p. 96101, Mar. 2004.

[198] Z. Xie et al., Plasmonic Nanolithography: A Review, vol. 6. 2011.

[199] J. M. Brockman, B. P. Nelson, and R. Corn, Brockman JM, Nelson BP, and Corn RM. Surface plasmon Resonance İmaging Measurements of Ultrathin Organic Films Annu Rev Phys Chem 51: 41-63, vol. 51. 2000.

[200] J. Yguerabide and E. E. Yguerabide, Light-Scattering Submicroscopic Particles as Highly Fluorescent Analogs and Their Use as Tracer Labels in Clinical and Biological Applications: I. Theory, vol. 262. 1998.

[201] L. J. Sherry, S.-H. Chang, G. C. Schatz, R. P. Van Duyne, B. J. Wiley, and Y. Xia,

Localized Surface Plasmon Resonance Spectroscopy of Single Silver Nanocubes, Nano Lett., vol. 5, no. 10, pp. 2034–2038, 2005.

[202] E. Gür, A. Baltakesmez, S. Tüzemen, and A. Yenisoy, Improved Growth Quality of the ZnO Thin Films on Au Nano-Particles/p-Si, IEEE Regional Symposium on Micro and Nanoelectronics (RSM), 2015, pp. 1–4.

[203] R. Wang, T. Li, X. Shao, X. Li, and H. Gong, The Simulation of Localized Surface Plasmon and Surface Plasmon Polariton in Wire Grid Polarizer Integrated on InP Substrate For InGaAs Sensor, AIP Adv., vol. 5, no. 7, p. 77128, Jul. 2015.

[204] P. Le, Optical Properties of Small Metal Clusters École Polytechnique Fédérale De Lausanne, vol. 6718, 2015.

[205] E. Townsend and G. W. Bryant, Plasmonic Properties of Metallic Nano-particles: The Effects of Size Quantization, Nano Lett., vol. 12, no. 1, pp. 429–434, 2012.

[206] V. Khanna, V. K. Khanna, Nanosensors: Physical, Chemical and Biological, CRC Press, Taylor & Francis, 2011.

[207] K. L. Kelly, E. Coronado, L. L. Zhao, and G. C. Schatz, The Optical Properties of Metal Nano-particles: The Influence of Size, Shape, and Dielectric Environment, J. Phys. Chem. B, vol. 107, no. 3, pp. 668–677, 2003.

[208] W. A. Murray and W. L. Barnes, Plasmonic Materials, Adv. Mater., vol. 19, no. 22, pp. 3771–3782, 2007.

[209] E. Petryayeva and U. J. Krull, Localized Surface Plasmon Resonance: Nanostructures, Bioassays and Biosensing—A review, Anal. Chim. Acta, vol. 706, no. 1, pp. 8–24, 2011.

[210] H. A. Atwater and A. Polman, Plasmonics for İmproved Photovoltaic Devices., Nat. Mater., vol. 9, no. 3, pp. 205–13, 2010.

[211] D. Guzatov, S. V. Vaschenko, V. Stankevich, A. Ya. Lunevich, Y. F. Glukhov, and S. Gaponenko, Plasmonic Enhancement of Molecular Fluorescence near Silver Nano-particles: Theory, Modeling, and Experiment, vol. 116. 2012.

[212] E. Roduner, Size matters: Why Nanomaterials are Different, Chem. Soc. Rev., vol. 35, no. 7, pp. 583–592, 2006.

[213] C. N. R. Rao, G. Kulkarni, P. J. Thomas, and P. P. Edwards, Metal Nano-particles and Their Assemblies, vol. 29. 2000.

[214] K. M. Mayer and J. H. Hafner, Localized Surface Plasmon Resonance Sensors, Chem. Rev., vol. 111, no. 6, pp. 3828–3857, Jun. 2011.

[215] M.-C. Daniel and D. Astruc, Gold Nano-particles: Assembly, Supramolecular Chemistry, Quantum-Size-Related Properties, and Applications Toward Biology, Catalysis, And Nanotechnology, vol. 104. 2004.

[216] E. M. Larsson, S. Alekseeva, and C. Langhammer, Nanoplasmonic Sensing for

Nanomaterials Science, vol. 1. 2012.

[217] E. Hutter and J. H. Fendler, Exploitation of Localized Surface Plasmon Resonance , vol. 16. 2004.

[218] N. E. Motl, A. F. Smith, C. J. DeSantis, and S. E. Skrabalak, Engineering Plasmonic Metal Colloids Through Composition and Structural Design, Chem. Soc. Rev., vol. 43, no. 11, pp. 3823–3834, 2014.

[219] L. Brus, Noble Metal Nanocrystals: Plasmon Electron Transfer Photochemistry and Single-Molecule Raman Spectroscopy, Acc. Chem. Res., vol. 41, no. 12, pp. 1742–1749, 2008.

[220] P. K. Jain, X. Huang, I. H. El-Sayed, and M. A. El-Sayed, Noble Metals on the Nanoscale: Optical and Photothermal Properties and Some Applications in Imaging, Sensing, Biology, and Medicine, Acc. Chem. Res., vol. 41, no. 12, pp. 1578–1586, 2008.

[221] S. Nie and S. R. Emory, Probing Single Molecules and Single Nano-particles by Surface-Enhanced Raman Scattering, Science, vol. 275, no. 5303, p. 1102 LP-1106, 1997.

[222] K. Catchpole and A. Polman, Plasmonic Solar Cells, vol. 16. 2009.

[223] D. Thrithamarassery Gangadharan, Z. Xu, Y. Liu, R. Izquierdo, and D. Ma, Recent Advancements in Plasmon-Enhanced Promising Third-Generation Solar Cells, vol. 6. 2016.

[224] S. Pillai and M. A. Green, Plasmonics for photovoltaic applications, Sol. Energy Mater. Sol. Cells, vol. 94, no. 9, pp. 1481–1486, 2010.

[225] E. M. Larsson, C. Langhammer, I. Zorić, and B. Kasemo, Nanoplasmonic Probes of Catalytic Reactions, Science, vol. 326, no. 5956, p. 1091 LP-1094, Nov. 2009.

[226] P. K. Jain, K. S. Lee, I. H. El-Sayed, and M. A. El-Sayed, Calculated Absorption and Scattering Properties of Gold Nano-particles of Different Size, Shape, and Composition: Applications in Biological Imaging and Biomedicine, J. Phys. Chem. B, vol. 110, no. 14, pp. 7238–7248, Apr. 2006.

[227] J. Wang et al., Effect of Plasmonic Au Nano-particles on Inverted Organic Solar Cell Performance, J. Phys. Chem. C, vol. 117, no. 1, pp. 85–91, Jan. 2013.

[228] E. Kowalska, O. O. P. Mahaney, R. Abe, and B. Ohtani, Visible-Light-Induced Photocatalysis Through Surface Plasmon Excitation of Gold on Titania Surfaces, Phys. Chem. Chem. Phys., vol. 12, no. 10, pp. 2344–2355, 2010.

[229] S. Carretero-Palacios, M. E. Calvo, and H. Míguez, Absorption Enhancement in Organic–Inorganic Halide Perovskite Films with Embedded Plasmonic Gold Nano-particles, J. Phys. Chem. C, vol. 119, no. 32, pp. 18635–18640, 2015.

[230] Y. H. Jang, Y. J. Jang, S. Kim, L. N. Quan, K. Chung, and D. H. Kim, Plasmonic Solar Cells: From Rational Design to Mechanism Overview, Chem. Rev., vol. 116,

no. 24, pp. 14982–15034, 2016.

[231] M. D. Brown et al., Plasmonic Dye-Sensitized Solar Cells Using Core−Shell Metal−Insulator Nano-particles, Nano Lett., vol. 11, no. 2, pp. 438–445, Feb. 2011.

[232] G. Sahu, S. W. Gordon, and M. A. Tarr, Synthesis and Application of Core-Shell Au–$TiO_2$ Nanowire Photoanode Materials for Dye Sensitized Solar Cells, RSC Adv., vol. 2, no. 2, pp. 573–582, 2012.

[233] Y. Ding et al., High Performance Dye-Sensitized Solar Cells with Enhanced Light-Harvesting Efficiency Based on Polyvinylpyrrolidone-Coated Au-$TiO_2$ Microspheres, vol. 9. 2016.

[234] S. P. Lim, A. Pandikumar, N. M. Huang, and H. N. Lim, Enhanced Photovoltaic Performance of Silver@Titania Plasmonic Photoanode in Dye-Sensitized Solar Cells, RSC Adv., vol. 4, no. 72, pp. 38111–38118, 2014.

[235] Y. H. Jang, Y. J. Jang, S. T. Kochuveedu, M. Byun, Z. Lin, and D. H. Kim, Plasmonic Dye-Sensitized Solar Cells Incorporated with Au–$TiO_2$ Nanostructures With Tailored Configurations, Nanoscale, vol. 6, no. 3, pp. 1823–1832, 2014.

[236] J. Henzie, J. Lee, M. H. Lee, W. Hasan, and T. W. Odom, Nanofabrication of Plasmonic Structures, Annu. Rev. Phys. Chem., vol. 60, no. 1, pp. 147–165, 2009.

[237] A. J. Haes, C. L. Haynes, A. D. McFarland, G. C. Schatz, R. P. Van Duyne, and S. Zou, Plasmonic Materials for Surface-Enhanced Sensing and Spectroscopy, MRS Bull., vol. 30, no. 5, pp. 368–375, 2005.

[238] R. P. Van Duyne, Molecular Plasmonics, Science, vol. 306, no. 5698, p. 985 LP-986, 2004.

[239] X. Lu, M. Rycenga, S. E. Skrabalak, B. Wiley, and Y. Xia, Chemical Synthesis of Novel Plasmonic Nano-particles, Annu. Rev. Phys. Chem., vol. 60, no. 1, pp. 167–192, 2009.

[240] S. Verbruggen et al., Plasmonic Gold–Silver Alloy on $TiO_2$ Photocatalysts with Tunable Visible Light Activity, vol. s 156–157. 2014.

[241] X. Zhou, G. Liu, J. Yu, and W. Fan, Surface Plasmon Resonance-Mediated Photocatalysis by Noble Metal-Based Composites Under Visible Light, J. Mater. Chem., vol. 22, no. 40, pp. 21337–21354, 2012.

[242] N. Zhang, S. Liu, X. Fu, and Y.-J. Xu, Synthesis of M@$TiO_2$ (M = Au, Pd, Pt) Core–Shell Nanocomposites with Tunable Photoreactivity, J. Phys. Chem. C, vol. 115, no. 18, pp. 9136–9145, 2011.

[243] D. B. Ingram, P. Christopher, J. L. Bauer, and S. Linic, Predictive Model for the Design of Plasmonic Metal/Semiconductor Composite Photocatalysts, ACS Catal., vol. 1, no. 10, pp. 1441–1447, 2011.

[244] J. Qi, X. Dang, P. T. Hammond, and A. M. Belcher, Highly Efficient Plasmon-Enhanced Dye-Sensitized Solar Cells through Metal@Oxide Core–Shell

Nanostructure, ACS Nano, vol. 5, no. 9, pp. 7108–7116, 2011.

[245] Z. S. Seddigi, S. A. Ahmed, S. Sardar, and S. K. Pal, Carbonate Doping in $TiO_2$ Microsphere: The Key Parameter Influencing Others for Efficient Dye Sensitized Solar Cell, Sci. Rep., vol. 6, no. March, 2016.

[246] D. D. Usta, K. Salimi, A. Pinar, I. Coban, T. Tekinay, and A. Tuncel, A Boronate Affinity-Assisted SERS Tag Equipped with a Sandwich System for Detection of Glycated Hemoglobin in the Hemolysate of Human Erythrocytes, ACS Appl. Mater. Interfaces, vol. 8, no. 19, pp. 11934–11944, 2016.

[247] Q. Liu and J. Wang, Dye-Sensitized Solar Cells Based on Surficial $TiO_2$ Modification, Sol. Energy, vol. 184, no. April, pp. 454–465, 2019.

[248] A. Atli, A. Atilgan, and A. Yildiz, Multi-Layered $TiO_2$ Photoanodes From Different Precursors of Nanocrystals for Dye-Sensitized Solar Cells, Sol. Energy, vol. 173, pp. 752–758, 2018.

[249] P. Knipping and M. Von Laue, X-ray Diffraction, pp. 1–18, 1952.

[250] Royal Society of Chemistry, Spectroscopy in a Suitcase: Ultraviolet -Visible Spectroscopy (UV), pp. 1–7, 2009.

[251] N. Musila, M. Munji, J. M. Simiyu,N. Eric,K. Raphael, Miriam, Characteristics of $TiO_2$ Compact Layer Prepared for DSSC Application, Path of Science, 2018.

[252] Lee, Chang Woo Rhee, Seung Choi, Hyung, Preparation of $TiO_2$ Nanotube/Nanoparticle Composite Particles and Their Applications in Dye-Sensitized Solar Cells,Nanoscale Research Letters, 2012.

[253] M. Nouri Sbeta, A. Yildiz, Optical Response Enhancement of GZO/p-Si Heterostructures via Metal Nanoparticles, Materials Research Express, 2019.

[254] Zhao-Qian Li, Ya-Ping Que, Li-E Mo, Wang-Chao Chen, Yong Ding, Yan-Mei Ma, Ling Jiang, Lin-Hua Hu, and Song-Yuan Dai, One-Pot Synthesis of Mesoporous $TiO_2$ Microphores and Its Application for High-Efficiency Dye-Sensitized Solar Cells, ACS Applied Materials & Interfaces, 7 (20), 10928-10934, 2015.

[255] Zhao-Qian Li, Yong Ding, Li-E Mo, Lin-Hua Hu, Ji-Huai Wu, and Song-Yuan Dai, Fine Tuning of Nanocrystal and Pore Sizes of TiO2 Submicrospheres toward High Performance Dye-Sensitized Solar Cells, ACS Applied Materials & Interfaces, 7 (40), 22277-22283, 2015.

[256] Zhao-Qian Li, Li-E Mo, Wang-Chao Chen, Xiao-Qiang Shi, Ning Wang, Lin-Hua Hu, Tasawar Hayat, Ahmed Alsaedi, and Song-Yuan Dai, Solvothermal Synthesis of Hierarchical $TiO_2$ Microstructures with High Crystallinity and Superior Light

Scattering for High-Performance Dye-Sensitized Solar Cells, ACS Applied Materials & Interfaces, 9 (37), 32026-32033, 2017.

[257]. Aseel Hadi, Qian Chen, Michele Curioni, Rongshi Xiao, Ting Huang, and Zhu Liu,

One-Step Fiber Laser Fabrication of Mesoporous and Compact $TiO_2$ Layers for Enhanced Performance of Dye-Sensitized Solar Cells, ACS Sustainable Chemistry & Engineering, 6 (9), 12299-12308, 2018.

[258] Yuewu Huang, Haigang Wu, Qingjiang Yu, Jianan Wang, Cuiling Yu, Jinzhong

Wang, Shiyong Gao, Shujie Jiao, Xitian Zhang, and Peng Wang, Single-Layer $TiO_2$ Film Composed of Mesoporous Spheres for High-Efficiency and Stable Dye-Sensitized Solar Cells, ACS Sustainable Chemistry & Engineering, 6 (3), 3411-3418, 2018.

[259] Zhao-Qian Li, Ya-Ping Que, Li-E Mo, Wang-Chao Chen, Yong Ding, Yan-Mei Ma,

Ling Jiang, Lin-Hua Hu, and Song-Yuan Dai, The synthesis and application of $TiO_2$ microspheres as scattering layer in dye-sensitized solar cells, ACS Applied Materials & Interfaces, 7 (20), 10928-10934, 2015.

[260] Muhammad, Niaz, Zanoni, Kassio, Yukie Murakami Iha, Neyde, Ahmed, Safeer,

The Use of Rutile- and Anatase- Titania Layers towards Back Light Scattering in Dye- Sensitized Solar Cells, Chemistry Select. 3. 10475-10482, 2018.

[261] Marandi, Maziar, Bayat, Samaneh, Naeimi Sani Sabet, Mahboubeh, Hydrothermal

growth of a composite $TiO_2$ hollow spheres/TiO2 nanorods powder and its application in high performance dye-sensitized solar cells, Journal of electroanalytical chemistry. 833. 143-150, 2018.

[262] Xie, Fengyan, Wang, Jingjing, Li, Yafeng, Dou, Jie, Wei, Mingdeng, One

step synthesis of hierarchical $SnO_2/TiO_2$ composite hollow microspheres as an efficient scattering layer for dye-sensitized solar cells, Electrochimica Acta. 296, 2018.

[263] Suresh Thogiti, Ji Young Park, Chau Thi Thanh Thuy, Do Kyung Lee, Bong-Ki Min,

Hyeong Jin Yun, and Jae Hong Kim, High-Performance Dye-Sensitized Solar Cells through Graded Electron Transport in Band-Engineered W-$TiO_2$ Cascade Layer, ACS Sustainable Chemistry, Engineering, 6 (10), 13025-13034, 2018.

[264] Zhou, Li, Wei, Liguo, Yang, Yulin, Xia, Xue, Wang, Ping, Yu, Jia, Luan,

Tianzhu, Improved performance of dye sensitized solar cells using Cu-doped TiO2 as photoanode materials: Band edge movement study by spectroelectrochemistry, Chemical Physics. 475, 2016.

[265] Dhonde, Mahesh, sahu, kirti, Murty, Vvs, Novel synergistic combination of Al/N

Co-doped TiO2 nanoparticles for highly efficient dye-sensitized solar cells, Solar Energy. 173. 551, 2018.

[266] Wang, Wei, Xu, Xiaomin, Liu, Yu, Zhong, Yijun, Shao, Zongping, Rational

Design of Metal Oxide–Based Cathodes for Efficient Dye- Sensitized Solar Cells., Advanced Energy Materials. 8. 1800172, 2018.

[267] Hyunbong Choi, Wei Ta Chen, and Prashant V. Kamat, Know Thy Nano Neighbor.

Plasmonic versus Electron Charging Effects of Metal Nanoparticles in Dye-Sensitized Solar Cells, ACS Nano, 6 (5), 4418-4427, 2012.

[268] Jung, Heesuk, Koo, Bonkee, Jae-Yup, Kim, Kim, Taehee, Jung Son, Hae,

Kim, Bongsoo, Young Kim, Jin, Lee, Doh-Kwon, Kim, Honggon, Cho, Jinhan, Jae Ko, Min, Enhanced Photovoltaic Properties and Long-Term Stability in Plasmonic Dye-Sensitized Solar Cells via Noncorrosive Redox Mediator, ACS applied materials, interfaces. 6, 2014.

[269] Dajiang Zheng, Xinchang Pang, Mengye Wang, Yanjie He, Changjian Lin, and Zhiqun

Lin, Unconventional Route to Hairy Plasmonic/Semiconductor Core/Shell Nanoparticles with Precisely Controlled Dimensions and Their Use in Solar Energy Conversion, Chemistry of Materials 27 (15), 5271-5278, 2015.

[270] Chunyu Liu, Chaoyang Zhao, Xulin Zhang, Wenbin Guo, Kun Liu, and Shengping

Ruan, Unique Gold Nanorods Embedded Active Layer Enabling Strong Plasmonic Effect To Improve the Performance of Polymer Photovoltaic Devices, The Journal of Physical Chemistry C, 120 (11), 6198-6205, 2016.

[271] Yue-Ying Li, Jian-Gan Wang, Xing-Rui Liu, Chao Shen, Keyu Xie, and Bingqing

Wei, Au/$TiO_2$ Hollow Spheres with Synergistic Effect of Plasmonic Enhancement and Light Scattering for Improved Dye-Sensitized Solar Cells, ACS Applied Materials, Interfaces, 9 (37), 31691-31698, 2017.

[272] Yoon Hee Jang,⊥ Yu Jin Jang, Seokhyoung Kim, Li Na Quan, Kyungwha Chung, and

Dong Ha Kim, Plasmonic Solar Cells: From Rational Design to Mechanis Overview, Chemical Reviews, 116 (24), 14982-15034, 2016.

[273] Holly F. Zarick, William R. Erwin, Abdelaziz Boulesbaa, Olivia K. Hurd, Joseph A.

Webb, Alexander A. Puretzky, David B. Geohegan, and Rizia Bardhan, Improving Light Harvesting in Dye-Sensitized Solar Cells Using Hybrid Bimetallic Nanostructures, ACS Photonics, 3 (3), 385-394, 2016.

[274] Erwin, William, F. Zarick, Holly, Talbert, Eric, Bardhan, Rizia, Light Trapping

in Mesoporous Solar Cells with Plasmonic Nanostructures, Energy Environ. Sci.. 9, 2016.

[275] Juyoung Yun, Sun Hye Hwang, and Jyongsik Jang ,Fabrication of Au@Ag Core/Shell Nanoparticles Decorated $TiO_2$ Hollow Structure for Efficient Light-Harvesting in Dye-Sensitized Solar Cells, ACS Applied Materials, Interfaces, 7 (3), 2055-2063, 2015.

# CURRICULUM VITAE



## PERSONAL INFORMATION


| | | |
|---|---|---|
| **Name Surname** | **:** | Hilal YILDIRIM |
| **Date of Birth** | **:** | 1991 |
| **Phone** | **:** | 5315838821 |
| **E-mail** | **:** | hlalyildirim@gmail.com |


## EDUCATION

| | | |
|---|---|---|
| **Bachelor** | **:** | Abant İzzet Baysal Üniversitesi, Food Engineering |
| **Bachelor** | **:** | Ankara Yıldırım Beyazıt Üniversitesi, Material Engineering |
| **Master Degree** | **:** | Ankara Yıldırım Beyazıt Üniversitesi, Material Engineering |

## WORK EXPERIENCE

| | | |
|---|---|---|
| **Internship** | **:** | COMOC - Center for Ordered Materials, Organometallics and Catalysis, Ghent University, Gent (Belgium) |
| **Internship** | **:** | ISA - Analytical Science Institut of Université Claude Bernard Lyon1, Lyon (France) |
| **Internship** | : | ETİ Maden İşletmeleri, Teknoloji Anabilim Dalı: Analitik Kimya ve Karakterizasyon Laboratuvarı, Ankara (Turkey) |

## TOPICS OF INTEREST

Nanomaterials, Development of Micro/Mesoporous MOFs and COFs for Energy Storage, Organometallic Catalysis, Hybrid Organic/ Inorganic Solar Cells, Functionalization of Surface Materials, Electrochemical Characterization